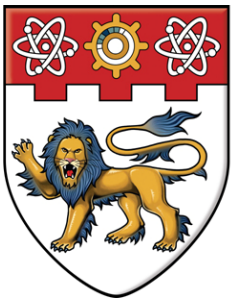

NANYANG TECHNOLOGICAL UNIVERSITY

# INFLUENCE OF ALLOY CHEMISTRY ON THE TRANSFORMATION TEMPERATURES AND LOCAL ATOMIC STRUCTURE OF SHAPE MEMORY ALLOYS:

## WITH A FOCUS ON NiTi-BASED INTERMETALLICS

**MEHRDAD ZARINEJAD**

**SCHOOL OF MECHANICAL AND AEROSPACE ENGINEERING**

**2009**

# INFLUENCE OF ALLOY CHEMISTRY ON THE TRANSFORMATION TEMPERATURES AND LOCAL ATOMIC STRUCTURE OF SHAPE MEMORY ALLOYS:

# WITH A FOCUS ON NiTi-BASED INTERMETALLICS

**MEHRDAD ZARINEJAD**

**SCHOOL OF MECHANICAL AND AEROSPACE ENGINEERING**

**A thesis submitted to the Nanyang Technological University in fulfillment of the requirements for the degree of**

**Doctor of Philosophy**

**2009**

# Acknowledgements and Dedication

I would like to express my sincere gratitude to my supervisor, Prof. Yong Liu for his guidance and support. His patience and kindness has been inspiring.

I am also grateful to Prof. Timothy John White for his guidance and fruitful discussions on Rietveld refinement and EXAFS analyses.

The author is also especially indebted to Dr. Tao Liu for EXAFS data analysis, Dr. Herbert Moser and Dr. Ping Yang from the Singapore Synchrotron Light Source (SSLS) facility for support and help in EXAFS measurements.

Many thanks are also due to the technicians of Materials Laboratories A and B, and Smart Materials and main Aircraft Laboratories, especially Mr. Sa'adon Bin Ahmad and Mr. Lim Yong Seng for their assistance and support.

I also would like to thank my friends and fellow graduate students who created a friendly and pleasant working environment during this study.

Special thanks go to the staff of the graduate office of the School Mechanical and Aerospace Engineering, and secretary of the aerospace division Ms. Amy Tan for their kind help regarding administrative issues.

Last but not least, I thank my mother, sister and brother for their patience, support, and encouragement.

To the spirit of my father,

To my kind mother, sister and brother

# Publications

1) Mehrdad Zarinejad, Yong Liu, Timothy John White, The crystal chemistry of NiTiHf shape memory alloys, ***Intermetallics*** 50 (2008), 176-189.

2) Mehrdad Zarinejad, Yong Liu, Dependence of transformation temperatures of NiTi-based shape memory alloys on the number and concentration of valence electrons, ***Advanced Functional Materials*** 18 (2008), 2789-2794.

3) Mehrdad Zarinejad, Yong Liu, Dependence of transformation temperatures of Shape Memory Alloys on the Number and Concentration of Valence Electrons, ***Book Chapter*** **in Shape Memory Alloys, Manufacture, Processing, Properties**, Nova Science Publishers, New York, (2009).

4) Mehrdad Zarinejad, Yong Liu, Yunxiang Tong, Transformation temperature changes due to second phase precipitation in NiTi-based shape memory alloys ***Intermetallics*** 51 (2009) 46-53.

5) Mehrdad Zarinejad, Yong Liu, Tao Liu, Tim White, Ping Yang, Qiming Chen, Evolution of local structure in a melt-spun $Ni_{25}Ti_{50}Cu_{25}$ shape memory alloy during crystallization, (submitted to ***Philosophical Magazine***).

6) Yunxiang Tong, Yong Liu, Zheliang Xie, Mehrdad Zarinejad, Effect of precipitation on the shape memory effect of $Ti_{50}Ni_{25}Cu_{25}$ melt-spun ribbon, ***Acta Materialia*** 56 (2008) 1721-1732.

7) Mehrdad Zarinejad, Yong Liu, Tim White, Tao Liu, Ping Yang, Change of local structure in $Ni_{25}Ti_{25}Cu_{25}$ shape memory alloy ribbon during crystallization, ***2nd SSLS Synchrotron Symposium***, Singapore, (2008).

8) Mehrdad Zarinejad, Yong Liu, Transformation Temperatures of NiTi-Based Shape Memory Alloys: A Valence Electron Study, ***Tohoko University-NTU Symposium on Materials***, Sendai, Japan, (2009).

9) Mehrdad Zarinejad, Yong Liu, Transformation Temperatures of Shape Memory Alloys, ***NTU Symposium on Materials***, Singapore, (2009).

# List of Parameters

| | |
|---|---|
| $M_s$ | Martensite start temperature |
| $A_s$ | Austenite start temperature |
| $e_v$/a | Number of valence electrons per atom |
| $e_t$ | Total number of electrons |
| $c_v$ | Valence electron concentration |
| Z | Atomic number |
| $f$ | Atomic fraction of the element in the alloy |
| ΔH | Transfomrtion latent heat |
| T | Temperature |
| $\varepsilon_0$ | Transformational strain |
| $\eta_M$ | Lattice distortion |
| ΔS | Entropy change |
| a,b,c | Lattice parameters |
| β | Monoclinic angle |
| x,y,z | Atomic parameters of the crystal |
| $m$ | weight of the element in alloy formula |
| $A$ | Atomic weight of the element |
| $w$ | Weight fraction of the element in the alloy |
| $I$ | Total weight of the alloy sample |
| $M_{Alloy}$ | Molecular weight of the alloy |
| $P$ | Weight fraction of the precipitate |
| $f'$ | Atomic fraction of element in the precipitate |
| $m'$ | Weight of the element in the precipitate formula |
| $w'$ | Weight of the element in the precipitate |
| $M_{precipitate}$ | Molecular weight of the precipitate |
| $w''$ | Weight of the element in the matrix after precipitation |
| $f^*$ | Number of moles of elemnet in the matrix after precipitation |
| $f''$ | Atomic fraction of the element in the matrix after precipitation |
| $(c_v)_{aged}$ | Valence electron concentration of the matrix after aging |
| $N$ | Coordination number |
| $R$ | Interatomic distance |
| $\sigma$ | Relative displacement of the atom |

# Abstract

The dependence of transformation temperatures of shape memory alloys on the number and concentration of valence electrons are studied. This dependence is further analyzed for NiTi-based alloys followed by an investigation of the effect of precipitation on the $M_s$ temperature, and the influence of composition change on the local atomic structure and transformation temperature of NiTiHf alloys. The bond evolution and change of transformation temperature during the local chemistry change of a $Ni_{25}Ti_{50}Cu_{25}$ melt-spun ribbon during crystallization is also studied.

The shape memory alloys are categorized into low ($e_v$/a<5), medium (5≤$e_v$/a≤7.50), and high ($e_v$/a>7.50) valence electron groups. For majority of alloys in medium and high valence electron group, clear correlations between transformation temperatures and their valence electron concentration ($c_v$) are found. The $M_s$ and $A_s$ both decrease from 1100 and 1150˚C to as low as -206˚C and -153˚C respectively, with increasing $c_v$ from 0.10 to around 0.30. When the number of valence electrons per atom is high ($e_v$/a>7.50), the transformation temperatures show much less dependence on $c_v$. High electron NiMnX (X=Ga, In, Al) Heusler alloys containing Mn (>30 at%) show high transformation temperatures at high $c_v$ values most likely due to anti-ferromagnetism of excess Mn which reduces the elastic moduli. The low valence electron group shows significantly lower transformation temperatures for their $c_v$ values compared to the main group. The influence of valence electron concentration is discussed on the basis of the variations of elastic moduli of the alloys as a result of composition change.

For NiTi-based alloys, two distinct trends of transformation temperatures with respect to the number of valence electrons per atom are found depending on whether $e_v$/a = 7 or $e_v$/a ≠ 7. Clear correlations between transformation temperatures and $c_v$ exist. $M_s$ and $A_s$ decrease consistently with increasing $c_v$. The possible influence of alloying elements atomic size on transformation hysteresis is also introduced. Furthermore, for these alloys, the changes of martensite start temperature ($M_s$) as a result of second phase precipitation are studied. The alteration of $M_s$ as a result of precipitation is mainly due to the change of electron concentration of the matrix because of its composition change.

The extrinsic effect of the precipitates on $M_s$ is also discussed on the basis of their quantity in the as-quenched and aged microstructures.

Local atomic structure investigation of a number of NiTiHf shape memory alloys are carried out using quanititative X-ray diffraction (XRD). At the same Hf content, Ti-rich alloys exhibit larger cell volumes than Ni-rich alloys. The equiatomic alloys show smaller unit cell volumes than Ti-rich and Ni-rich groups possibly due to more isotropic bonding. The $e_v$/a and $c_v$ of the alloys influence the atomic bond lengths and unit cell dimensions. The similar tendency of Hf towards occupancy in Ni and Ti sites, results in its preference for available sites in the structure.

The local atomic environment of an amorphous $Ni_{25}Ti_{50}Cu_{25}$ met-spun ribbon and bond evolution during its crystallization were studied as an example of the change of local chemistry and its effect on transformation temperature of the alloy, by extended x-ray absorption fine structure (EXAFS) spectroscopy and differential scanning calorimetry (DSC). In the amorphous alloy the interatomic distances of Ni-Ti and Cu-Ti are distinct from Ti-Ti and can be indicative of the formation of two types of dominant polyhedra or distorted polyhedral clusters centered with Ni and Cu, with majority of shell atoms being Ti. The overall increase of the coordination numbers of Ni, Ti, and Cu by crystallization and an evidence for structural relaxation suggest the melt-spun alloy ribbon contains a combination of ordered structures and free volume prior to the heat treatment. Copper and nickel are co-located as their absorption spectra are similar. Although crystallization occurs rapidly (within 4 mins), the local atomic environment change persists at longer annealing times (up to 10 mins). An increase in the Ti-Ti and Cu-Cu homo-bond fractions at early and intermediate annealing times suggests these species segregate between two phases. Crystallization continues by a short-range Ti and Cu diffusion dominated process, as the near-neighbor structures of Ti and Cu change considerably more than Ni during annealing to homogenize the microstructure followed by possible precipitation of a TiCu compound. The segregation of Cu and Ti results in the change of chemical composition of the crystalline phase and brings about the variation of transformation temperature of the alloy during crystallization.

# Table of Contents

# List of Figures

# List of Tables

# Chapter 1

# 1 Introduction

## 1.1 Background

Shape memory alloys (SMAs) are a group of metallic materials which have the ability to undergo large deformations while reverting back to their original undeformed shape through either heating (shape memory effect) or removal of the load (superelastic effect). Although shape memory was discovered in the 1930's, it was not until the discovery of shape memory properties in near equiatomic NiTi (also known as Nitinol) by Buehler and Wiley at the Naval Ordnance Laboratory that research into the mechanics and applications of shape memory alloys began [1]. During the past two decades, several advances have been made in understanding the mechanisms associated with the shape memory and superelastic effects, their thermomechanical behavior, and the fabrication and production of SMAs leading to higher quality and more reliable materials at lower costs. Shape memory alloys are produced through casting and thermomechanical processing in the form of bulk, wire or sheets, or through melt-spinning technique in the form of thin ribbons with initially nearly amorphous microstructure. These advances have prompted increased interest in the use of these materials in a number of functional engineering and commercial applications.

The shape memory properties of SMAs are due to a temperature-dependent or magnetic-induced martensitic phase transformation from a low-symmetry to a highly symmetric crystallographic structure. In shape-memory alloys, the martensitic phase change is reversible and often termed thermoelastic [2,3]. When cooling a shape-memory alloy from high temperature, the transformation produces a martensitic microstructure which can completely transform to the parent phase (high temperature, high symmetry) upon reheating [4].

Transformation temperatures of shape memory alloys are of paramount importance from both fundamental and technological points of view [4-12]. For instance, in NiTi as the most famous shape memory alloy, the transformation temperature and hysteresis can be altered by introducing alloying elements to satisfy the high or low temperature applications. Addition of various transition metals to NiTi that either elevate or lower the transformation temperatures has been studied [13-47], part of which has been reviewed by Otsuka et al [11]. Apart from the selection of alloying elements, their replacement for either Ni or Ti, or both is also of paramount importance. For instance, when W is added to replace Ni, the $M_s$ temperature is above room temperature; whereas when it replaces Ti, the $M_s$ temperature drops to below room temperature [22]. Similarly, For $Ni_{50}Mn_{25}Ga_{25}$ which is another shape memory system of magnetic nature alloying elements have been added to alter the properties and/or transformation temperatures. Despite many efforts to relate transformation temperatures to chemical composition, the dependence of $M_s$ and $A_s$ on alloy composition has remained unclear, and the design of shape memory alloys, is rather empirical, due to the lack of an in-depth understanding about the effect of composition change. The key influential factors that have been referred to are elastic constants of the parent crystal and microstructural features such as precipitates [11].

## 1.2 Present Research

It has been shown that in shape memory alloys, prior to martensitic transformation a softening of elastic constant occurs with lowering temperature. Experimental results, mainly in Cu-based and also in NiTi-based shape memory alloys [8-10,12] and the studies of Clapp [48,49] show that there is a critical value of elastic constant at which transformation takes place. This value is not sensitive to alloy compositions, and is only slightly dependant on temperature [11]. However, it is not clear how the change of alloy chemical composition is linked with the elastic properties and therefore the transformation temperatures.

In order to understand the influential factors that control the transformation temperatures of shape memory alloys, a profound knowledge of how the atomic

bonding is influenced by chemical composition change is necessary. This undermines the importance of the knowledge on the electronic, crystal chemistry and local atomic structure changes and includes interatomic bonding characteristics. Despite their importance these areas have not been systematically studied in shape memory alloys. The inter-relationship of electronic structure, local atomic and crystal structures and their influence on mechanical properties and martensitic transformation characteristics are not known. The limited research in these fields has been mainly done independently on either microstructure level, atomic level, or electronic level. Specifically the influence of the latter on mechanical properties and martensitic transformation has been overlooked. There is a need to explore the relationship of electronic structure, local atomic and crystal structure as a result of compositional changes in shape memory alloys in general and NiTi-based alloys specifically as the most commercial group of these alloys,

It is well known that in metallic materials the delocalized valence electrons hold the non-valence electrons and nuclei of atoms (ion cores) together and form metallic bonds [50]. Therefore, knowledge of how the chemistry change alters the electronic structures of shape memory alloys is essential. Theoretical studies of Parlinski et al [51] and Kulkova et al [52] offer some understanding of the lattice dynamics and electronic structure in NiTi and Ti-based shape memory alloys. In order to clarify the mechanism by which alloying elements alter the transformation temperatures in NiTi-based alloys further electronic structure studies are required. Moreover, how the interatomic bonding is influenced by alloying and the interatomic distances (bond lengths) and coordination behavior of parent Ni, Ti and alloying elements are important.

In the present work, the valence electron changes of various alloys are studied. Two parameters are paid attention to: 1) the number of valence electron per atom, and 2) the valence electron concentration of the alloys. The correlations of these parameters with transformation temperatures are investigated. Furthermore, the crystal structure and local atomic structure of a number of Ni-rich, Ti-rich and equiatomic NiTiHf alloys are studied which represent alloys with dfferent transformation temperatures. Also, the local atomic and microstructure changes in a $Ni_{25}Ti_{25}Cu_{25}$ amorphous ribbon as a result of crystallization annealing are studied. These investigations will take place through quantitative X-ray diffraction (XRD) X-ray

diffraction fine structure (EXAFS) and scanning electron microscopy (SEM) analyses. Hence the main objectives of the present work are:

To determine the effect of chemical composition on the transformation temperatures of shape memory alloys through the understanding of the influence of valence electron factors of these materials with a focus on NiTi-based compositions.

To investigate the crystal chemistry and local atomic structures of NiTiHf alloys (with an emphasis on bond length variations, and substitutional site preference of alloying elements) as a function of composition and their possible relationship to transformation temperatures.

To study the effect of second precipitate on the martensitic transformation temperature of NiTi-based shape memory alloys.

To determine the local atomic structure and transformation temperature variation of an amorphous $Ni_{25}Ti_{25}Cu_{25}$ alloy as a result of crystallization.

## 1.3 Organization of the Thesis

A literature survey of the shape memory effect, diversity of shape memory compositions, NiTi-based shape memory alloys with an emphasis on the effect of chemical composition on the transformation temperatures, along with a brief review of the local atomic and electronic structure studies are presented in Chapter 2.

In Chapter 3 the experimental procedures and analysis methods are presented. These include alloy production using vacuum arc melting, melt spinning and heat treatment, chemical analysis, differential scanning calorimetry (DSC), data compilation and analysis for valence electron study, X-ray diffraction (XRD) and extended X-ray absorption fine structure (EXAFS) spectroscopy for crystal chemistry and local atomic structure study.

The results and discussion of electronic structure analysis and its relationship to transformation temperatures for all the transition-metal shape memory alloys and NiTi-based alloys are given in Chapters 4 and 5, respectively.

The influence of second phase precipitation on the transformation temperatures in aged NiTi-based shape memory alloys is presented in Chapter 6.

The crystal chemistry, local atomic structure, and transformation temperatures of a select group of NiTi-based alloys, i.e. NiTiHf alloys, are analyzed in Chapter 7.

The possible presence of short range order in a $Ni_{25}Ti_{50}Cu_{25}$ melt-spun ribbon and the evolution of chemical bonding and change of transformation temperature during crystallization are explored in Chapter 8.

Finally, conclusions are given in Chapter 9, followed by a note on the contributions to the knowledge and recommendations for further work.

## 1.4 Summary

Despite many efforts to relate transformation temperatures to chemical composition, the design of shape memory alloys, is rather empirical, due to the lack of an in-depth understanding about the effect of composition change. Therefore, knowledge of how the chemistry change alters the electronic structures of shape memory alloys is essential. In the present work, the valence electron changes of various alloys are studied. Two parameters are paid attention to: 1) the number of valence electron per atom, and 2) the valence electron concentration of the alloys. The correlations of these parameters with transformation temperatures are investigated. Furthermore, the crystal structure and local atomic structure of a number of Ni-rich, Ti-rich and equiatomic NiTiHf alloys and the local atomic in a $Ni_{25}Ti_{25}Cu_{25}$ amorphous ribbon as a result of crystallization annealing are studied. These investigations will take place through quantitative X-ray diffraction (XRD) X-ray diffraction fine structure (EXAFS) and scanning electron microscopy (SEM) analyses.

# Chapter 2

# 2 Literature Survey

## 2.1 Martensitic Transformation and Shape Memory Effect

Martensitic transformations are diffusionless, solid-to-solid phase transitions, and have been observed in metals, alloys, ceramics and proteins [3,4]. They are characterized by a rapid change of crystal structure, accompanied by the development of a rich microstructure. The low symmetry martensitic phase is stable in either a multi-variant twinned form or a single variant detwinned form where the multi-variants represent a change in the orientation of the crystalline structure. Conversely, the austenitic phase only takes on a single form and tends to be harder and stronger [53]. A two-dimensional general schematic view of the martensitic and austenitic phases can be seen in Fig. 2.1. The unique ability of SMAs to recover their shape is in part due to the ordered crystalline structure between the austenitic and martensitic phases. As a result, the ordering of the atoms in the martensitic phase and austenitic phase does not change. This ordering 2.1a: 2.1b: 2.1c allows the material to undergo a displacive (diffusionless) martensitic phase transformation either through a temperature change or the application of stress rather than the diffusional transformation associated with solid-state transformations of typical metals.

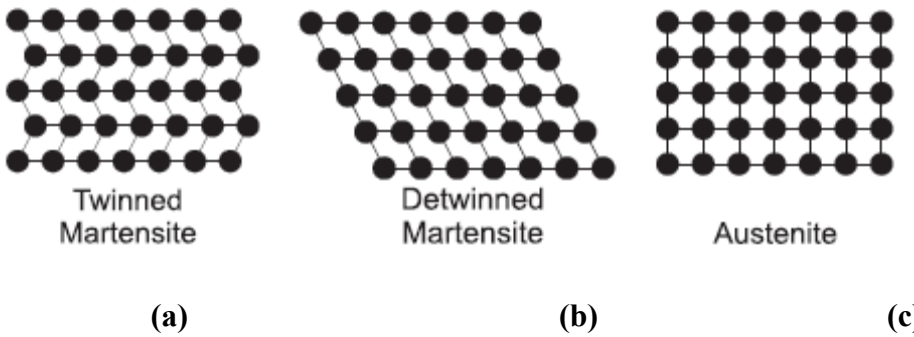


Figure 2.1: Schematic view of a typical SMA microstructure: (a) multi-variant twinned martensite, (b) single variant detwinned martensite, (c) austenite [4].

The martensitic phase transformation takes place through both a lattice deformation (atomic movement) and lattice accommodation (invariant shear) process. The lattice deformation process consists of small atomic movements in either the austenite phase (Fig. 2.1c) or twinned martensite phase (Fig. 2.1a) layer by layer to create a single variant detwinned martensite structure (Fig. 2.1b). This process consists only of a shape change with no permanent slip allowing the shape change to be reversible and providing the unique ability of SMAs to be able to undergo large deformations while returning to their original undeformed shape [53]. The martensite start temperature, $M_s$, martensite finish temperature, $M_f$, austenite start temperature, $A_s$, and austenite finish temperature, $A_f$, define the temperatures at which the phase transformations occur and result in hysteretic behavior during cooling and heating. At temperatures below $M_f$, SMAs are in their twinned martensite phase while at temperatures above $A_f$, the SMAs are in their austenite phase. Significant property changes are associated with passing these transformation points and the transformation temperatures themselves are highly dependent on the composition and processing of the SMA [1].

### 2.1.2 Shape Memory Effect

There are two mechanisms by which the deformation of SMAs can be recovered, the shape memory effect and the superelastic effect. The shape memory effect occurs at temperatures below $M_f$, resulting in the SMA being in its twinned martensite form. Upon loading, the twinned martensite undergoes typical elastic deformation until the "yield" stress is reached at which point twin boundary movement occurs and detwinning initiates. After the completion of the phase transformation, further elastic deformation of the detwinned martensite occurs provided the critical slip stress has not been reached. Upon unloading, there remains residual strain which is recovered by heating the material above $A_f$ causing a phase change to the high temperature austenite phase. Upon cooling, the structure returns to the original twinned martensite form with little or no residual strain [53]. Figure 2.2 [54] provides the stress-strain curve associated with the shape memory effect.

### 2.1.3 Superelastic Effect

The second means of shape recovery in SMAs is the superelastic effect. The superelastic effect occurs at temperatures above the $A_f$, resulting in the SMA being in its austenitic phase at the start of loading. Upon loading, the austenite undergoes typical elastic deformation until the "yield" stress (stress at which martensite becomes stable) is reached. At this point, the martensitic phase transformation initiates. Detwinning then occurs along the stress plateau until the NiTi is in its fully detwinned martensite phase.

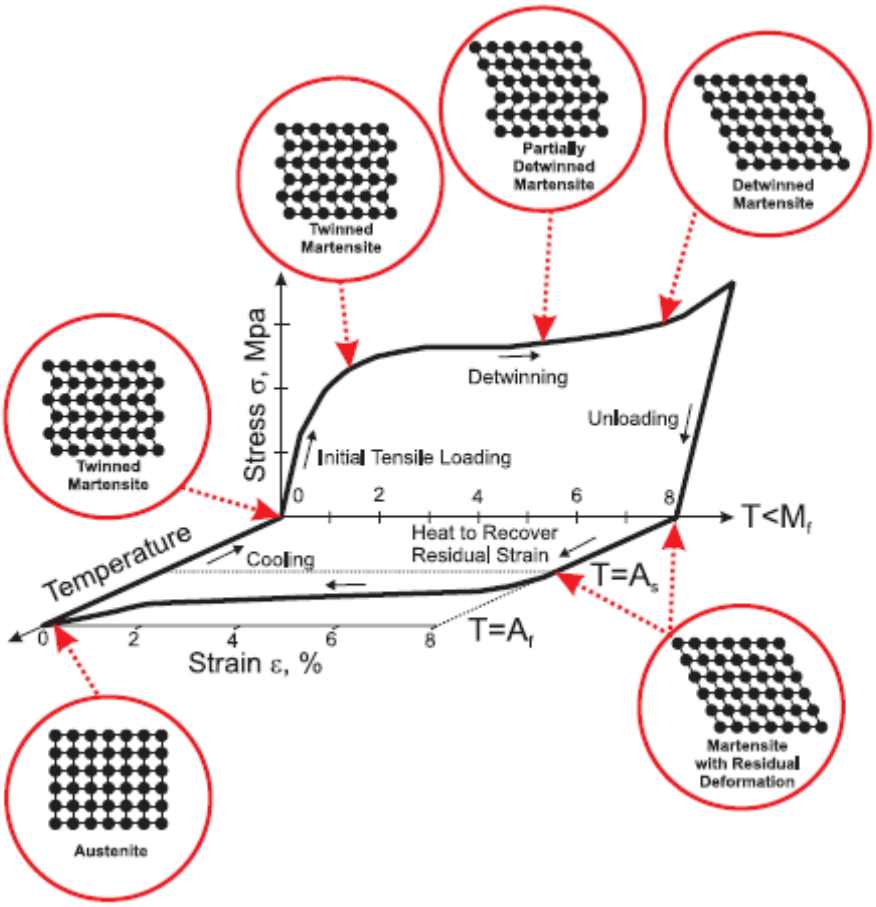


Figure 2.2: Typical stress-strain curve for an SMA undergoing the shape memory effect [54]

After completion of the phase transformation, further elastic deformation can occur provided the critical slip stress has not been reached. Upon removal of the load,

the detwinned martensite is no longer stable and reverts back to its original austenite phase. The energy driving this reverse transformation is the chemical free energy between the austenite phase and martensite phase [55]. In order for the superelastic effect to occur, the critical slip stress must be above the critical stress to cause stress-induced martensite. If this is not true, permanent deformation occurs [56]. Fig. 2.3 provides a schematic of the stress-strain curve associated with the superelastic effect.

### 2.1.4 Mechanical Behavior of Shape Memory Alloys

A further property to note is that the martensitic phase transformation is a thermoelastic process. The thermoelastic nature means that a decrease in the SMAs temperature equivalently acts as an increase in stress due to growth of martensitic plates causing an increase in internal stresses [53]. This is the main contribution to the formation of the shape memory effect and the superelastic effect at different temperatures as can be seen from the three dimensional plot of stress, strain, and temperature in Fig. 2.4 [57].

The relationship between stress required to induce martensite and the temperature can be described by the Clausius-Clapeyron equation (Equation 2.1):

$$d\sigma/dM_s=-\Delta H/T\varepsilon_0 \qquad (2.1)$$

The left side of Equation 2.1 refers to the change in stress with respect to a change in martensite start temperature, while $\Delta H$, T, and $\varepsilon_0$ represent the transformation latent heat, temperature, and transformational strain, respectively.

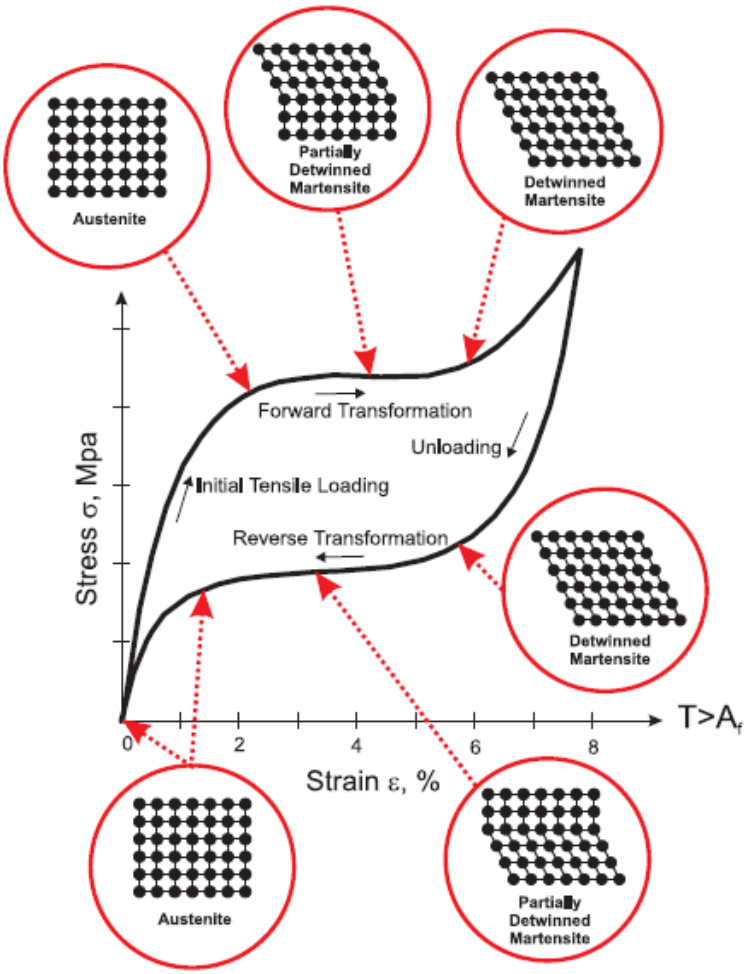


Figure 2.3: Typical stress-strain curve for an SMA undergoing the superelastic effect [54].

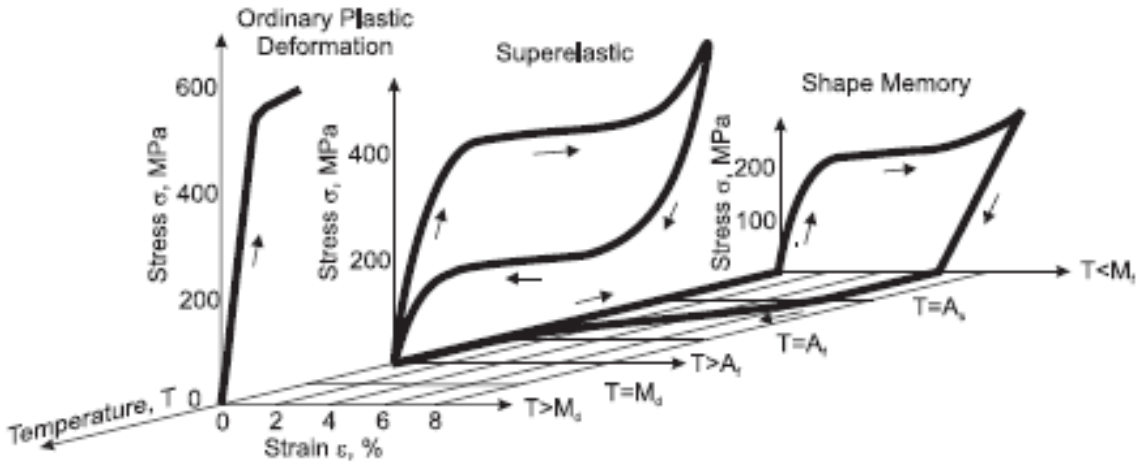


Figure 2.4: Three dimensional stress, strain, temperature relationship for the mechanical behavior of the alloys [57].

This temperature effect needs to be considered when considering SMAs for applications which may experience a broad temperature range.

### 2.1.5 Aerospace Applications of Shape Memory Alloys

The unique properties of SMAs, such as the shape recovery, hysteretic damping, good corrosion resistance, and biocompatibility, coupled with a significant reduction in price, higher quality, and better reliability has led to the development of several applications for SMAs in the biomedical, commercial, and aerospace fields. The ability to use SMAs to enhance behavior of SMAs less invasive medical procedures has led to several developments in the medical field including: arterial stents, medical guide wires, catheters, orthodontic braces, and orthopedic prostheses [58]. Commercial applications which have taken advantage of the superelastic properties of SMAs include eyeglass frames, cellular telephone antennas, and golf clubs [59,60]. The aerospace industry implemented SMAs in adaptive aircraft wings and smart helicopter blades for increased efficiency and reduced noise and vibration [61,62]. The success of these applications has increased interest in the use of SMAs in other fields, such as for applications in the seismic resistant design and retrofit of civil engineering structures. With the increased emphasis on both reliability and multi-functionality in the aerospace industry, active materials are fast becoming an enabling technology capturing the attention of an increasing number of engineers and scientists worldwide.

Designers in many fields have been developing ways to convert thermal energy into mechanical work via the crystallographic phase change of SMAs, which have now been used in real-world applications for several decades. One of the most well-known of these early applications was the hydraulic tubing coupling used on the F-14 in 1971 [63]. Since that time, designers have continued to utilize both the shape memory and pseudoelastic effects of SMAs in solving engineering problems in the aerospace industry. Such implementations of SMA technology have spanned the areas of fixed wing aircraft, rotorcraft, and spacecraft; work continues in all three of these areas.

- *Fixed-wing aircraft and rotorcraft applications*

Two of the most well-known fixed-wing projects of the past are the Smart Wing program and the Smart Aircraft and Marine Propulsion System demonstration (SAMPSON) [63]. SMA wire tendons were used to actuate hingeless ailerons while an SMA torque tube was used to initiate spanwise wing twisting of a scaled-down F-18. In each of these applications, the SME is used to provide actuation via shape recovery, and the recovery occurs at a non-zero stress. Although the SMA was able to provide satisfactory actuation at 16 per cent scale, it was found that the SMA torque tube in particular was not of sufficient strength to actuate a full-scale wing. Fabrication of larger SMA components for stronger actuation is now practical. The SAMPSON program was designed to demonstrate the usefulness of active materials in tailoring the inlet geometry and orientation of various propulsion systems. Portions of the SAMPSON project also studied the use of SMA 'cables' wrapped circumferentially around the aft portion of the fan cowling of a high-bypass jet engine in order to increase/decrease fan nozzle area in different regions of the flight regime. In the design, high exhaust temperature produced during take-off and landing (slow speed flight) was used to cause SMA structural elements to transform into austenite, thus providing recovery strain and opening the nozzle to its maximum cross-sectional area. At cruise, however, lower temperatures would allow the nozzle to close, optimizing performance at high altitudes. The experiment, which utilized SMA cable bundles for both opening and closing of the nozzle, proved the technology to be practical. Again, actuation was based on the principle of changing flow temperature with altitude. In addition to propulsion system applications, SME actuation is also commonly applied to the problem of adaptable lifting bodies, including the morphing of the wing structure. The concept of integrating SMA elements into an aerostructure has been the topic of a number of studies. It was shown that the wing configuration could be changed during flight to optimize performance.

-*Spacecraft applications*

Space applications seek to address the unique problems of release, actuation, and vibration mitigation during either the launch of a spacecraft or its subsequent operation in a microgravity and zero atmosphere environment. Although actuated structures in

space are subject to low gravitational forces which reduce required actuator power, heat transfer can quickly become problematic because of the lack of a convective medium. Perhaps the most prolific use of SMAs in space is in solving the problem of low-shock release [63]. Pyrotechnic release mechanisms were often found to be the root cause. Because they can be actuated slowly by gradual heating, SMA components are suited for use in low-shock release mechanisms and have been introduced for use on both averagesized and smaller 'micro'-sized satellites. The advent of these smaller satellites has created a need for more compact release devices which are an order of magnitude smaller than their off-the-shelf counterparts. Another SMA application is the actuation of various spacecraft components via SME. One early example includes an SMA-actuated solar collector utilizing torsional elements which can modify its shape to optimize performance. Such a design could be used to tailor the shape of spacecraft antennae. Another example of potential structural morphing is the antagonistic flexural unit cell discussed earlier in reference to fixed-wing aircraft. A different and well-known SMA space actuation application of SMAs is the Mars Pathfinder mission in 1997. The mission included an SMA actuator which served to rotate a dust cover froma specific region of a solar cell so that the power output of this protected and clean region could be compared to the power output of non-protected regions, thereby quantifying the negative effects of dust settling on the solar panels. Finally, researchers have investigated using SMA strips to support inflatable structures for use in space. This interesting application can utilize both the shape memory and pseudoelastic effects. The actuation of SME is used to help deploy the structure, while the large yet fully recoverable deformations provided during pseudoelastic loading help preserve its shape. Research is also being performed which takes into account the tunable nature of SMA vibration isolators. Because of the large change in elastic as well as transformation properties with temperature, SMA elements properly placed in structural attenuators allow for attenuation across a range of frequencies. Also interesting is an MEMS implementation of such vibration isolation. Finally, new investigation is being performed into the detailed dynamic response of SMA vibration isolation systems.

As a summary of the various advantageous and challenges exhibited by SMAs, Table 2.1 has been provided.

Table 2.1: Summary of various SMA properties and their effects [63].

| SMA traits | Consequences |
|---|---|
| Shape memory effect | Material can be used as an actuator, providing force during shape recovery |
| Pseudoelasticity | Material can be stressed to provide large, recoverable deformations at relatively constant stress levels |
| Hysteresis | Allows for dissipation of energy during pseudoelastic response |
| High actuation stress (400–700 MPa) [18, 74] | Small component cross-sections can provide substantial forces |
| High actuation strain (8%) [18, 74] | Small component lengths can provide large displacements |
| High energy density (~1200 J/kg) [69] | Small amount of material required to provide substantial actuation work |
| Three-dimensional actuation | Polycrystalline SMA components fabricated in a variety of shapes, providing a variety of useful geometric configurations |
| Actuation frequency | Difficulty of quickly cooling components limits use in high frequency applications |
| Energy efficiency (10–15%) [69] | Amount of thermal energy required for actuation is much larger than mechanical work output |
| Transformation-induced plasticity | Plastic accumulation during cyclic response eventually degrades material and leads to failure |

Note that while some behaviors are clearly positive or negative, others will depend upon the details of the use. Although some of the challenges can be met by creative engineering solutions, others will only be solved by future improvement of the material itself. At present high transformation temperature hysteresis of the commercially available wire does not provide fast enough responses for high frequency applications. This problem needs to be solved by development of the materials coupled with the design.

## 2.2 Crystal Chemistry and Reversibility of Martensitic Transformation

Martensitic transformations can be irreversible, as seen in steels upon quenching [2,6], or they can be reversible, such as those observed in shape memory alloys [6,64,65]. Reversibility of structural phase transformations has profound

technological implications in a wide range of applications from fatigue life in shape memory alloys (SMAs) to magnetism in multiferroic oxides. The geometric nonlinear theory of martensite universally applicable to all structural transitions has been recently developed. It predicts the reversibility of the transitions as manifested in the hysteresis behavior based solely on crystal symmetry and geometric compatibilities between phases. These sharp differences in behavior on the basis of the change in crystal symmetry during the transition have recently been explained [6,66]. It has been proposed [6] that in order to have a reversible transformation it is required that the symmetry groups of the parent and product phases to be in a common finite symmetry group. In such conditions, the lattice invariant shear is faced with a bigger energy barrier than that of the phase change; hence transformations in this condition can occur without plasticity. Once the energy barrier to plastic deformation (via lattice-invariant shears) is not more than the barrier to the phase change itself, martenstic transformation becomes irreversible.

### 2.2.1 Weak versus Reconstructive Martensitic Transformation

When cooling a shape memory alloy like Nitinol from high temperature, the transformation produces a microstructure with a (twinned) plate-like morphology. This microstructure can easily be changed by the application of loads. The transformation can be completely reversed, with the disappearance of the microstructure upon reheating and the appearance of little or no dislocation or twinning in the parent (high temperature, high symmetry) phase. In contrast, the martensitic transformation is not reversible in materials like steel and other alloys, such as CoNi [2]. Materials that undergo irreversible transformations are characterized by significant dislocations and twinning in the parent phase. An explanation for this difference in reversibility on the basis of the symmetry change during the transformation has been provided [6]. 'Weak' martensitic transformations has been labeled as in which the symmetry group of both the parent and product phase are included in a common finite symmetry group [6,64] (which includes symmetry breaking), and all other martensitic transformations as 'reconstructive' [65]. It has been shown that irreversibility is inevitable in a reconstructive phase transformation, but not in a weak one [6]. Fig. 2.5 illustrates the main idea through a square-to-hexagonal reconstructive phase change in a two-

dimensional crystal [6]. Consider the square lattice shown on the left, and suppose the solid square unit cell is transformed to the solid unit cell of the hexagonal lattice (middle). By symmetry the solid and dashed unit cells shown in the middle are equivalent. If the crystal is transformed back to the square phase, the dashed hexagonal cell can go to, say, the dashed cell on the right. Crucially, the square cell on the left is then transformed to the sheared cell of the square lattice on the right. Thus, upon transforming, performing a symmetry operation, and transforming back, the crystal has undergone a lattice-invariant shear, that is, a shearing deformation that leaves the entire lattice invariant.

### 2.2.2 Ordering and Reversibility

The results of analysis of Bhattacharya et al [6] which was presented above are related to those explained by Otsuka and Shimizu [67] who discuss the effects of ordering on crystallographic reversibility of martensitic transformation in alloys. They observe that in ordered alloys the transformation path must be such that the order is not destroyed, whereas in disordered ones only the atomic positions need to be recovered. Their results are consistent with many experiments, but they also note that the f.c.c.-to-face-centred tetragonal (fct) transformation is an 'exception', which, they argue, is a consequence of the fact that "the lattice correspondence is unique in the reverse transformation because of the so simple lattice change and lower symmetry of the f.c.t. phase". Battachrya has proposed that the essential difference resides in the crystal symmetry, rather than in order and disorder [6].

### 2.2.3 Volume Change and Reversibility

The common explanation [68] for the irreversibility in Fe (or low Ni or C steels) is based on the volume change that accompanies the transformation. The idea is that a partially transformed region causes stress and plastic deformation. The crystal symmetry explanation is independent of such a volume effect. It is possible, however, that both mechanisms (crystal symmetry and volume change) contribute to the irreversibility in Fe. Battacharya argues that the barrier to lattice-invariant shears in

reconstructive transformations is as high as to the phase transition itself. A remarkable implication is that reconstructive transformations are accompanied by plastic deformation through dislocations and twinning in the parent phase, making this phase

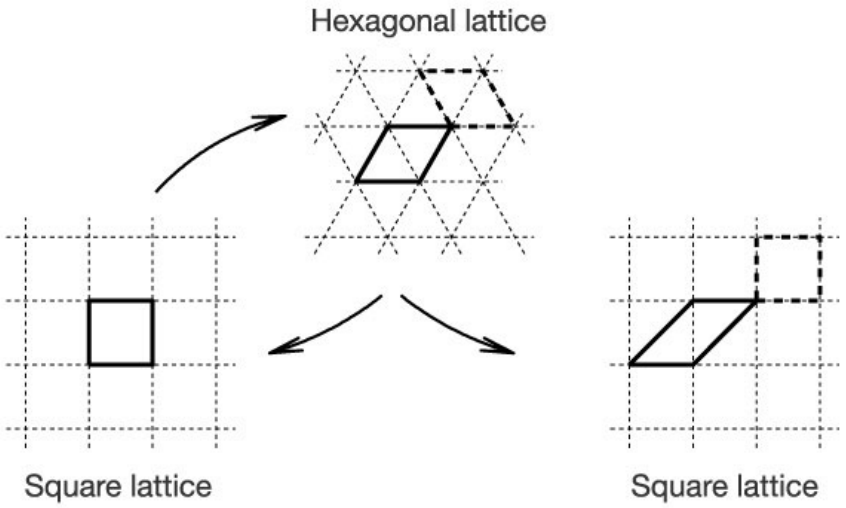


Figure 2.5: A lattice-invariant shear can be generated by a forward and reverse square-to-hexagonal phase transformation [6].The transformation takes the solid square on the left to the solid rhombus in the middle. The hexagonal symmetry implies the equivalence of the solid rhombic cell to the dashed rhombic one. The reverse transformation takes the latter to the dashed square on the right. In the process, the original solid square on the left has sheared by a lattice-invariant shear to the solid parallelogram on the right.

changes irreversible. In contrast, weak transformations have the potential to be reversible, because the energy barriers to lattice-invariant shears and to the phase transition are independent of each other. This, for example, is the case in NiTi, where plastic deformation masks the reversibility. In summary, a transformation must be weak to be reversible [6].

### 2.2.4 Transformation Hysteresis

The subject of hysteresis in shape memory alloys is a very broad subject, with important technological consequences in the design and operation of these materials. A complete overview of the subject should cover many different aspects [69]. At first

it is appropriate to just look at the features essential to hysteresis in SMA and disregard the factors that differentiate systems from each other.

A hysteresis loop is formed when temperature of the sample is changed in a cyclic way through the martensitic transformation. Fig. 2.6 shows a set of typical cycles measured on CuAlNi single crystals (left) and polycrystals (right)[70,71]. In single crystals the single interface transformations (A) take place at two constant temperatures whose difference characterizes the energy dissipation. The multiple-interface transformations (b), on the contrary, extend in temperature range, indicative of build-up and partial storage of elastic strain energy, with dissipation comparable to the previous case. In polycrystals of various grain sizes, (0.5 mm C), 1.5 mm (D), 4.0 mm E, the transformation takes places via multiple interfaces. The behavior is then comparable to (B), except that the extension in temperature is much larger due to the misorietation between grains and the associated build-up of strain energy. This is demonstrated by transformations in a single crystal spark-cut from a coarse-grained polycrystal, shown in (F), which behave very similarly to (B).

The evolution of the energy dissipation as the transformation proceeds can be derived from the area enclosed by partial cycles [72]. This kind of experiments show that energy dissipated increases monotonously with the volume fraction of martensite.

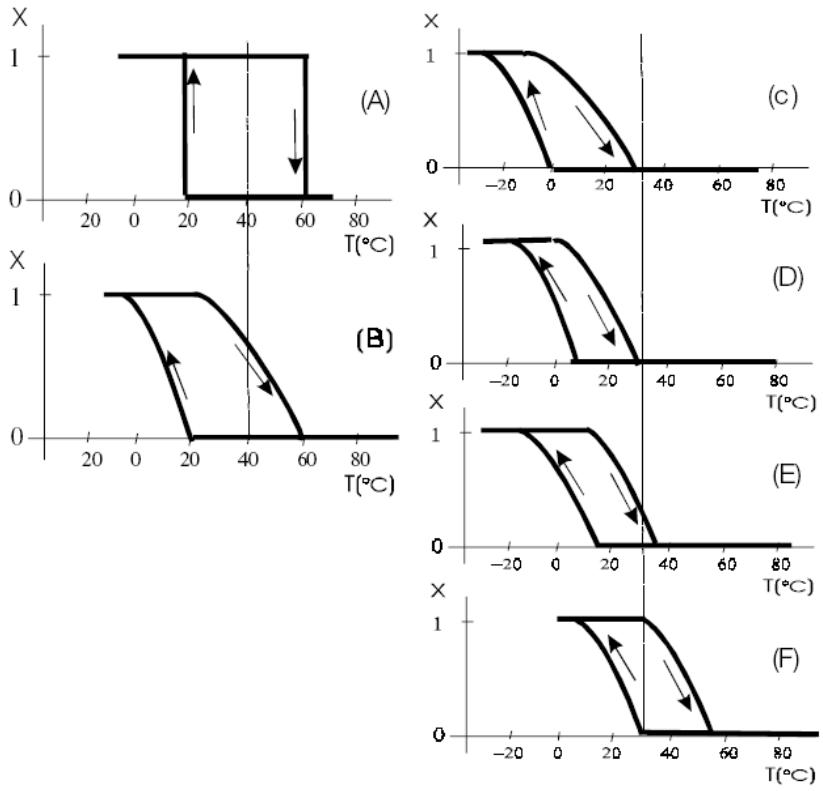


Figure 2.6: Hysteresis cycles in thermally induced transformations of a Cu-14Al-2.5Ni (wt%) alloy [69]. X- denotes parameters such as stored elastic energy.

The amount of energy dissipated in thermally induced transformations is always small compared to the latent heat of transformation. Table 2.1 gives an estimate of the order of magnitude of these contributions in copper-based alloys. It is noticeable from the table that transformation to the hexagonal phase $\gamma_1$', involves larger energy dissipation than to the rombohedrical phase $\beta_1$'.The two following factors can influence the hyteresis in shape memory alloys: 1) thermal or thermomechanical treatments and cycling, 2) alloying and composition. As a result, it is expected that the crystal structure and microstructural features of the alloys are affected. Very little systematic study on the influence of the second factor has been done. It has been shown that alloying elements, precipitates, and stress can change the transformation hsyteresis by enhancing the methods contributing to the energy dissipation in the alloys during transformation [73]. In Section 2.3, the influence of alloying elements on the hsyteresis in NiTi-based shape memory alloys is introduced.

Table 2.2: Estimates of the latent heat and energy dissipated in the thermally induced transformations of copper-based alloys [71].

| Alloy composition (at%) | Cu-27.7Al-2.3Ni | Cu-16.1Zn-15.9Al | Cu-7.2Zn-23.1Al |
|---|---|---|---|
| Type of crystal transformation | Single crystal—multiple interface | Single crystal—multiple interface | Polycrystal |
| | $\beta_1 \leftrightarrow \gamma_1'$ | $\beta_1 \leftrightarrow \beta_1'$ | $\beta_1 \leftrightarrow \gamma_1'$ |
| Latent heat (J/mol) | 526 | 320 | 350 |
| Energy dissipated (J/mol) | 48 | 8 | 29 |

#### 2.2.4.2 Effect of Alloying Element on Transformation Hysteresis

As pointed out previously, the transformation hysteresis in shape memory alloy is of significant importance when the application is of concern. Narrow hsyteresis for actuation applications and wide hysteresis for damping applications are desired. For instance, alloying elements affect the hystersis of NiTi considerably (Table 2.3). The influence of Cu as an alloying element replacing Ni, and Hf replacing Ti is particularly of interest. The former narrows the transformation hysteresis while the latter widens it significantly. The relevant underlying mechanism is presently unknown.

There is a need for systematic studies on the mechanisms by which the influential factors, especially alloying elements and composition affect the transformation hsyteresis.

## 2.3 Shape Memory Alloy Compositions and Transformation Temperatures

A survey of the literature reveals numerous transition-metal shape memory alloy systems with a wide range of martensitic transformation temperatures [11,19-22,25-39,46,47,74-155]. There are many alloy systems with or without magnetic effects. These alloys systems include NiTi, NiMn CuAlNi, AuCd, FeMn, ZrCu, NbRu, TaRu, CoNi, CoAl, $Ni_3Ta$, CuZn, MnCu, TiPt, TiPd, TiNb, ZrNb, $Fe_3Pt$, $Fe_3Ge$, etc. Table 2.2 presents more than 200 alloy compositions that comprise nearly all the transition-metal-based shape memory alloys, together with their transformation temperatures ($M_s$, $A_s$) in ascending order. The Table indicates that the effect of

composition on transformation temperature change is immense. The change of transformation temperatures by chemical composition will be the subject of analysis of the present work.

Table 2.3: Shape memory alloy compositions

| Alloy Composition [at.%] | $M_s$ [C] | $A_s$ [C] | Ref |
|---|---|---|---|
| $Au_{50}Zn_{50}$ | -206 | - | [103] |
| $Fe_{75}Pt_{25}$ | -188 | - | [104] |
| $Ni_{47.25}Mn_{23}Ga_{24.5}Fe_{5.25}$ | -173 | - | [78] |
| $Fe_{60.4}Mn_{8.5}Si_{13}Cr_{10.2}Ni_{7.9}$ ($Fe_{65}Mn_9Si_7Cr_{10}Ni_9$ (wt)) | -168 | -58 | [79] |
| $Fe_{58.6}Mn_{15.4}Si_{9.4}Cr_{12.2}Ni_{4.4}$ ($Fe_{62}Mn_{16}Si_5Cr_{12}Ni_5$ (wt)) | -153 | -53 | [79] |
| $Ni_{52}Mn_6Fe_{15}Ga_{27}$ | -153 | -153 | [105] |
| $Fe_{58.7}Mn_{19.2}Si_{9.4}Cr_{8.1}Ni_{4.6}$ ($Fe_{62}Mn_{20}Si_5Cr_8Ni_5$ (wt)) | -133 | -33 | [79] |
| $Ni_{51}Fe_{22}Ga_{27}$ | -132 | - | [106] |
| $Co_{38.5}Ni_{32.5}Al_{29}$ | -131 | -113 | [107] |
| $Ni_{49.6}Mn_{27.7}Ga_{20.6}Si_{2.1}$ | -128 | -111 | [84] |
| $Ni_{52}Mn_{16}Fe_5Ga_{27}$ | -123 | -98 | [105] |
| $Ni_{49.5}Mn_{23}Ga_{24.5}Fe_3$ | -108 | - | [78] |
| $Ni_{43}Ti_{50}Co_7$ | -100 | - | [11] |
| $Ni_{44}Ti_{50}Fe_6$ | -100 | - | [27] |
| $Ni_{47}Ti_{50}Fe_3$ | -98 | - | [11] |
| $Ni_{48.5}Ti_{50}Cr_{1.5}$ | -95 | - | [11] |
| $Ni_{48}Ti_{50}Mn_2$ | -95 | - | [11] |
| $Ni_{51.7}Mn_{28.5}Ga_{15.6}In_{4.2}$ | -95 | -73 | [84] |
| $Cu_{54.74}Al_{29.75}Zn_{15.51}$ ($Cu_{72.3}Al_{6.66}Zn_{21.04}$(wt)) | -94 | -108 | [108] |
| $Ti_{72}Nb_{28}$ | -93 | - | [74] |
| $Co_{38}Ni_{33}Al_{29}$ | -91 | -73 | [108] |
| $Ni_{47.5}Ti_{50}Fe_2Mo_{0.5}$ | -90 | 5 | [33] |
| $Fe_{49.8}Ni_{28.11}Co_{17.35}Ti_{4.74}$ ($Fe_{50}Ni_{33}Co_{12}Ti_5$ (wt)) | -90 | 10 | [109] |
| $Ni_{50}Mn_{35}Sb_{15}$ | -88 | -128 | [110] |
| $Ni_{42}Co_2Mn_{45}Sn_{11}$ | -81 | -84 | [111] |

| | | | |
|---|---|---|---|
| $Ni_{45}Ti_{50}V_5$ | -80 | - | [11] |
| $Ni_{43}Mn_{46}Sn_{11}$ | -73 | -78 | [112] |
| $Fe_{70}Pd_{24}Pt_6$ | -73 | -78 | [113] |
| $Ni_{50}Mn_{25}Ga_{25}$ | -71 | - | [80] |
| $Ni_{52}Mn_{11}Fe_5Co_5Ga_{27}$ | -68 | 27 | [105] |
| $Ni_{40}Mn_{30}Ga_{20}Fe_{10}$ | -67 | -82 | [115] |
| $Co_{37}Ni_{34}Al_{29}$ | -58 | -43 | [107] |
| $Co_{41}Ni_{32}Al_{27}$ | -54 | -85 | [114] |
| $Pd_{29.5}Fe_{64.25}Co_{6.25}$ | -53 | - | [116] |
| $Ni_{43}Co_1Mn_{45}Sn_{11}$ | -53 | -52 | [111] |
| $Fe_{65.9}Mn_{12.9}Si_{4.5}Ni_{6.7}Cr_{9.5}Nb_{0.5}$ | -50 | 83 | [117] |
| $Fe_{71.4}Mn_{12.5}Ni_{6.2}Cr_{9.4}Ti_{0.5}$ | -50 | 69 | [117] |
| $Ni_{46}Ti_{50}V_4$ | -50 | - | [11] |
| $Ni_{47.6}Ti_{46.4}Nb_6$ | -50 | -29 | [28] |
| $Ni_{49}Mn_{23.5}Ga_{27.5}$ | -46 | - | [81] |
| $Ni_{50}Mn_{36}Sb_{14}$ | -38 | -58 | [118] |
| $Ni_{50}Ti_{48}W_2$ | -37 | -26 | [30] |
| $Ni_{42.5}Ti_{42.5}Cu_{15}$ | -34 | -30 | [12] |
| $Cu_{68.0}Al_{28.2}Ni_{3.8}$ ($Cu_{81.7}Al_{14.1}Ni_{4.2}$ (wt)) | -33 | - | [116] |
| $Ni_{51}Mn_{23}Ga_{24.5}Fe_{1.5}$ | -33 | - | [79] |
| $Ti_{72}Nb_{22}Ta_6$ | -33 | - | [75] |
| $Ni_{41.75}Mn_{44.65}Sn_{10.65}B_{2.95}$ | -31 | -33 | [112] |
| $Ni_{46}Ti_{50}Cu_3Mo_1$ | -30 | - | [35] |
| $Pd_{56.8}In_{25.4}Fe_{17.8}$ | -29 | -21 | [120] |
| $Ni_{50}Ti_{49}W_1$ | -28 | -12 | [30] |
| $Cu_{70.6}Al_{25.3}Mn_{4.1}$ | -25 | -18 | [121] |
| $Fe_{62.40}Mn_{12.76}Si_{9.50}Cr_{8.84}Ni_{6.37}C_{0.13}$ ($Fe_{65.92}Mn_{13.25}Si_{5.05}Cr_{8.70}Ni_{7.05}C_{0.03}$ (wt)) | -22 | 113 | [117] |
| $Fe_{70}Pd_{28}Pt_2$ | -20 | -24 | [113] |
| $Ni_{48.3}Ti_{51}Mo_{0.7}$ | -13 | 20 | [29] |
| $Co_{39}Ni_{33}Al_{28}$ | -5 | 17 | [107] |
| $Ni_{50}Mn_{29}Ga_{21}$ | -5.3 | -4.4 | [122] |

| | | | |
|---|---|---|---|
| $Ti_{74}Nb_{26}$ | 0 | - | [76] |
| $Ni_{40..95}Mn_{43.81}Sn_{10.47}B_{4.77}$ | 2 | -1 | [112] |
| $Cu_{70.9}Al_{20.4}Mn_{8.7}$ | 3 | 7 | [121] |
| $Pd_{29.43}Fe_{68.55}Co_{2.02}$ | 3 | - | [116] |
| $Ni_{54}Fe_{19}Ga_{27}$ | 3 | 7 | [123] |
| $Pd_{29.23}Fe_{66.67}Co_{4.10}$ | 6 | - | [81] |
| $Ni_{49}Ti_{50}Mo_{1}$ | 10 | 20 | [29] |
| $Ni_{52}Mn_{24.5}Ga_{23.5}$ | 12 | 16 | [124] |
| $Cu_{69}Al_{27.5}Ni_{3.5}$ | 15 | 40 | [125] |
| $Fe_{70}Pd_{30}$ | 15 | 14 | [113] |
| $Ni_{50}Mn_{37}Sb_{13}$ | 17 | 2 | [118] |
| $Ni_{52}Mn_{1}Fe_{15}Co_{5}Ga_{27}$ | 17 | 297 | [105] |
| $Fe_{70}Pd_{30}$ | 17 | 14 | [126] |
| $Au_{43.3}Cu_{31.8}Al_{24.9}$ | 17 | 70 | **[127]** |
| $Fe_{70.1}Pd_{29.9}$ | 18 | 6 | [128] |
| $Ni_{50}Mn_{28}Ga_{22}$ | 18 | 19 | [129] |
| $Co_{66.66}Ni_{28.34}Ga_{5}$ | 20 | - | [130] |
| $Co_{41}Ni_{32}Al_{24}Sb_{3}$ | 20 | 24 | [114] |
| $Ni_{45}Ti_{50}Pd_{5}$ | 20 | - | [11] |
| $Fe_{72.6}Mn_{25.6}Mo_{1.8}$ ($Fe_{72}Mn_{25}Mo_{3}$ (wt)) | 21 | - | [131] |
| $Fe_{58.92}Mn_{14.59}Si_{12.99}Cr_{9.09}Ni_{4.41}$ ($Fe_{63.43}Mn_{15.45}Si_{7.03}Cr_{9.11}Ni_{4.98}$ (wt)) | 24 | 112 | [82] |
| $Ni_{50.4}Mn_{28.8}Ga_{19.8}Si_{1}$ | 25 | -3 | [121] |
| $Ni_{39.5}Ti_{49.5}Cu_{10}Cr_{1}$ | 25 | 30 | [38] |
| $Ni_{49}Fe_{18}Ga_{27}Co_{6}$ | 27 | - | [132] |
| $Au_{43.75}Cu_{31.25}Al_{25}$ | 27 | - | **[133]** |
| $(Co_{45}Ni_{25}Ga_{30})_{0.95}Ta_{5}$ | 27 | 37 | [83] |
| $Fe_{59.85}Mn_{13.99}Si_{12.98}Cr_{8.90}Ni_{4.28}$ ($Fe_{64.44}Mn_{14.82}Si_{7.03}Cr_{8.87}Ni_{4.84}$ (wt)) | 28 | 97 | [82]] |
| $Au_{50.5}Cd_{49.5}$ | 31 | - | **[134]** |
| $Ni_{49.7}Mn_{28.7}Ga_{21.6}$ | 32 | 38 | [84] |
| $Fe_{80}Mn_{20}$ | 33 | 154 | [87] |
| $Cu_{73.7}Sn_{26.3}$ ($Cu_{60}Sn_{40}$ (wt)) | 37 | - | [135] |

| | | | |
|---|---|---|---|
| $Fe_{58.2}Mn_{30.6}Si_{11.2}$ ($Fe_{62}Mn_{32}Si_6$ (wt)) | 37 | - | [79] |
| $Ni_{52}Ti_{46.74}Re_{1.26}$ | 37 | 87 | [31] |
| $Ni_{50.5}Mn_{28.2}Ga_{21.3}$ | 38 | 41 | [84] |
| $Ni_{45}Co_5Mn_{36.7}In_{13.3}$ | 39 | 37 | [136] |
| $Ni_{47.9}Mn_{26.1}Ga_{26}$ | 39 | 52 | [84] |
| $Co_{60.7}Ni_{29.9}Si_{9.4}$ ($Co_{63.9}Ni_{31.4}Si_{4.7}$ (wt)) | 39.6 | 264.8 | [137] |
| $Ni_{50}Mn_{38}Sb_{12}$ | 42 | 17 | [118] |
| $Ni_{50}Ti_{45}Ta_5$ | 44 | 76 | [22] |
| $Ni_{50}Mn_{34}In_{16}$ | 47 | - | [120] |
| $Pd_{57}In_{25}Fe_{18}$ | 50 | - | **[120]** |
| $Fe_{61.96}Mn_{30.47}Co_{7.57}$ ($Fe_{62}Mn_{30}Co_8$ (wt)) | 52 | 162 | [139] |
| $Fe_{73}Mn_{24.52}Ge_{2.48}$ ($Fe_{72}Mn_{24}Ge_4$ (wt)) | 52 | - | [140] |
| $Ti_{32}Hf_{18}Ni_{49.8}Re_{0.2}$ | 52 | 101.5 | [85] |
| $Ni_{55}Fe_{18}Ga_{27}$ | 54 | 27 | [123] |
| $Ni_{48}Ti_{50}W_2$ | 55 | 70 | [30] |
| $Ni_{52}Fe_{18}Ga_{27}Co_3$ | 58 | - | [132] |
| $Ni_{50}Ti_{47}Ta_3$ | 58 | 90 | [22] |
| $Ni_{30}Ti_{50}Cu_{20}$ | 58 | 60 | [36] |
| $Co_{50}Ni_{23.5}Ga_{26.5}$ | 60 | - | [130] |
| $Ni_{50}Mn_{28}Ga_{21}Y_1$ | 60 | 62 | [129] |
| $Ni_{50}Ti_{50}$ | 60 | 80 | [11] |
| $Ni_{25}Ti_{50}Cu_{25}$ | 61 | 62 | [86] |
| $Ni_{42}Ti_{49}Ag_9$ | 61 | 20 | [25] |
| $Ni_{50}Mn_{30}Ga_{15}Al_5$ | 62 | -1 | [115] |
| $Ni_{44}Ti_{49}Ag_7$ | 63 | 23 | [25] |
| $Co_{50}Ni_{22}Ga_{28}$ | 64 | - | [141] |
| $Fe_{85}Mn_{15}$ | 67 | 197 | [87] |
| $Cu_{67.71}Zn_{19.45}Al_{12.84}$ (($Cu_{72.65}Zn_{21.5}Al_{5.85}$ (wt)) | 69 | 70 | [142] |
| $Ni_{50}Mn_{29}Ga_{20}Gd_1$ | 70 | 78 | [122] |
| $Ni_{49.5}Ti_{45.5}Zr_5$ | 70 | 110 | [19] |
| $Ni_{44}Ti_{40}Hf_{10}Cu_6$ | 72 | 90 | [32] |
| $Ni_{48}Ti_{50}Au_2$ | 75 | - | [21] |

| | | | |
|---|---|---|---|
| $Ni_{50}Mn_{29}Ga_{20}Dy_1$ | 75.9 | 76.3 | [122] |
| $Cu_{68.5}Zn_{18.8}Al_{12.7}$ | 76 | - | [142] |
| $Co_{50}Ni_{22}Ga_{27}Al_1$ | 77 | - | [141] |
| $Co_{45}Ni_{25}Ga_{30}$ | 77 | 105 | [83] |
| $Ni_{51.4}Mn_{27.2}Ga_{21.4}$ | 78 | 80 | [31] |
| $Mn_{85}Cu_{15}$ | 80 | - | [144] |
| $Pt_{10}Ni_{40}Mn_{25}Ga_{25}$ | 82 | 77 | [145] |
| $Cu_{68.3}Zn_{20.4}Al_{11.3}$ | 85 | - | [143] |
| $Ni_{29}Ti_{51}Pd_{20}$ | 85 | - | [39] |
| $Ni_{51.3}Mn_{14.4}Ga_{26.3}Fe_8$ | 86 | 88 | [84] |
| $Ni_{40}Mn_{30}Ga_{20}Co_{10}$ | 88 | 91 | [115] |
| $Ni_{49.5}Ti_{40.5}Zr_{10}$ | 90 | 170 | [32] |
| $Ni_{30}Ti_{50}Pd_{20}$ | 90 | - | [11] |
| $Ni_{40}Ti_{50}Pt_{10}$ | 90 | 100 | [46] |
| $Ni_{26.5}Ti_{51}Pd_{22.5}$ | 95 | - | [39] |
| $Fe_{69.9}Mn_{25.37}Co_{4.73}$ ($Fe_{70}Mn_{25}Co_5$ (wt)) | 97 | 177 | [139] |
| $Fe_{67}Mn_{25.41}Co_{7.59}$ ($Fe_{67}Mn_{25}Co_8$(wt)) | 100 | 175 | [139] |
| $Cu_{58.51}Al_{32.43}Zn_{9.06}$ ($Cu_{78.9}Al_{8.54}Zn_{12.56}$ (wt)) | 102 | 48 | [108] |
| $N_{50}Mn_{29}Ga_{19}Gd_2$ | 105 | 115 | [126] |
| $Ni_{54}Mn_{23}Ga_{23}$ | 110 | 115 | [146] |
| $Zr_{48}Cu_{50}Ti_2$ | 110 | | [88] |
| $Co_{86}Al_{14}$ | 112 | 236 | [141] |
| $Co_{50}Ni_{22}Ga_{26}Al_2$ | 115 | - | [141] |
| $Ni_{50}Ti_{40}Hf_{10}$ | 120 | 165 | [32] |
| $Ni_{50}Mn_{29}Ga_{19}Dy_2$ | 126.2 | 123.7 | [122] |
| $Ti_{50}Pd_{43.5}Cr_{6.5}$ | 127 | - | [89] |
| $Ni_{50}Mn_{28}Ga_{19}Y_3$ | 130 | 132 | [129] |
| $Ti_{78}Nb_{22}$ | 137 | - | [75] |
| $Zr_{50}Cu_{50}$ | 140 | 230 | [90] |
| $Ni_{40}Ti_{50}Hf_{10}$ | 140 | 185 | **[10]** |
| $Co_{50}Ni_{22}Ga_{23}Al_5$ | 150 | - | [141] |
| $Zr_{50}Cu_{50}$ | 150 | | [88] |

| | | | |
|---|---|---|---|
| $Ni_{55.6}Mn_{11.4}Fe_{7.4}Ga_{25.6}$ | 166 | 180 | [147] |
| $Co_{35}Ni_{40}Al_{25}$ | 167 | - | [148] |
| $Ni_{55}Mn_{22.5}Ga_{22.5}$ | 175 | 200 | [146] |
| $Ni_{48.75}Mn_{35.5}Ga_{15.75}$ | 175.1 | 178.7 | [149] |
| $Ni_{50}Mn_{40}In_{10}$ | 177 | - | [138] |
| $Zr_{42.3}Cu_{29.9}Ni_{11}Co_{10.2}Ti_{6.6}$ | 177 | 137 | [91] |
| $Mn_{85.5}Fe_{9.5}Cu_5$ | 182 | 180 | [92] |
| $Ni_{49.5}Ti_{35.5}Zr_{15}$ | 190 | 235 | [19] |
| $Ni_{49.5}Ti_{35.5}Hf_{7.5}Zr_{7.5}$ | 195 | 230 | [37] |
| $Ti_{50}Rh_{40}Ni_{10}$ | 210 | - | [93] |
| $Ti_{80}Nb_{20}$ | 217 | - | [74] |
| $Ni_{50}Mn_{29}Ga_{18.8}Co_{2.2}$ | 223 | 224 | [31] |
| $Ni_{15}Ti_{50}Pd_{35}$ | 225 | - | [39] |
| $Ni_{36}Ti_{49}Hf_{15}$ | 230 | - | [11] |
| $Ni_{35}Ti_{50}Hf_{15}$ | 235 | 256 | **[10]** |
| $Ni_{75}Ta_{25}$ | 250 | - | [150] |
| $Zr_{49.6}Cu_{28.2}Ni_{6.8}Co_{15.4}$ | 253 | 212 | [91] |
| $Cu_{72.12}Al_{26.45}Pd_{1.43}$ ($Cu_{84.13}Al_{13.08}Pd_{2.79}$ (wt)) | 262.8 | 262.8 | [151] |
| $Cu_{79.23}Al_{20.77}$ ($Cu_{90}Al_{10}$ (wt)) | 265 | - | [152] |
| $Ni_{30}Ti_{50}Pt_{20}$ | 266 | 271 | [46,47] |
| $Ti_{80}Nb_{18.40}Pd_{1.60}$ | 288 | 405 | [77] |
| $Ni_{49.5}Ti_{30.5}Hf_{10}Zr_{10}$ | 290 | 315 | [38] |
| $Ni_{50}Ti_{30}Hf_{20}$ | 290 | 317 | **[10]** |
| $Zr_{50}Cu_{40}Ni_{10}$ | 300 | - | [88] |
| $Ti_{50}Rh_{45}Ni_5$ | 300 | 100 | [93] |
| $Ti_{50}Rh_{46}Co_4$ | 300 | 150 | [93] |
| $Ti_{67}Nb_{30}Pd_3$ | 300 | - | [77] |
| $Ni_{50.7}Mn_{34.6}Ga_{14.7}$ | 311 | 319 | [153] |
| $Ti_{50}Rh_{50}$ | 345 | 140 | [94] |
| $Ni_{50}Mn_{40}Ga_{10}$ | 347 | - | [154] |
| $Cu_{73.1}Al_{21.5}Ag_{5.4}$ ($Cu_{80}Al_{10}Ag_{10}$(wt)) | 350 | - | [152] |
| $Ni_{31}Ti_{49}Hf_{20}$ | 350 | - | [11] |

| | | | |
|---|---|---|---|
| $Ti_{43.33}Pd_{50}Hf_{6.67}$ | 360 | - | [89] |
| $Ni_{50}Mn_{37.5}Al_{12.5}$ | 390 | - | [154] |
| $Ni_{25}Ti_{50}Pt_{25}$ | 430 | 450 | [39] |
| $Ni_{50}Mn_{45}Sn_{5}$ | 437 | - | [154] |
| $Zr_{50}Rh_{50}$ | 480 | 570 | [95] |
| $Ni_{49.6}Mn_{45.5}In_{4.9}$ | 487 | 509 | [155] |
| $Zr_{50.59}Cu_{29.56}Ni_{19.85}$ | 497 | 597 | [91] |
| $Ti_{50}Pd_{50}$ | 537 | 577 | [96] |
| $Ti_{50}Pd_{50}$ | 544.7 | 574 | [97] |
| $Ni_{20}Ti_{50}Pt_{30}$ | 560 | 594 | [47] |
| $Ni_{50}Mn_{50}$ | 627 | - | [155] |
| $Ru_{43}Nb_{50}Fe_{7}$ | 650 | - | [98] |
| $Ni_{15}Ti_{50}Pt_{35}$ | 680 | 750 | [46] |
| $Zr_{50}Ir_{50}$ | 740 | 880 | [94] |
| $Nb_{50}Ru_{36}Fe_{14}$ | 795 | 797 | [98] |
| $Ni_{10}Ti_{50}Pt_{40}$ | 810 | 850 | [46] |
| $Nb_{50}Ru_{43}Fe_{7}$ | 841 | 830 | [98] |
| $Ru_{50}Nb_{50}$ | 865 | - | [99] |
| $Nb_{50}Ru_{50}$ | 887 | 890 | [98] |
| $Ni_{5}Ti_{50}Pt_{45}$ | 900 | 950 | [47] |
| $Ti_{50}Pt_{50}$ | 1020 | 1040 | [100] |
| $Ru_{50}Ta_{50}$ | 1050 | 1030 | [99,101] |
| $Ru_{46}Ta_{54}$ | 1100 | 1150 | [102] |

The alloy compositions in parentheses () are the weight percent formula of the alloys as presented in the original references.

## 2.4 NiTi-Based Shape Memoy Alloys

### 2.4.1 NiTi Intermetallics

Although several different types of materials have shown shape memory properties, the most readily available and commercially used SMAs are NiTi-based alloys. The phase diagram associated with a binary NiTi system can be seen in Figure

2.7 [156]. From the phase diagram, it is clear that small changes in the composition of near-equiatomic NiTi can lead to the formation of additional phases such as $NiTi_2$ and $Ni_3Ti$ which consequently do not exhibit shape memory behavior [157-159]. Exposure to elevated temperatures for a sufficiently long time results in the formation of a $TiNi_3$ phase which precipitates through a diffusion-based process. However, most heat treatment processes after manufacturing are done at temperatures below those mapped by the phase diagram resulting in the formation of metastable phases.

It has also been shown that prior to the formation of the $TiNi_3$ phase, metastable $Ti_3Ni_4$ precipitates can form from a solid solution of Ni in NiTi at moderate aging temperatures (300˚C to 600˚C) [158-160]. The influence of composition must be considered in looking at the overall macroscopic behavior of NiTi SMAs.

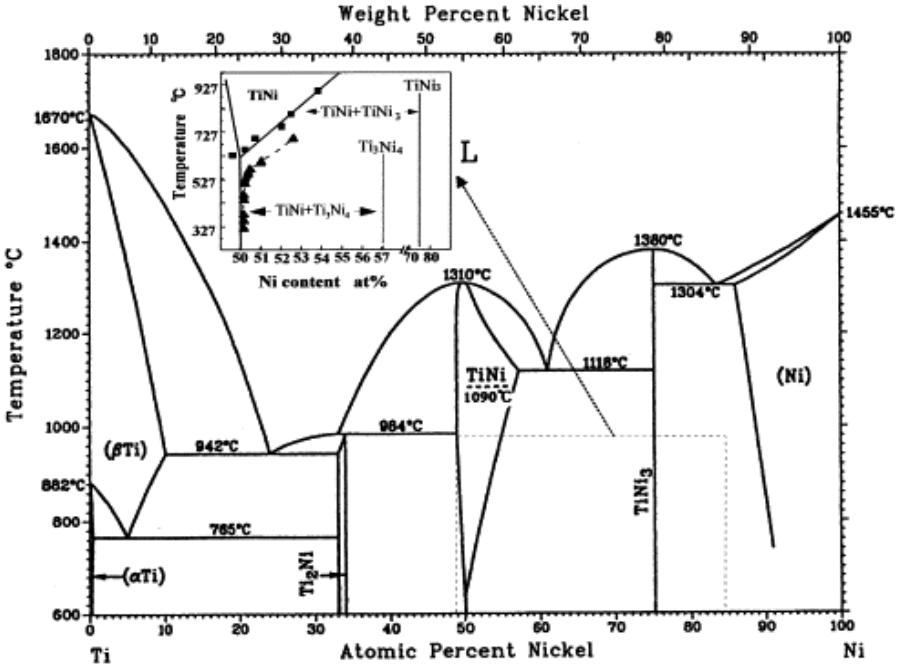


Figure 2.7: Phase diagram of binary NiTi systems [156]

## 2.4.2 Crystal Structure of Austenite and Martensite

The parent phase of all NiTi and NiTi-based alloys has a cubic B2 (ordered BCC) structure as shown as shaded cubic in Fig. 2.9a [161]. The stable martensite

structures are usually of B19 Orthorohbic (*Pmma,* and *Pmmb*) symmetry (Fig. 2.9b), or B19' monoclinic ($P2_1/m$) structure (Fig. 2.8c) which is sometimes considered stress-stabilized [161].

## 2.4.3 Phase Stability, Martensitic Transformation and Transformation Temperatures

### 2.4.3.1 Transformation Rroutes of NiTi-Based Alloys and Structure Relationship

Depending on composition, thermomechanical treatment, the B2 phase may take one of three transformation paths shown in Fig. 2.10 [11], B2–B19′ transformation occurs in quenched NiTi alloys; B2–R–B19′ transformation occurs in aged NiTi (with $Ti_3Ni_4$ precipitation) or cold-worked NiTi, and in ternary Ti–Ni–Fe(Al) alloys; B2–B19–B19′ transformation occurs in NiTiCu alloys [162]. The end product of all martensitic transformations in NiTi-based alloys is B19′ martensite. Therefore, B19′ martensite is considered as the ground state of all NiTi and NiTi-based alloys. Depending upon the composition and heat-treatment only the first transformation may occur, and the second one may be lost, because the possible transformation temperatures for the second one to B19′ become too low in that case. Symmetry analysis of various phases by Barsch [163] shows interesting symmetry relationship between B2 and three different martensites. He showed that except R–B19′ transformation, all other transformations, B2–B19′, B2–R, B2–B19, B19–B19′ follow a group–subgroup relation (i.e., the symmetry group of low-temperature phase is a subgroup of that of the high-temperature phase), as the usual case for shape memory alloys.

The R–B19′ transformation does not follow a group–subgroup relation. B19′ martensite has a space group of $P2_1/m$; it is not a subgroup of R, which has a space group of *P3*. It is schematically shown in Fig. 2.11 [167], which shows the structure relationship among B2 (Fig. 2.11a), B19 (Fig. 2.11b), and B19′ (Fig. 2.10c).

The B19′ martensite can be viewed as a "normal" martensite B19, but being distorted by a monoclinic shear $\{001\}\langle 1\bar{1}0\rangle$ [164]. Recently results from elastic

constant measurement have enabled some understanding of the monoclinicity of the B19′ martensite [10,11,165-166].

A typical example is that NiTi undergoes a direct B2–B19′ transformation; but with the addition of Fe, NiTiFe alloy shows a two-stage transformation B2–R–B19′ [162], as shown in Fig. 2.12. It can be seen that with increasing Fe content, B2–R transformation becomes more and more separated from the R–B19′ transformation (Fig.2.12a) This feature enables a characterization of R-phase over wide temperature range without being interrupted by the second transformation R–B19′.

Another important system is Ti–Ni–Cu. Addition of Cu exceeding 5 at.% can change the transformation route into B2–B19–B19′. B2–B19 transformation is associated with a small transformation hysteresis (about 4 K at 20 at.%Cu) (Fig. 2.12b) [162].

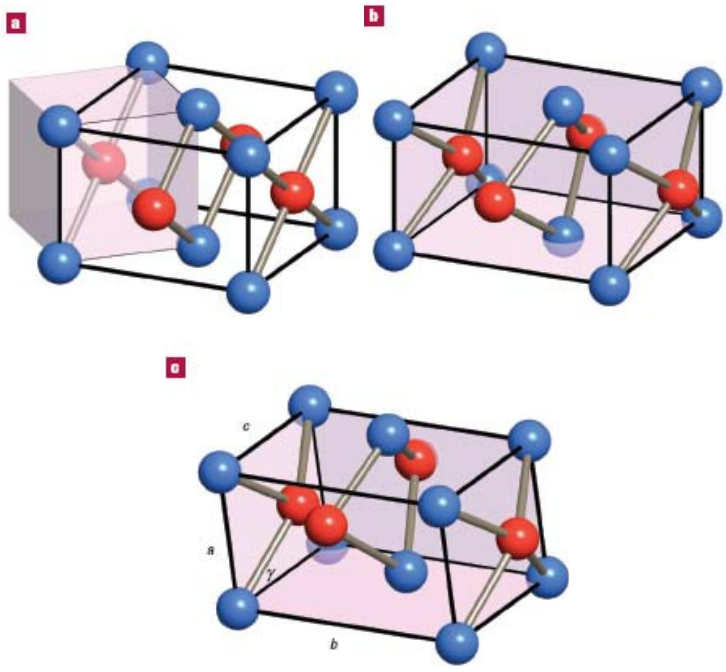


Figure 2.8: Martensitic distortions of the *B*2 crystal structure of NiTi. a,The relation between the cubic *B*2 cell (shaded box) and the undistorted (tetragonal) *B*19 cell.b,The orthorhombic *B*19 structure. **c**,The distortion to the stress-stabilized *B*19′ structure. Ni and Ti atoms are represented by red balls and blue balls, respectively [162].

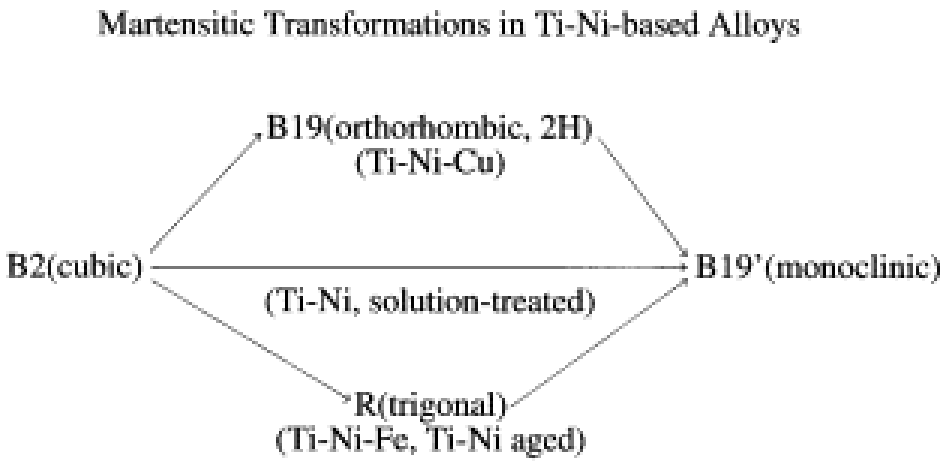


Figure 2.9: Three transformation paths in Ti–Ni-based alloys [11].

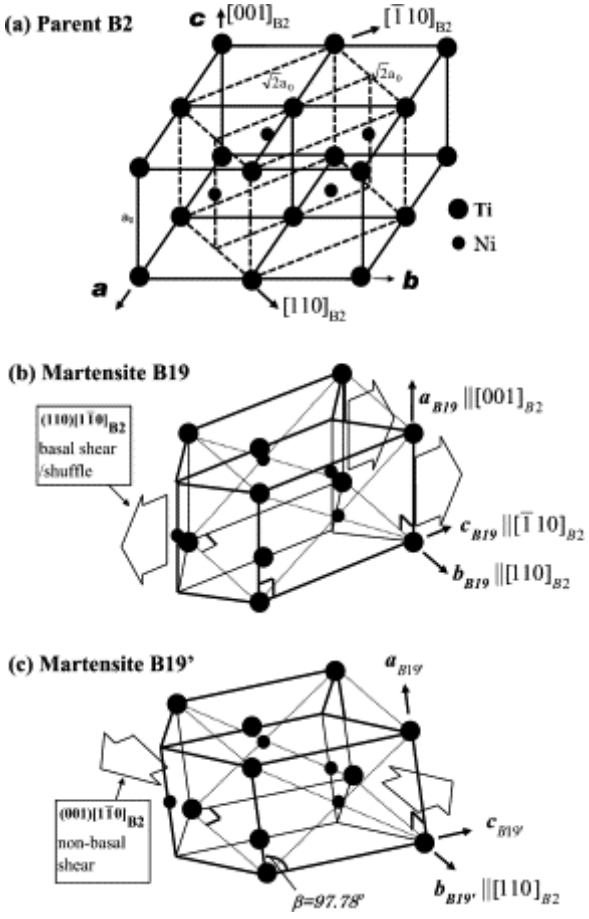


Figure 2.10: Structure relationship among B2 parent phase and two kinds of martensite, B19, and B19′: (a) the parent phase B2 structure with a FCT cell delineated; (b) orthorhombic martensite B19, formed by shear/shuffle of the basal plane $(1\ 1\ 0)_{B2}$ along $[1\ \bar{1}\ 0]$ direction; (c) monoclinic martensite B19′, which is viewed as a B19 structure sheared by a non-basal shear $(0\ 0\ 1)[\bar{1}\ \bar{1}\ 0]_{B2}$[167].

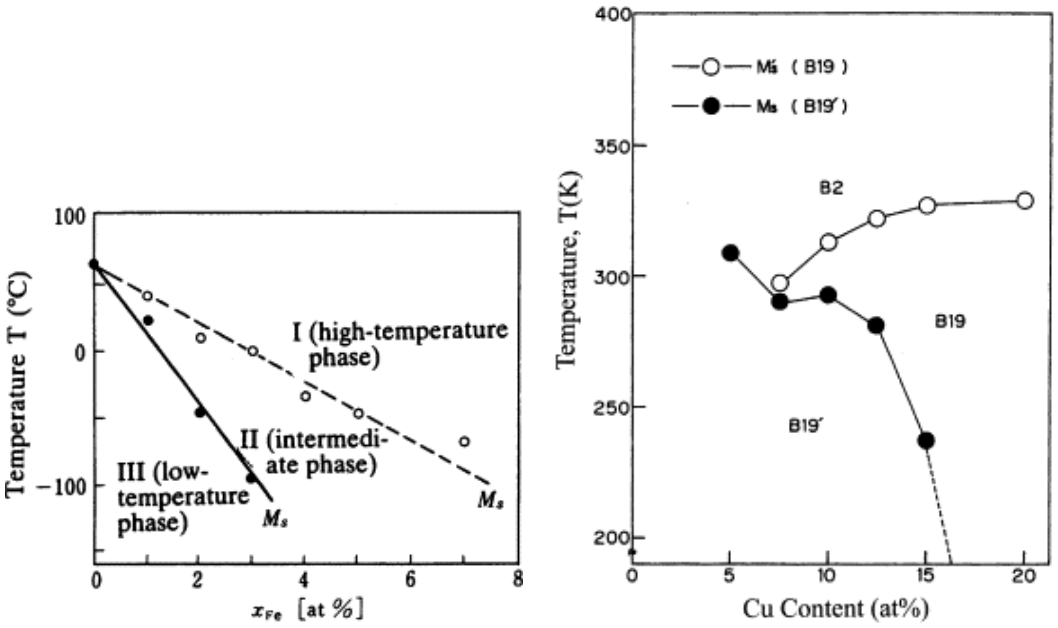


(a) (b)

Figure 2.11:(a) Effect of Fe addition on the martensitic transformation temperature and transformation paths, I, II and III regime represents parent B2 phase, R phase and B19′ martensite [168], respectively (b) Cu-content dependence of transformation temperatures for $Ti_{50}Ni_{50-x}Cu_x$ alloys [162].

### 2.4.3.2 Phase Transformation Sequence: Thermodynamic Approach

It has been show that entropy change during transformation is related to the martensite volume (Eq. 2.2) [11]:

$$\Delta S = -a\,\eta^2_M \qquad (2.2)$$

where $\Delta S$ is the entropy change, $\eta_M$ is the lattice distortion (or transformation strain) at transformation temperature, and a proportionality factor. The minus sign of Eq. 2.2 clearly shows that martensitic transformation always leads to entropy decrease. This equation also leads to an important conclusion: the magnitude of entropy change associated with martensitic transformation is proportional to the square of lattice distortion (or transformation strain), i.e., the larger the transformation strain the larger the entropy change is [11].

In NiTi-based alloys, three possible martensite candidates, R, B19, and B19′, exist. The transformation strain for R-phase is very small (~1%), next is the B19

(~8%), B19′ is the largest (~10%). It is deduced that $|\Delta S_{B19'}| > |\Delta S_{B19}| > |\Delta S_R|$. Since the entropy change means slope change of martensite (including R-phase) relative to that of the parent phase in free energy vs. temperature line, we can deduce that R-phase line makes the smallest angle from the B2 line, next is the B19 line, while B19′ line makes the largest angle, as shown in Fig. 2.12 [11,169] Depending on the relative stability of these three candidates, it is possible to have three situations.

From Fig. 2.12, we can draw an important general conclusion: the necessary condition for an intermediate martensite to appear before the formation of final product is that the intermediate phase must have smaller transformation strain (or smaller entropy change during transformation) than the final product, or in other words, the intermediate martensitic transformation must be more weakly first order transformation than the final transformation.

This important conclusion has been summarized in a simple statement: multi-stage martensitic transformation occurs in the sequence of increasing transformation strain. Considering the relationship between transformation strain and entropy change shown in Equ. 2.2, we can restate this conclusion in an equivalent form: multi-stage transformation occurs in the sequence of increasing transformation entropy.

There is a thermodynamic requirement that intermediate martensite phase must have smaller transformation strain than the final product. However, whether or not the intermediate phase appears or which intermediate phase is realized depends on competition in both intrinsic and extrinsic energies. The intrinsic energy is governed by lattice dynamics (phonon softening and elastic softening), while the extrinsic energies arise from resistance to lattice distortion (i.e., transformation) by precipitates or dislocations.

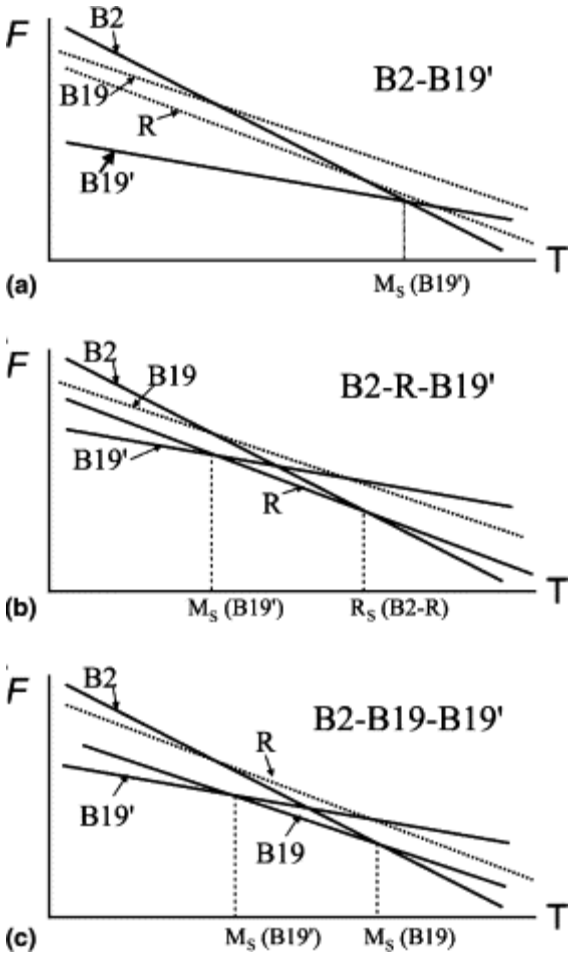


Figure 2.12: Schematic of the three possible transformation paths of NiTi-based alloys in relation to the relative stability of three competing martensite candidates, R, B19 and B19′, with respect to B2 parent phase. (a) B2–B19′ one-stage transformation, (b) B2–R–B19′ two-stage transformation, and (c) B2–B19–B19′ two-stage transformation. The dotted lines indicate martensite(s) that is unstable at any temperature [11,169].

### 2.4.3.3 Phase Transformation Sequence: Elastic Softening

The origin of the unique B19′ martensite can be traced from a remarkable difference in the precursory elastic softening between NiTi and common β-phase alloys. Common β-phase alloys are known to show softening only in elastic constant $c'$ [170-175] with other elastic constants behaving normal. This yields an anisotropy factor $A$ ($=c_{44}/c'$) as large as 10–20, which further increases with lowering temperature. In sharp contrast, NiTi shows softening in both $c'$ and $c_{44}$; this leads to a very low anisotropy ($A \sim 2$), which further decreases with lowering temperature. This difference has been noticed by previous studies [176,177]; but the underlying meaning has not been figured out until very recently [178]. By definition, $c'$ corresponds to the

$\{1\,1\,0\}\langle 1\,\bar{1}\,0\rangle$ shear modulus, which is naturally related to the formation of basal-plane-based martensites. On the other hand, $c_{44}$ is the $0\,0\,1\ \langle 1\,0\,0\rangle$ shear modulus, which seems at first sight to have nothing to do with the B19′ martensite. However, for cubic crystals, $c_{44}$ also equals to the $\{0\,0\,1\}\langle 1\,\bar{1}\,0\rangle$ shear modulus. This $\{0\,0\,1\}\langle 1\,\bar{1}\,0\rangle$ shear is just what is required for the monoclinic distortion to make the B19′ structure, as was shown in Fig. 2.10c. Therefore, the unique monoclinic structure B19′ of NiTi originates from the additional softening in $c_{44}$ besides softening in $c'$. For many years, martensitic transformation has been regarded as solely due to the softening in basal shear/shuffle mode; the discovery of the non-basal mode for B19′ martensite strongly suggests that in some cases non-basal mode may also play an important role in martensitic transformations. Elastic constant measurements have been performed on some NiTi-based alloys in order to verify the above view. Three kinds of NiTi-based alloys were tested, corresponding to three transformation-paths, B2–B19′, B2–B19–B19′, and B2–R–B19′. The results are shown in Fig. 2.13 [169].

A common feature among all NiTi-based alloys: for all the tested alloys can be seen, $c_{44}$ exhibits significant softening besides a softening in $c'$. The softening in $c_{44}$ just corresponds to the fact that all these alloys ultimately transform into B19′ martensite. Therefore, the soft $c_{44}$ is a signature for the ultimate transformation to B19′, although other transformations (R, B19) may intervene before the formation of this final product. The softer the $c_{44}$ the higher is the transformation temperature to B19′.

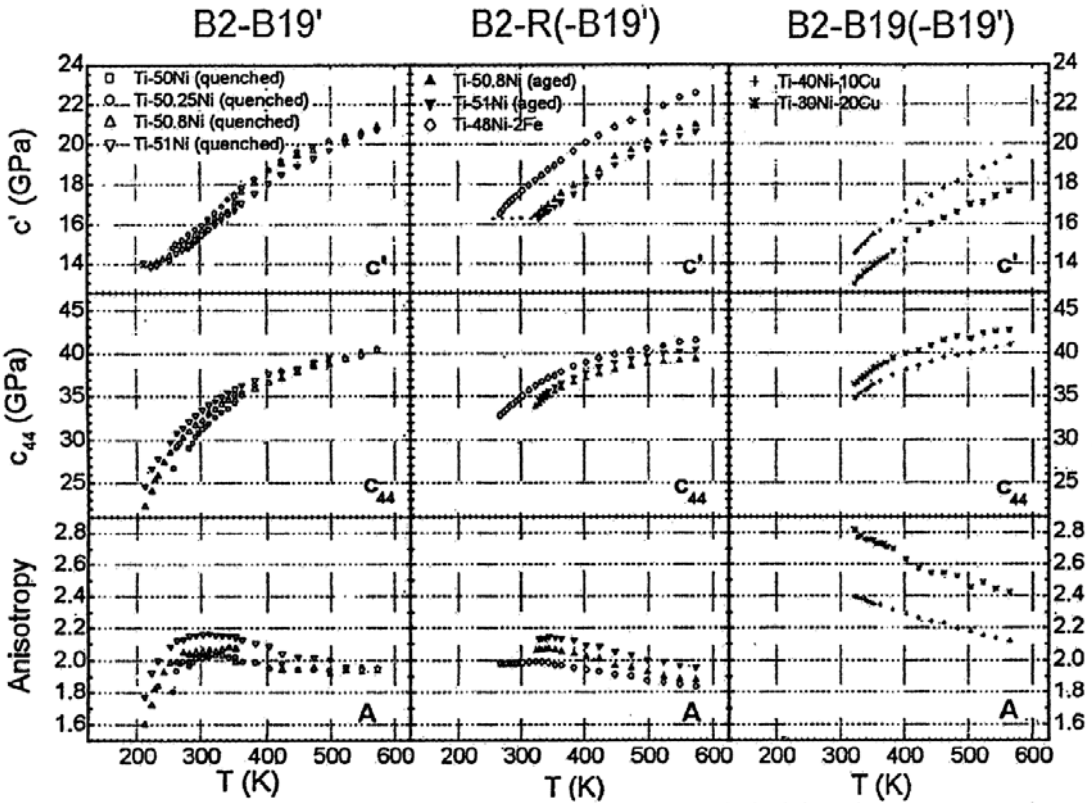


Figure 2.13:Single crystal elastic constants of NiTi binary and NiTiX (X = Fe, Cu) as a function of temperature in B2 phase prior to (a) B2–B19′ transformation, (b) B2–R (–B19′) transformation, and (c) B2–B19 (–B19′) transformation. It is noted that solution-treated and directly quenched binary Ti–Ni undergoes a direct B2–B19′ transformation, but after aging it undergoes a B2–R–B19′ transformation [169].

#### 2.4.3.4 The Influence of composition on the $M_s$ Temperature of NiTi-based alloys

The effect of composition can be related to the effect of Ni content in binary alloys and the effect of alloying elements. Binary NiTi is an intermetallic compound with B2 order although it is not a line-compound with a fixed composition. It shows certain solubility of excess Ni on Ni-rich side but cannot dissolve excess Ti. Ti-rich side is almost vertical but Ni-rich side has some solubility at high temperature (up to about 6 at% at 1000 °C). Quenched NiTi alloys show one-stage B2–B19′ transformation. The transformation temperature is strongly dependent on Ni concentration, as shown in 2.14 [11,178]. On Ti-rich side the transformation temperature is almost composition independent being about 60 °C; this has been attributed to the fact that the solubility limit of NiTi phase on Ti-rich side is almost vertical and thus it is not possible to get Ti-rich NiTi solid solution. So the Ti-rich

alloys show a behavior being the same as NiTi alloy. On Ni-rich side, increasing Ni causes a rapid decrease in transformation temperature. Martensitic transformation temperature almost drops to 0 K for Ni content exceeding 51.5 at.%, but experimental data show a large scattering.

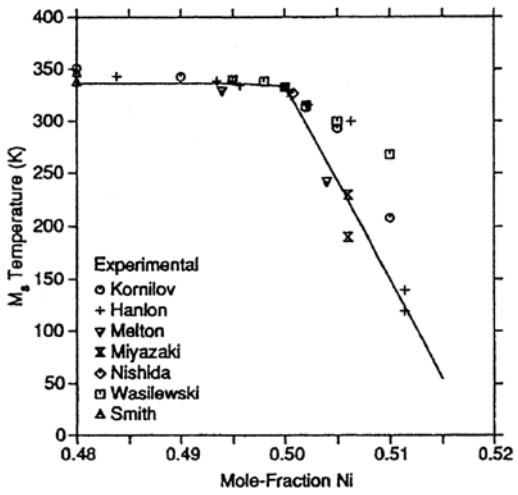


Figure 2.14:$M_s$ temperature as a function of Ni content for binary Ni-Ti alloys. Different data symbols represent data from different authors. The solid line is given by thermodynamic calculations [11,178].

The transformation temperature and hysteresis can be adjusted by introducing ternary elements to satisfy the high or low temperature applications. Addition of various transition metals to NiTi that either elevate or lower the transformation temperatures has been studied, part of which has been reviewed by Otsuka et al [11]. Apart from the selection of alloying elements, their replacement for either Ni or Ti, or both is also of paramount importance. As it is evident from Table 2.3, alloying elements influence the transformation temperatures of NiTi shape memory alloy remarkably. The mechanism by which the alloying elements affect the transformation temperatures is presentably unclear. What is known is the elastic softening of austenite before martensitic transformation with lowering temperature.

Experimental results, mainly in Cu-based and also in NiTi-based shape memory alloys [7-10] suggest that there is a critical value of elastic constant at which transformation takes place which is not sensitive to alloy compositions [4] and is only slightly dependant on temperature [11]. Based on this, the elastic modulus of the alloy, which is dependent on both composition and temperature [11,12] is thought to

influence the transformation temperatures. However, it is not clear how the addition of different alloying elements to NiTi is linked with the elastic properties and therefore the transformation temperatures. The current research focuses mainly on the understanding of this relationship. Therefore, a brief explanation of how the elastic constants can be affected by composition is presented in the following section.

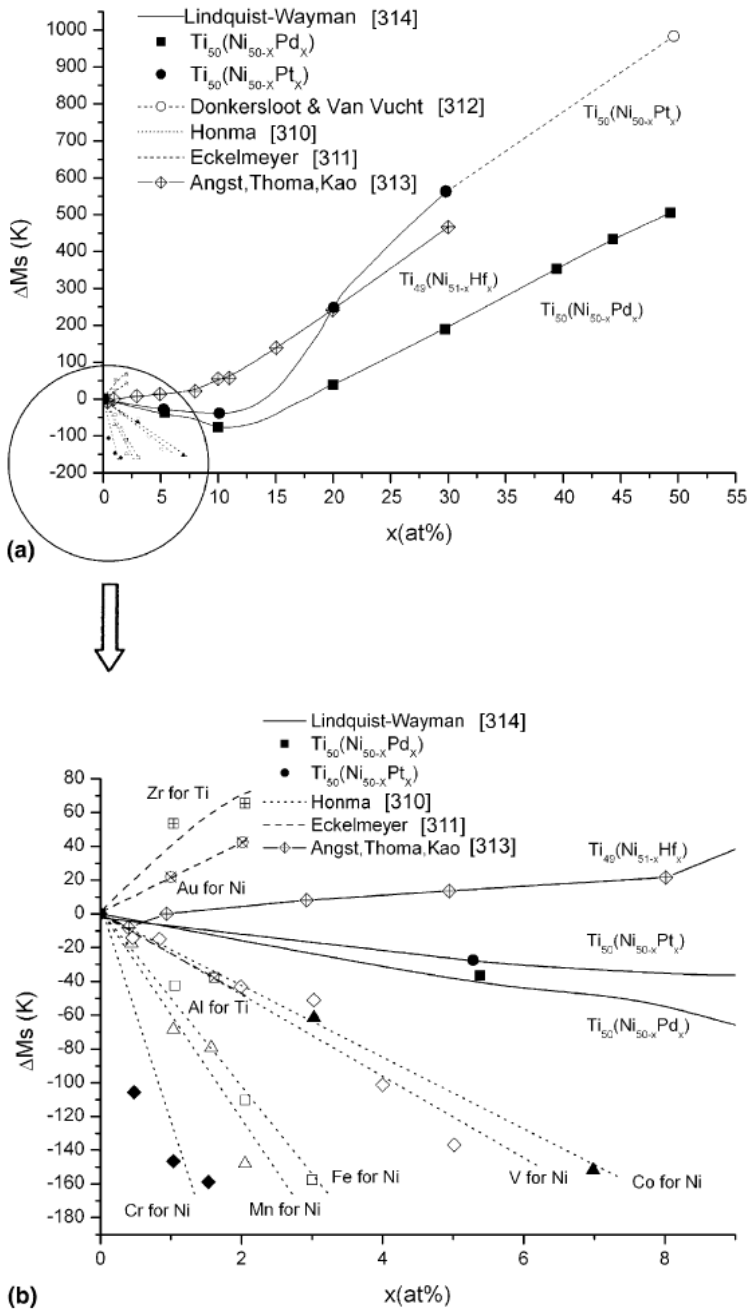


Figure 2.15:The effect of alloying element Fe, Pd, Pt, Hf, Co, V, Mn Au, Zr, Al and Cr on martensitic transformation temperature of Ti–Ni system: (a) wide alloying range, (b) narrow alloying range (low alloying level). The data were compiled from the data in references indicated in the figure [11].

## 2.5 Electronic Basis of the Strength of Crystals, Bulk and Shear Moduli

### 2.5.1 Atomic Number, Orbital Electron Occupancy

Bulk modulus is a measure of resistance of a crystal (solid) to volume change and shear modulus is a measure of resistance to shape change [179,180]. A major source of information on the trends in elastic stiffness is the Periodic Table of Elements. Figure 2.15 is a plot showing the dependence of the bulk moduli of the elements on their atomic numbers. It may be seen that there are six peaks in bulk stiffness corresponding to each of the standard Periodic Table [180]. The maxima fall at when the valence shells of rows one and two are half full of electrons; and then when each of the transitions shells (3d,4d, and 5d) is roughly half filled. Three of these peaks are related to transition metals [180-182]. Therefore, atomic number and electron occupancy of orbitals are two major factors influencing the elastic constants.

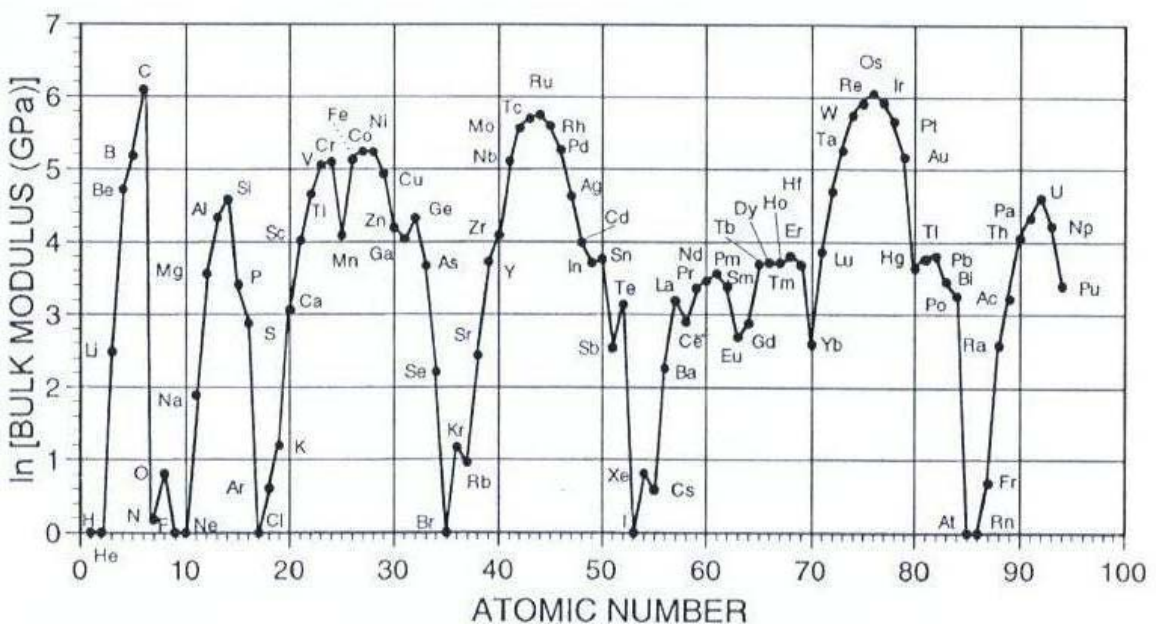


Figure 2.16: Bulk Moduli of Elements [179].

### 2.5.2 Number of Valence Electrons, Size of Ion Cores

In addition to the patterns of Figure 2.15, there are other patterns that relate to the sizes of ion cores of the atoms in the metallic bonding and their net charges (nuclear charge minus the ion core charge). Both of these depend on the number of valence electrons (column of the periodic table) as well as the sizes of the ion cores (atomic numbers).

### 2.5.3 Valence Electron Concentration (Density)

A simple pattern for the elastic constants of transition metals and alloys exists. It correlates to the majority of alloys. It is a linear relationship between the valence electron concentration (density) and the bulk modulus. By increasing the valence electron concentration, the bulk modulus increases [179,183]. This relationship is illustrated for the metals and alloys of the first, second and third long rows of the Periodic Table in Figure 2.16 [180].

### 2.5.4 Magnetism

The d-orbitals play a critical role in the transition metals but they do not usually act alone. They become hybridized with p- and s-oribitals. The evidence of their importance is that as one proceeds across one of the long rows of transition metal row in the periodic table, the atomic volume changes relatively little but the elastic stiffness changes markedly, reaching a maxmimum near the middle of each row. Manganese is an exception in which the bonding is strongly affected by its anti-ferromagnetism [184]. Other elements that are influenced by their magnetism, but to a lesser extent than Mn, are Cr, Fe, and Co. Figure 2.17 [180,184] shows the difference between the magnetic and non-magnetic cases as calculated by Moruzzi and Marcus [184]. This effect can be maintained in the alloys containing more than a certain quantity of these elements as well.

We will use this anti-ferromagnetism effect of Mn on elastic constant to explain the increase of the transformation temperature in Mn-rich Hesuler shape memory alloys in Chapter 4.

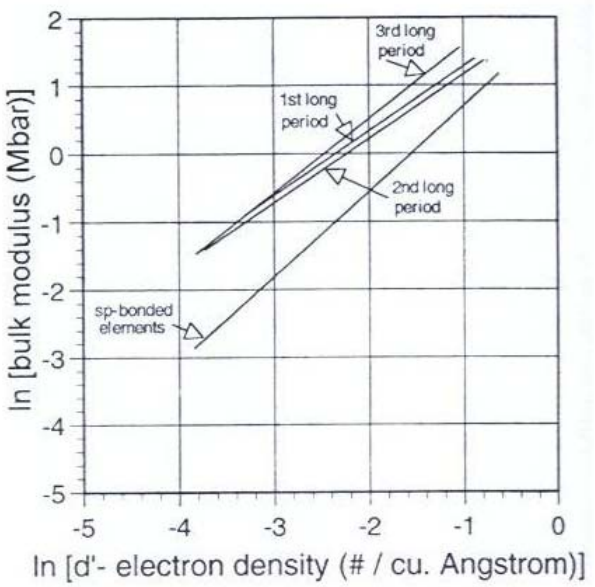


Figure 2.17: Trend lines for the logarithm of the bulk moduli versus the logarithm of the valence electron density [179].

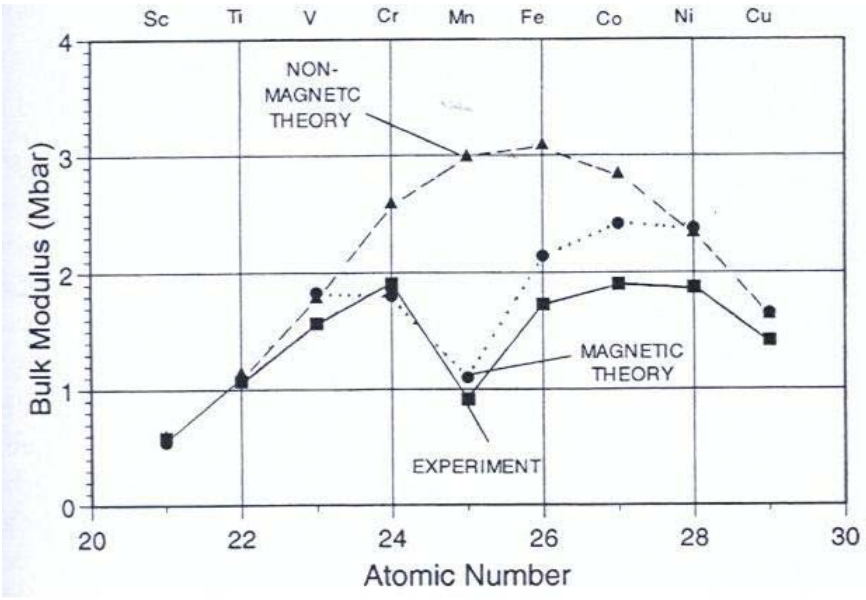


Figure 2.18: Effect of magnetism on the stiffness of the elements in the first long period [179,184].

## 2.6 Site Occupancy of Alloying Elements

A pointed out, martensitic transformation temperature is strongly dependent on composition and alloying. In spite of the importance of the site preference behavior of the additions to the base alloy for the understanding of their effect on the shape memory characteristics and transformation temperatures, very limited studies have been performed to determine the actual site preference of ternary additions to NiTi. Electron configuration, atomic size, chemical affinity of alloying elements towards Ni or Ti has been thought to influence the site preference and occupancy of the ternary elements [11]. Zr and Hf which are iso-electronic with Ti, are thought to prefer Ti sites in NiTi crystal. The reliability of suggestions is under the question as no experimental verification has been done. Relative chemical affinity of alloying element to Ti and Ni is another important factor. If an alloying element has strong affinity to Ti (represented by a large negative formation enthalpy) but has only weak affinity to Ni, this element tends to substitute for Ni, as it has similar chemical property as Ni. Co and Fe satisfy this condition and thus are thought to substitute for Ni. Atomic size factor is another factor. If other factors are the same, an alloying element tends to substitute for species of a similar size [11].

### 2.6.1 Experimental and Theoretical Attempts for Site Occupancy Determination

The only experimental effort to determine the site occupancy of alloying element in NiTi has been made by Nakata et al. [178,185,186]. Atom location by channeling enhanced microanalysis (ALCHEMI) method was used to determine the site preference of alloy element Cr, Mn, Fe, Co, Cu, Pd. Within the limited accuracy of ALCHEMI, they suggest that: (i) Fe, Co and Pd have strong preference for entering into Ni-site, irrespective of the formula of adding alloying element. (ii) Sc has strong preference for entering into Ti-site, irrespective of the formula of adding alloying element. (iii) V, Cr, Mn, Cu and Au seem to have less preference for a particular site; their occupancy fractions are strongly affected by the formula of adding alloying element.

A technique for atomistic modeling of the site substitution behavior of alloying elements in NiTi has been used by Bozzolo et al [187,188] to determine the site preference of alloying elements in NiTi structure. It was found that all elements, to a varying degree, displayed absolute preference for available sites in the deficient sublattice. However, the energetics of the different substitutional schemes, coupled with large-scale simulations indicates that the general trend in all cases is for the ternary addition to want to form stronger ordered structures with Ti. Fig. 2.16 summarizes the tendency of element towards Ni and Ti site. Higher energy gap indicates more relative preference for Ni site occupancy. This theoretical modeling needs to be experimentally verified. It was concluded that the site preference behavior is largely driven by the XTi bonds created when X occupies Ni sites, in spite of the energy cost of creating Ni(Ti) anti-site defects [187]. The result of this theoretical modeling requires experimental verification.

## 2.7 Local Atomic Structure

Despite extensive research on many aspects of the NiTi-shape memory alloys, the knowledge of local atomic structure (structure of neighboring atomic species to an atom) and also electronic structure of the alloys is very limited [189-191]. X-ray absorption spectroscopy which is a relatively new technique has been only briefly used in NiTi-based shape memory alloy.

### 2.7.1 Local Atomic Structure (XAFS Studies)

The structure of nanocrytalline NiTi with different annealing temperatures, prepared by sputtering was investigated by extended X-ray absorption fine structure (EXAFS) [189]. It was found that the structure of nano-phase powder is different from bulk NiTi. By increasing the annealing temperature, a small fraction of the (Ni,Ti) type nanocrystal with a hexagonal structure was present with a random atomic occupation.

The most interesting and in depth local atomic structure study pertains to the recent structural study of austenite and martensite of $Ni_{2+x}Mn_{1-x}Ga$ $0 \leq x \leq 16$ by Bhobe

et al [190]. In this work, in order to understand the atomic re-arrangements that occur upon martensitic transformation, room-temperature and low-temperatures EXAFS measurements were carried out. The Fourier transform (FT) magnitude in R space of $k^3$ weighted Mn K-edge EXAFS at room temperature and low temperature are shown in Fig. 2.17 [190]. Fitting the absorption behavior data by a structural model reveals the local atomic structure of the atoms around the absorbing atoms.

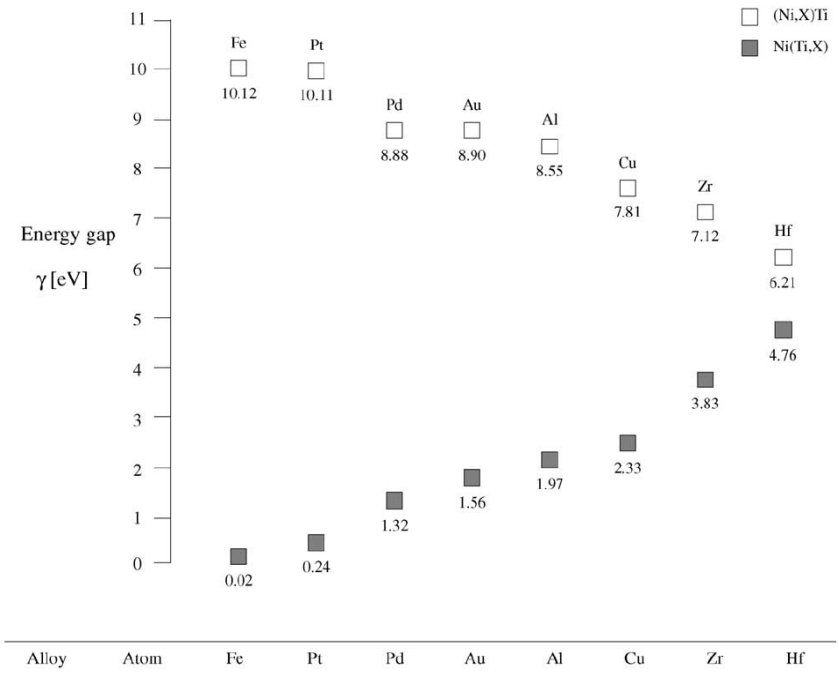


Figure 2.19: Absolute site preference behavior for X (=Fe, Pt, Pd, Au, Al, Cu, Zr, Hf) additions to (Ni, X)Ti (open squares) and Ni(Ti, X) (solid squares) alloys. Solid squares denote the energy gap $\gamma$ (in eV) between X(Ti) and X(Ni)Ni(Ti) substitutions in Ni(Ti, X) alloys. Open squares denote the energy gap between X(Ni) and X(Ti)Ti(Ni) substitutions in (Ni, X)Ti alloys. Open squares high in this chart indicate that the element has a strong preference for Ni sites in (Ni, X)Ti alloys. Solid squares low in this chart indicate that the element has a very weak preference for Ti sites in Ni (Ti, X) alloys. The energy gap (in eV) is defined as the difference in energy between the lowest energy configuration (X(Ti) and X(Ni), respectively), and the average of the two states higher in energy ($X(Ti)Ti(Ni)_l$ and $X(Ti)Ti(Ni)_f$ for (Ni, X)Ti, and $X(Ni)Ni(Ti)_l$ and $X(Ni)Ni(Ti)_f$ for Ni(Ti, X) alloys, respectively) [199].

The modulation amplitudes over which the constituent atoms move, giving rise to the shuffling of the atomic planes in the modulated structure due to austenite to martensite transition have been clearly determined by this study. Typical structures model of the local structure around Ga atoms concluded from fitting EXAFS data of $Ni_{2+x}Mn_{1-x}Ga$ alloys are presented in Fig. 2.18 [190].

In another work, X-ray absorption near edge spectroscopy (XANES) has been briefly used to understand the evolution of R phase before formation of martensite in Ni-rich NiTi shape memory alloy by Mehta et al [191].

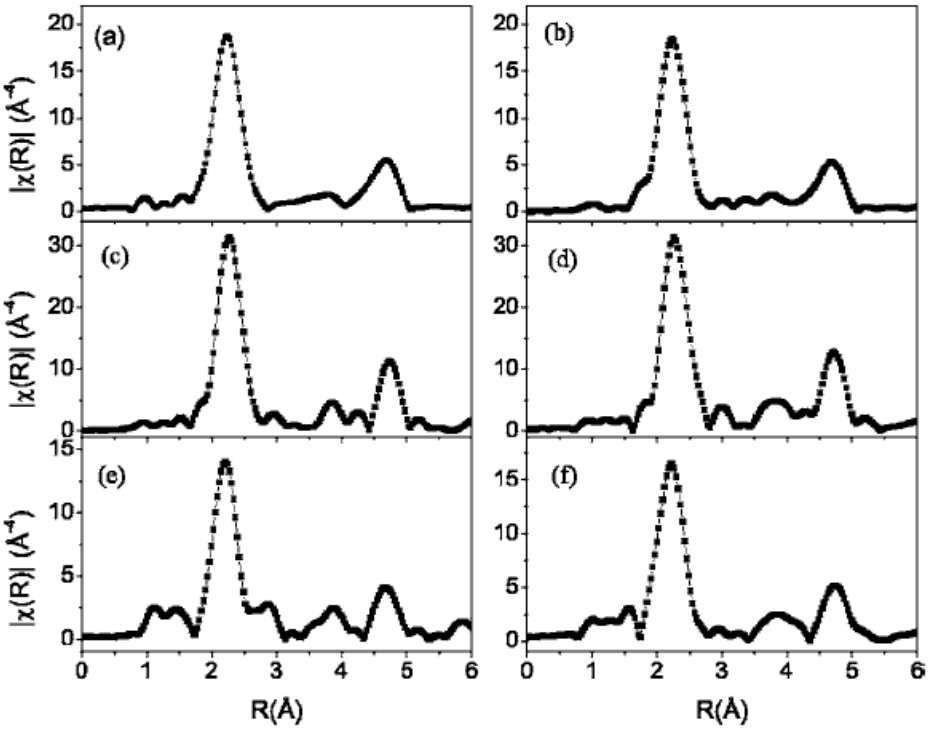


Figure 2.20: The magnitude of Fourier-transform spectra of Mn *K*-edge EXAFS in the austenitic phase (room) temperature_ for (a) $x$=0, (b) $x$ =0.1, and in the martensitic phase for (c) $x$=0, (d) $x$=0.1, (e) $x$=0.13, and (f) $x$=0.16 [190].

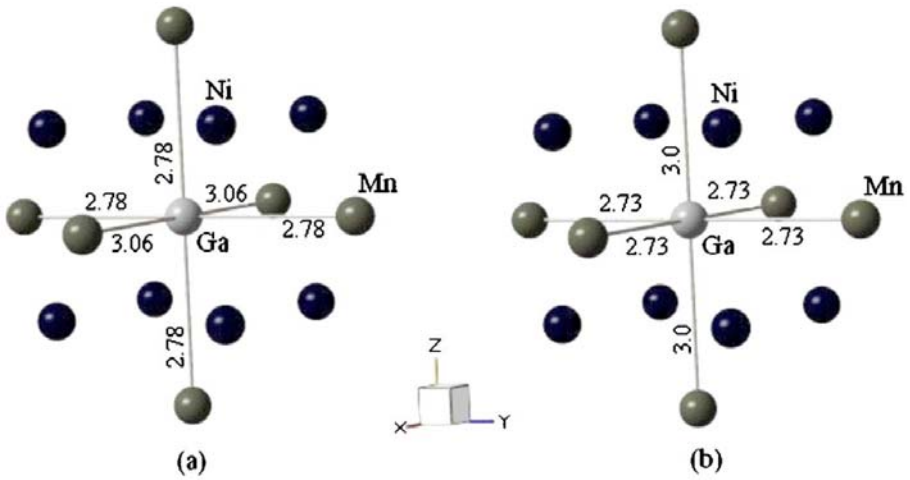


Figure 2.21: The local environment around the central Ga atom in martensitic phase (a) for $x$=0.1and (b) for $x$=0.13 [190].

### 2.7.2 Local atomic structure of melt-Spun NiTiCu shape memory Ribbon

It is known that the properties of NiTi shape memoy alloys can be changed by alloying. However, most of the ternary alloys are too brittle to be deformed plastically. The melt-spinning technique has been introduced to tackle this problem by skipping the thermomechanical shaping procedure and to achieve fine grain [192]. During the process, the starting alloy is induction melted in a quartz crucible and then ejected with a pressurized argon gas out of a nozzle onto a high speed rotating copper roller quenched by water.

Since the melt-spinning is a non-equilibrium technique, the structure of the as-melt-spun ribbon depends on the cooling rate controlled by the processing parameters [192-194]. The initial structure of $Ni_{25}Ti_{50}Cu_{25}$ ribbon can be amorphous by adjusting the melt temperature of the alloy. Previous experimental work on this ribbon confirms the amorphous structure of the alloy [193]. The amorphous alloy is crystallized to activate its shape memory effect. Some aspects of the crystallization of this alloy have been studied [195-197], however, the details of its local atomic structure in the as-prepared condition and subsequent local atomic changes during crystallization which gives rise to some transformation temperature change are unclear. The possible presence of short range order in a $Ni_{25}Ti_{50}Cu_{25}$ melt-spun ribbons and the evolution of chemical bonding during crystallization is an important step to understand crystallization. An ideal tool to directly investigate local structures is X-ray absorption fine structure (XAFS). The analysis of the extended x-ray absorption fine structure (EXAFS) allows one to obtain information about the number of nearest neighbors (coordination number), the bond lengths, degree of disorder, and also the chemical nature of the surrounding species. This technique will be used to study the structural evolution of a $Ni_{25}Ti_{50}Cu_{25}$ ribbon during crystallization.

## 2.8 Summary

The characteristics of shape memory alloys including their thermoelastic martensitic transformation, transformation hysteresis, and crystal structure change

during transformation were decribed. A collection of almost all transition metal shape memory alloys with martensitic transformation temperatures in the range of -206 to 1100˚C are presented. The number and concentration of valence electrons, atomic number, ion core size and antiferromagnetism have been explained to be influential on the elastic properties and therefore transformation temperatures of transition metals. The necessity of the study of these factors on the transformation temperatures of shape memory alloys has been indicated. The importance of local atomic structure of metallic materials to understand their properties have also been shown.

# Chapter 3

# 3 Experimental Procedures and Analysis Methods

The experimental procedures and analysis methods of the current work are illustrated in the chart of Fig. 3.1. The description of the methods and procedures follow in this chapter.

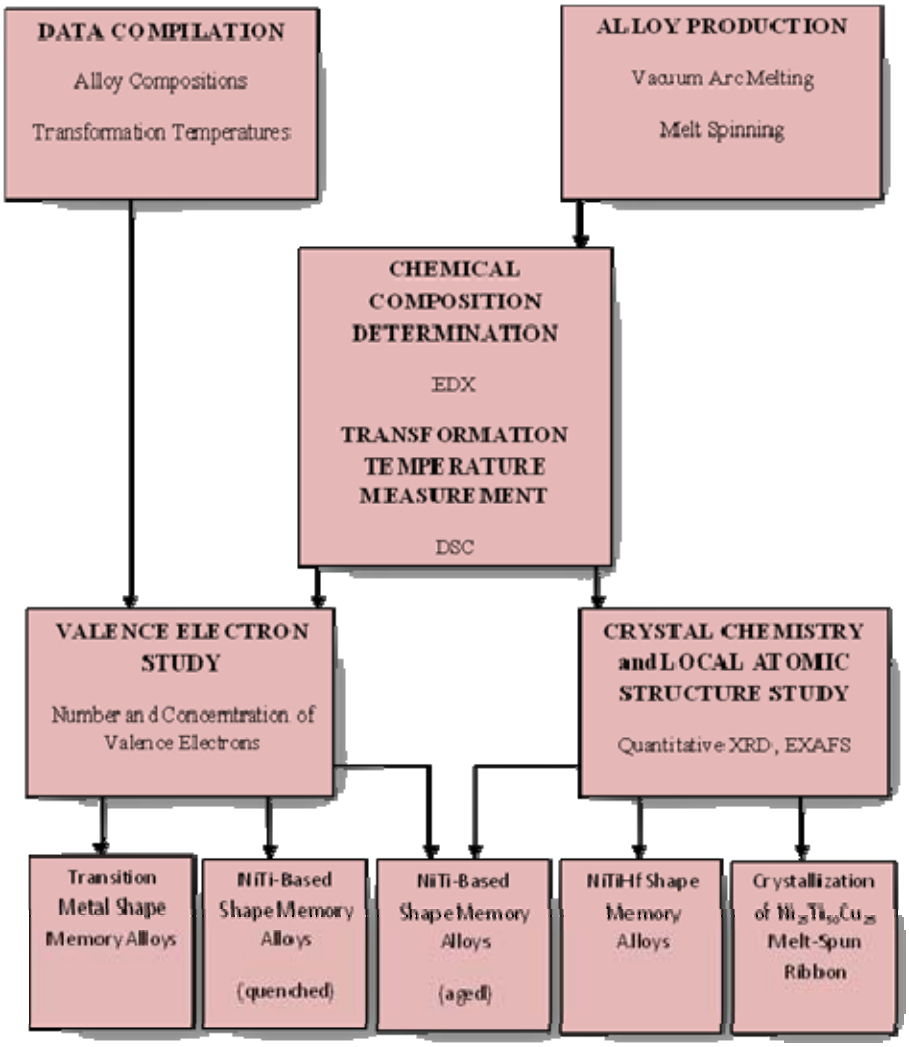


Figure 3.1: Flow chart showing the experimental procedures and analyses methods.

## 3.1 Alloy Production

Bulk NiTiHf shape memory alloys containing 5-20at% Hf or Cu were prepared in 20 g batches by combining high purity (MaTecK, 99.97%) Ti, Ni, and (MaTecK, 99.9%) Hf pellets in stoichiometric amounts, and arc melting under argon atmosphere in an Emund Buhler mini arc melting system. The resulting disc-shaped precursors of approximately 3 cm diameter were initially homogenized at 950ºC for 8 hours in a high-vacuum furnace ($1.8 \times 10^{-5}$ Pa). The specimens were solution treated for a second time at 950ºC for 1 hour followed by water quenching to ambient temperature. Three solution treated Ni-rich NiTiHf containing 10-20at% Hf were aged at 650ºC for 2 hours. These specimens used to study the effect of aging on the transformation temperature in this group of alloys.

## 3.2 Chemical Analysis

For semi-quantitative analysis of elements in the alloy specimens, energy dispersive spectroscopy (EDS) was carried out on four different regions of the specimens polished to a mirror-finish surface. A JEOL JSM-5600LN scanning electron microscope (SEM), operated at the accelerating voltage of 15 KeV, was used. The chemical compositions for Ni and Ti were within 0.05-0.14 at% and for Hf and Cu within 0.10-0.34 at% of the nominal values of the alloys.

## 3.3 Differential Scanning Calorimetry

The transformation behavior was measured using differential scanning calorimeter (TA Instruments, MDSC 2920), and the transformation temperatures were determined using slope line extension method. A heating and cooling rate of 10˚C/min was used.

## 3.4 Valence Electron Analysis

In order to understand the mechanisms that control the transformation temperatures in NiTi-based alloys, a profound knowledge of how the atomic bonding is influenced by alloying elements is necessary. As it was pointed out, it is well known that in metallic materials the delocalized valence electrons hold the non-valence electrons and nuclei of atoms (ion cores) together and form metallic bonds [50,179,183] Therefore, knowledge of how the alloying elements alter the electronic structures of these alloys is essential. In the present work, the electronic structures of various ternary and quaternary NiTi-based alloys and correlated them to the transformation temperatures are investigated. Two parameters are paid attention to: 1) the number of valence electron per atom, and 2) the valence electron concentration of the alloy.

The number of valence electrons are usually considered as the number of d and s electrons for an atom of transition metals, and p and s electrons for an atom for non-transition ones. The valence electrons per atom of an alloy can be calculated based on the atomic fraction of the elements in the alloy by Eq. (3.1):

$$\frac{e_v}{a} = f_A e_v^A + f_B e_v^B + f_C e_v^C + f_D e_v^D + \ldots \tag{3.1}$$

where $f_A, f_B, f_C$ and $f_D$ represent the atomic fractions of A, B, C, and D elements in the alloy and, $e_v^A$ $e_v^B$, $e_v^C$ and $e_v^D$ are the corresponding number of valence electrons of elements A, B, C, D, respectively.

The average concentration of valence electrons $c_v$ of an alloy can be defined as the ratio of number of valence electrons to the total number of electrons of the alloy, $c_v = (e_v/e_t)$, which can be simply calculated as follows (Eq. 3.2):

$$c_v = \frac{e_v}{e_t} = \frac{f_A e_v^A + f_B e_v^B + f_C e_v^C + f_C e_v^D}{f_A Z_A + f_B Z_B + f_C Z_C + f_D Z_D} \tag{3.2}$$

where $Z_A, Z_B, Z_C, Z_D$ etc., represent the atomic numbers of elements A, B, C, D, etc., respectively. Similarly $f_A, f_B, f_C, f_D$ etc., represent their corresponding atomic fractions in the alloy. Depending on the alloying elements, atomic fractions of elements comprising an alloy, different $c_v$ values are resulted.

## 3.5 Quantitative X-ray Diffraction (Rietveld Refinement)

The parent phase of all NiTi-based alloys, austenite, has a cubic B2 (ordered body centered cubic) structure. Depending on composition and thermomechanical treatment, the B2 Austenite phase transforms to its ground-state martensite B19' by one of three transformation paths: B2(*Pm-3m*)-B19'($P2_1/m$), B2(*Pm-3m*)-B19(*Pmmb*)-B19'($P2_1/m$) or B2(*Pm-3m*)-R(*P3*)-B19'($P2_1/m$) [11]. B'19 has a monoclinic crystal structure of $P2_1/m$ space group. The martensitic transformation of B2-B19' is basically a group-subgroup symmetry change. In NiTiHf alloys the direct transformation of B2-B19' takes place [198]. In the present work B19' crystal structure is used as the starting model for the refinement of the crystal structure of martensite in NiTiHf alloys. Fig. 3.2, illustrates a schematic of the unit cell of NiTi B19' martensite.

X-Ray diffraction was used to analyze the crystal structures of the polycrystalline alloys. Patterns were collected using Cu Kα radiation by scanning in the 2θ range of 10-120˚ at intervals of 0.02˚ with a dwelling time of 4s. Crystal structure analysis was conducted using the fundamental parameter Rietveld procedure as implemented in TOPAS (Version 3) [199]. A Rietveld refinement involves fitting of the full experimental diffraction pattern with calculated profiles and background. All the parameters that define a diffraction pattern are parameterized in such a way that they can be changed in a recurrent process to minimize the weighted squared difference between the experimental data ($Y_i$) and the theoretically predicted value ($Y_{ical}$) at each angular position, according to Eq. 3.3:

$$\sum_i w_i (Y_i - Y_{ical})^2 \qquad (3.3)$$

where $i$ varies from 1 to the number of observation and $w_i=1/Y_i$ is the reciprocal of the variance associated to the $i$th observation. The crystallographic model of monoclinic ($P2_1/m$) B19' NiTi martensite and (*Pm-3m*) B2 austenite were used as starting models for the refinements (Table 3.1 [11,200,201]). For each refinement, the following parameters were varied: the background parameter, scale factor, cell parameters, zero point correction, Lorenzien crystal size, isotropic thermal parameters, site occupancy factors, and atom site coordinates. The strain factors and preferred orientation parameters were not refined. Fig. 3.3 illustrates a typical refined diffraction profile of

the alloys. The diffraction peaks correspond to B19' NiTi martensite. No evidence of precipitates is observed in the diffraction profiles. The refinements resulted in good fits to the experimental data and Bragg reliability factor ($R_b$) values from 3.4 % to 5.1% were obtained.

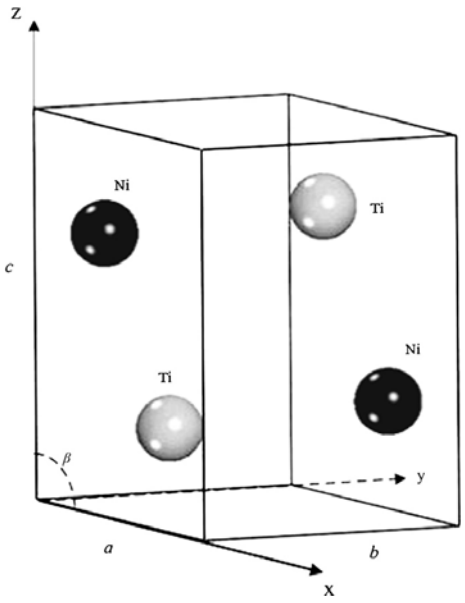


Figure 3.2: Schematic of the unit cell of NiTi B19' martensite structure. Atoms are shown indark (Ni) and light (Ti) colors.

Table 3.1: Crystallographic data of the monoclinic and cubic NiTi models [11,199,200]

| Phase (*Space group*) | Lattice parameters(Å) and monoclinic angle | Atomic parameters<br>x y z |
|---|---|---|
| B19' *($P2_1/m$)* | a=2.898, b=4.108<br>c=4.646, β=97.78º | Ni (0.04 0.25 0.67)<br>Ti (0.42 0.25 0.22) |
| B2 *(Pm-3m)* | a=3.015 | Ni (0 0 0)<br>Ti (0.5 0.5 0.5) |
| $Ni_4Ti_3$ | a=6.722 α=113.905º | Ni(0 0 0), Ni(0.5 0.5 0.5)<br>Ni(0.06 0.59 0.76)<br>Ti (0.50 011. 0.25) |

The structure analysis was carried out following the standard method of least-squares for the observed reflections. Here $R_b$ is defined by Eq. 3.4:

$$R_b = \frac{\sum (F_o - F_c)}{\sum F_o} \tag{3.4}$$

where $F_o$ and $F_c$ are the observed and calculated structure factors, respectively. The crystallite size of the specimens was in the range 25-35 nm. For the aged alloys the crystal structure model of the second phase ($Ni_4Ti_3$) was used together with the B19'. The crystallographic data of this compound [201] are reported in Table 3.1. Since the precipitate that is formed by aging at this temperature in NiTiHf system is known to be $Ni_4(Ti,Hf)_3$ [11], the occupancy of Ti site in the second phase were refined to obtain the optimal atomic fraction of Hf dissolved in the precipitate based on the best fit. The fraction was found to be nearly 0.15, hence a precipitate of $Ni_4(Ti_{0.85}Hf_{0.15})$ was considered in the calculations of this study.

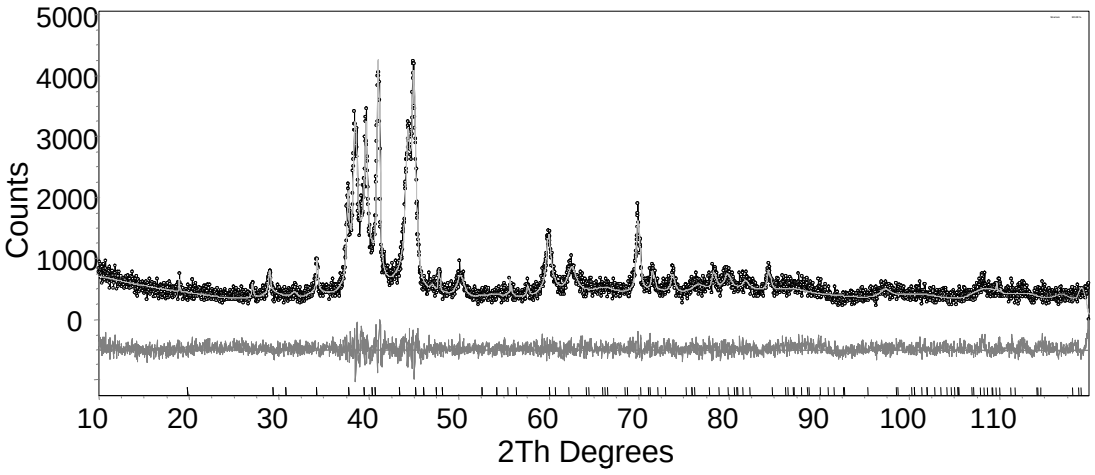


Figure 3.3: Rietveld refinement of room temperature diffraction profile of $Ni_{45}Ti_{45}Hf_{10}$ indicating the difference curve and only martensite peak positions.

## 3.6 X-ray Absorption Fine Structure (EXAFS) Analysis

An ideal tool to directly investigate local structures is X-ray absorption fine structure (XAFS). The analysis of the extended x-ray absorption fine structure (EXAFS) allows one to obtain information about the number of nearest neighbors (coordination number), the bond lengths, degree of disorder, and also the chemical nature of the surrounding species. In this letter, the results of an XAFS study of the structure of a melt-spun $Ni_{25}Ti_{50}Cu_{25}$ and its crystallization process are presented. Specifically, we explore the possible presence of short range order in a $Ni_{25}Ti_{50}Cu_{25}$ melt-spun ribbons and the evolution of chemical bonding during crystallization.

Melt-spun $Ni_{25}Ti_{50}Cu_{25}$ alloy ribbons 30 μm thick x 20 mm wide were produced. The ribbons were finely polished on both sides to a thickness of 10 μm which was appropriate for XAFS measurements and to increase structural homogeneity. The as-prepared amorphous ribbons were annealed at 500°C for 1, 3, 5, and 10 min. X-ray diffraction (XRD) measurements were carried out under ambient conditions using Cu-$K_\alpha$ radiation. Room-temperature extended X-ray absorption fine structure (EXAFS) measurements for all samples were performed at the XDD beam line at Singapore Synchrotron Light Source (SSLS) which has an accessible photon energy range of 2.5 ~ 10.5 keV [202,203]. Ni, Ti and Cu K-edge spectra were measured in transmission mode and the spectra analyzed by standard procedures of data reduction using WINXAS [204]. First, the EXAFS signal, $\chi(k)$, was extracted by background removal, spline function fit of the free atomic background, weighted by $k^3$ and multiplied by a Bessel window function, followed by subsequent Fourier transformation (FT) over the region where the amplitude of the non-weighted $\chi(k)$ is significant ($k$, the the wave number of the photo-electron, ranges for Ti is 3~14.2, for Cu is 2.0 ~ 12.5 and for Ni is 2.0~12.5 $Å^{-1}$). The FT gives a radial distribution function (RDF), modified by the phase shifts due to the absorbing and backscattering atoms. The data fit was carried out in R space to the first coordination shell by filtering out the first peak in FT spectra. The structural parameters $N$ (coordination number), $R$ (interatomic distance), and σ (relative displacement of atoms) were obtained, using theoretical phases and amplitude functions calculated by the FEFF-8 code [205], which were based on the pure metal and martensite $Ni_{50}Ti_{50}$ structure. The Ni-Ni, Cu-Cu and Ti-Ti distances in closely packed

pure metals are 2.49, 2.55 and 2.93 Å, respectively. Cu-Cu and Ni-Ni are the nearest neighbor atomic pairs, so in the fit of the first shell of the Cu edge in the FT data, only Cu-Ti and Cu-Cu coordination were employed, due to a the limited XAFS data range and similarity of bond lengths and scattering factors for Cu and Ni. XAFS cannot distinguish between Cu-Cu and Cu-Ni, and therefore, the fitted Cu-Cu coordination should contain the contributions from both species. The same analysis applies to the Ni and Ti edge data. The inelastic factor, $s_0^2$ was fixed to 0.80 for Ti-edge, 0.87 for Cu-edge and 0.88 for Ni edge, while the binding energy ($E_0$) for the two coordination components were made equal. A typical Fourier transform (FT) magnitude in *R* space of the $k^3$ weighted Ti, K-edge EXAFS at a $Ni_{25}Ti_{50}Cu_{25}$ are shown in Fig. 3.4.

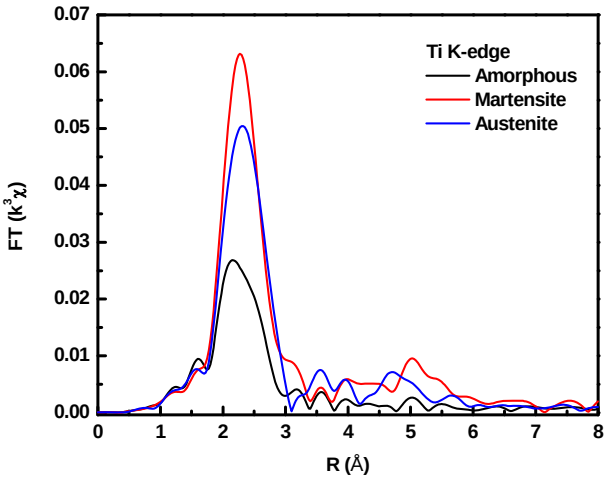


Figure 3.4: Fourier transform magnitude in R space of $k^3$ weighted Ti K-edge EXAFS in a $Ni_{25}Ti_{50}Cu_{25}$ alloy in austenite, martensite and amorphous states.

## 3.7 Summary

The experimental procudures and analysis methods to study the effect of alloy chemistry on the transformation temperature and local atomic structure of shape memory alloys are presented. The procedures for alloy production through vacuum arc melting, or melt-spinning, transformation temperature measurement by Differential scanning calorimetry, structural analysis by X-ray diffraction and Rietveld refinement and X-ray absorption Fine structure analysis are presented. Data Collection and method of investigation of the electronic structure of the alloys on their transformation temperature are also explained.

# Chapter 4

# 4 Dependence of Transformation Temperatures of Shape Memory Alloys on the Number and Concentration of Valence Electrons

## 4.1 Introduction

As introduced in Chapters 1 and 2, the transformation temperatures of shape memory alloys are of paramount importance from both fundamental and technological points of view [4-12]. Despite many efforts to relate transformation temperatures to chemical composition, the dependence of $M_s$ and $A_s$ on alloy composition has remained unclear, and the design of alloys, has been rather empirical, as an in depth understanding about the effect of composition change has not been achieved. The key influential factors that have been referred to are elastic constants of the matrix crystal before martensitic transformation and microstructural features such as precipitates [11]. In order to understand the factors influencing the transformation temperatures in NiTi-based shape memory alloys, it is necessary to acquire an in-depth knowledge of how the atomic bonding strength of the matrix crystal is influenced by chemical composition of the alloys. It is understood that prior to martensitic transformation a softening of elastic moduli occurs with lowering temperature [11,48,49]. Experimental works, in Cu-based and NiTi-based shape memory alloys [7-10] are indicative of the existence of a critical value of elastic constant at which transformation occurs which is not sensitive to alloy compositions [4] and is only slightly dependant on temperature [11]. Based on this, the elastic moduli of the alloy, which are dependent on both composition and temperature are the key parameters influencing the transformation temperatures [11,12]. Since in metallic materials the delocalized valence electrons dominate the strengths of bonds and elastic properties [50], it is of importance to study the electronic structure of alloys.

In the present work, the investigation is extended to nearly all existing transition-metal-based shape memory alloys in order to reveal a more in depth understanding of the dependence of transformation temperatures ($M_s$, $A_s$) on the electronic structure of transition metal based shape memory alloys. The electronic structures of nearly all the alloy systems are examined. Two parameters are considered: 1) the number of valence electron per atom, and 2) the valence electron concentration of the alloy. Furthermore, the possible influence of other factors such as, Mn antiferromagnetism, or electron orbital occupancy, on the transformation temperatures of shape memory alloys is introduced. The findings of this study are important steps towards understanding the influence of chemical composition on the transformation temperatures of shape memory alloys and will enable more effective alloy design.

## 4.2 Analysis

A survey of the literature reveals a number of transition-metal shape memory alloy systems with a wide range of martensitic transformation temperatures [11,19,22-25,46,47,74-155]. There are many alloy systems with or without magnetic effects. These alloys systems include NiTi, NiMn, CuAlNi, AuCd, FeMn, ZrCu, NbRu, TaRu, CoNi, CoAl, $Ni_3Ta$, CuZn, MnCu, TiPt, TiPd, TiNb, ZrNb, $Fe_3Pt$, $Fe_3Ge$, etc. Tables 4.1-4.3 present more than 200 alloy compositions which comprise nearly all the transition-metal-based shape memory alloys, together with their transformation temperatures ($M_s$, $A_s$) in ascending order. The transformation temperature data were extracted from the relevant literature as listed in tables or presented in graphs. The majority of these data correspond to solution treated alloys to minimize the effects of precipitates and mechanical work. Nonetheless, in few cases where solution-treated data were not available in the literature, the data pertaining to annealed conditions have been used. Thus, the possible effect of precipitates was not considered. Also, the possible influence of different crystal structures both in austenite and martensite for different alloy systems has not been considered in this work.

### 4.2.1 Dependence on the number of valence electrons

The number of valence electrons are usually considered as the number of d and s electrons for an atom of transition metals, and p and s electrons for an atom for non-transition ones. The valence electrons per atom of an alloy can be calculated based on the atomic fraction of the elements in the alloy by Eq. (3.1). The $e_v$/a values of the alloys examined in this study are within a wide range of 4.20-11.50 (Tables 4.1-4.3, and Figure 4.1). The $M_s$ ($A_s$) temperatures as high as 1100˚C (1150˚C) down to -206˚C (-153˚C) are examined. For analysis in this study, the alloys are categorized into three groups with low ($e_v$/a<5), medium (5≤$e_v$/a≤7.50) and high ($e_v$/a>7.50) number of valence electrons per atom as tabulated in Tables 4.1,4.2, and 4.3, respectively. A small group of shape memory alloys have $e_v$/a<5.

Table 4.1: Shape memory alloys with $e_v$/a<5

| Alloy Composition [at.%] | $M_s$ [C] | $A_s$ [C] | $e_v$/a [e atom$^{-1}$] | $c_v$ | Ref |
|---|---|---|---|---|---|
| $Ti_{72}Nb_{28}$ | -93 | - | 4.28 | 0.16 | [74] |
| $Ti_{72}Nb_{22}Ta_6$ | -33 | - | 4.28 | 0.15 | [75] |
| $Ti_{74}Nb_{26}$ | 0 | - | 4.26 | 0.16 | [76] |
| $Ti_{78}Nb_{22}$ | 137 | - | 4.22 | 0.16 | [75] |
| $Ti_{80}Nb_{20}$ | 217 | - | 4.20 | 0.16 | [74] |
| $Ti_{80}Nb_{18.40}Pd_{1.60}$ | 288 | 405 | 4.28 | 0.17 | [77] |
| $Ti_{67}Nb_{30}Pd_3$ | 300 | - | 4.48 | 0.16 | [77] |

These alloys are mostly of TiNb-based compositions. A considerable number of non-magnetic alloys happen to belong to the medium range. A majority of the NiTi-based and many of high temperature alloys are within this group. The highest $M_s$ is observed in this group when $e_v$/a is around 6.50 to 7.00, and tends to lower when $e_v$/a deviates from this range. While most of the non-magnetic alloys have $e_v$/a values in the medium range, the majority of magnetic alloys belong to the high valence electron category ($e_v$/a>7.50).Nearly all NiMn-based Heusler compositions, Co-based, Fe-based, and Cu-

based alloys fall into this category. An overall view indicates that $M_s$ temperatures of these alloys are comparatively lower compared to those of the alloys in the medium $e_v$/a group (Figure 4.1). A similar variation with the number of valence electrons is observed for $A_s$ temperature. The number of reported $A_s$ data is smaller than $M_s$ only due to unavailability of the $A_s$ data in the literature.

Table 4.2: Shape memory alloys with $5 \leq e_v/a \leq 7.50$

| **Alloy Composition [at.%]** | **$M_s$ [C]** | **$A_s$ [C]** | **$e_v$/a [e atom$^{-1}$]** | **$c_v$** | **Ref** |
|---|---|---|---|---|---|
| $Ni_{47.25}Mn_{23}Ga_{24.5}Fe_{5.25}$ | -173 | - | 7.47 | 0.27 | [78] |
| $Fe_{60.4}Mn_{8.5}Si_{13}Cr_{10.2}Ni_{7.9}$ ($Fe_{65}Mn_9Si_7Cr_{10}Ni_9$ (wt)) | -168 | -58 | 7.35 | 0.30 | [79] |
| $Fe_{58.6}Mn_{15.4}Si_{9.4}Cr_{12.2}Ni_{4.4}$ ($Fe_{62}Mn_{16}Si_5Cr_{12}Ni_5$ (wt)) | -153 | -53 | 7.31 | 0.30 | [79] |
| $Fe_{58.7}Mn_{19.2}Si_{9.4}Cr_{8.1}Ni_{4.6}$ ($Fe_{62}Mn_{20}Si_5Cr_8Ni_5$ (wt)) | -133 | -33 | 7.36 | 0.30 | [79] |
| $Ni_{43}Ti_{50}Co_7$ | -100 | - | 6.93 | 0.28 | [11] |
| $Ni_{44}Ti_{50}Fe_6$ | -100 | - | 6.88 | 0.28 | [27] |
| $Ni_{47}Ti_{50}Fe_3$ | -98 | - | 6.94 | 0.28 | [11] |
| $Ni_{48.5}Ti_{50}Cr_{1.5}$ | -95 | - | 6.94 | 0.28 | [11] |
| $Ni_{48}Ti_{50}Mn_2$ | -95 | - | 6.94 | 0.28 | [11] |
| $Ni_{47.5}Ti_{50}Fe_2Mo_{0.5}$ | -90 | 5 | 6.94 | 0.28 | [33] |
| $Ni_{45}Ti_{50}V_5$ | -80 | - | 6.75 | 0.27 | [11] |
| $Ni_{50}Mn_{25}Ga_{25}$ | -71 | - | 7.50 | 0.27 | [80] |
| $Ni_{46}Ti_{50}V_4$ | -50 | - | 6.80 | 0.27 | [11] |
| $Ni_{47.6}Ti_{46.4}Nb_6$ | -50 | -29 | 6.92 | 0.27 | [28] |
| $Ni_{49}Mn_{23.5}Ga_{27.5}$ | -46 | - | 7.37 | 0.26 | [81] |
| $Ni_{50}Ti_{48}W_2$ | -37 | -26 | 7.04 | 0.27 | [30] |
| $Ni_{46}Ti_{50}Cu_3Mo_1$ | -30 | - | 6.99 | 0.28 | [86] |
| $Ni_{50}Ti_{49}W_1$ | -28 | -12 | 7.02 | 0.27 | [85] |
| $Ni_{48.3}Ti_{51}Mo_{0.7}$ | -13 | 20 | 6.91 | 0.27 | [29] |
| $Ni_{49}Ti_{50}Mo_1$ | 10 | 20 | 6.96 | 0.28 | [29] |
| $Ni_{45}Ti_{50}Pd_5$ | 20 | - | 7.00 | 0.27 | [11] |
| $Fe_{58.92}Mn_{14.59}Si_{12.99}Cr_{9.09}Ni_{4.41}$ ($Fe_{63.43}Mn_{15.45}Si_{7.03}Cr_{9.11}Ni_{4.98}$ (wt)) | 24 | 112 | 7.24 | 0.30 | [82] |

| | | | | | |
|---|---|---|---|---|---|
| $Ni_{39.5}Ti_{49.5}Cu_{10}Cr_1$ | 25 | 30 | 7.08 | 0.28 | [38] |
| $(Co_{45}Ni_{25}Ga_{30})_{0.95}Ta_5$ | 27 | 37 | 7.33 | 0.24 | [83] |
| $Fe_{59.85}Mn_{13.99}Si_{12.98}Cr_{8.90}Ni_{4.28}$ ($Fe_{64.44}Mn_{14.82}Si_{7.03}Cr_{8.87}Ni_{4.84}$ (wt)) | 28 | 97 | 7.25 | 0.30 | [82] |
| $Fe_{58.2}Mn_{30.6}Si_{11.2}$ ($Fe_{62}Mn_{32}Si_6$ (wt)) | 37 | - | 7.25 | 0.29 | [79] |
| $Ni_{52}Ti_{46.74}Re_{1.26}$ | 37 | 87 | 7.16 | 0.28 | [31] |
| $Ni_{47.9}Mn_{26.1}Ga_{26}$ | 39 | 52 | 7.40 | 0.27 | [84] |
| $Ni_{50}Ti_{45}Ta_5$ | 44 | 76 | 7.05 | 0.26 | [22] |
| $Ti_{32}Hf_{18}Ni_{49.8}Re_{0.2}$ | 52 | 101.5 | 6.99 | 0.21 | [85] |
| $Ni_{48}Ti_{50}W_2$ | 55 | 70 | 6.92 | 0.27 | [30] |
| $Ni_{50}Ti_{47}Ta_3$ | 58 | 90 | 7.03 | 0.26 | [22] |
| $Ni_{30}Ti_{50}Cu_{20}$ | 58 | 60 | 7.20 | 0.28 | [36] |
| $Ni_{50}Ti_{50}$ | 60 | 80 | 7.00 | 0.28 | [11] |
| $Ni_{25}Ti_{50}Cu_{25}$ | 61 | 62 | 7.25 | 0.29 | [86] |
| $Ni_{42}Ti_{49}Ag_9$ | 61 | 20 | 7.15 | 0.27 | [25] |
| $Ni_{44}Ti_{49}Ag_7$ | 63 | 23 | 7.13 | 0.27 | [25] |
| $Fe_{85}Mn_{15}$ | 67 | 197 | 6.81 | 0.26 | [87] |
| $Ni_{49.5}Ti_{45.5}Zr_5$ | 70 | 110 | 6.97 | 0.27 | [19] |
| $Ni_{44}Ti_{40}Hf_{10}Cu_6$ | 72 | 90 | 7.06 | 0.24 | [32] |
| $Ni_{48}Ti_{50}Au_2$ | 75 | - | 7.02 | 0.27 | [21] |
| $Co_{45}Ni_{25}Ga_{30}$ | 77 | 105 | 7.45 | 0.26 | [83] |
| $Ni_{29}Ti_{51}Pd_{20}$ | 85 | - | 6.94 | 0.24 | [39] |
| $Ni_{49.5}Ti_{40.5}Zr_{10}$ | 90 | 170 | 6.97 | 0.26 | [32] |
| $Ni_{30}Ti_{50}Pd_{20}$ | 90 | - | 7.00 | 0.24 | [11] |
| $Ni_{40}Ti_{50}Pt_{10}$ | 90 | 100 | 7.00 | 0.23 | [46] |
| $Ni_{26.5}Ti_{51}Pd_{22.5}$ | 95 | - | 6.94 | 0.24 | [39] |
| $Zr_{48}Cu_{50}Ti_2$ | 110 | | 7.5 | 0.22 | [88] |
| $Ni_{50}Ti_{40}Hf_{10}$ | 120 | 165 | 7.00 | 0.23 | [32] |
| $Ti_{50}Pd_{43.5}Cr_{6.5}$ | 127 | - | 6.74 | 0.21 | [89] |
| $Zr_{50}Cu_{50}$ | 140 | 230 | 7.50 | 0.22 | [90] |
| $Ni_{40}Ti_{50}Hf_{10}$ | 140 | 185 | 6.40 | 0.22 | **[10]** |
| $Zr_{50}Cu_{50}$ | 150 | | 7.50 | 0.22 | [88] |

| | | | | | |
|---|---|---|---|---|---|
| $Zr_{42.3}Cu_{29.9}Ni_{11}Co_{10.2}Ti_{6.6}$ | 177 | 137 | 7.26 | 0.22 | [91] |
| $Mn_{85.5}Fe_{9.5}Cu_5$ | 182 | 180 | 7.29 | 0.29 | [92] |
| $Ni_{49.5}Ti_{35.5}Zr_{15}$ | 190 | 235 | 6.97 | 0.25 | [19] |
| $Ni_{49.5}Ti_{35.5}Hf_{7.5}Zr_{7.5}$ | 195 | 230 | 6.97 | 0.23 | [37] |
| $Ti_{50}Rh_{40}Ni_{10}$ | 210 | - | 6.60 | 0.21 | [93] |
| $Ni_{15}Ti_{50}Pd_{35}$ | 225 | - | 7.00 | 0.22 | [39] |
| $Ni_{36}Ti_{49}Hf_{15}$ | 230 | - | 6.16 | 0.20 | [11] |
| $Ni_{35}Ti_{50}Hf_{15}$ | 235 | 256 | 6.10 | 0.19 | **[10]** |
| $Zr_{49.6}Cu_{28.2}Ni_{6.8}Co_{15.4}$ | 253 | 212 | 7.15 | 0.21 | [91] |
| $Ni_{30}Ti_{50}Pt_{20}$ | 266 | 271 | 7.00 | 0.20 | [46,47] |
| $Ni_{49.5}Ti_{30.5}Hf_{10}Zr_{10}$ | 290 | 315 | 6.97 | 0.22 | [37] |
| $Ni_{50}Ti_{30}Hf_{20}$ | 290 | 317 | 7.00 | 0.20 | **[10]** |
| $Zr_{50}Cu_{40}Ni_{10}$ | 300 | - | 7.40 | 0.21 | [88] |
| $Ti_{50}Rh_{45}Ni_5$ | 300 | 100 | 6.55 | 0.20 | [93] |
| $Ti_{50}Rh_{46}Co_4$ | 300 | 150 | 6.50 | 0.20 | [93] |
| $Ti_{50}Rh_{50}$ | 345 | 140 | 6.50 | 0.19 | [94] |
| $Ni_{31}Ti_{49}Hf_{20}$ | 350 | - | 5.86 | 0.17 | [11] |
| $Ti_{43.33}Pd_{50}Hf_{6.67}$ | 360 | - | 7.00 | 0.19 | [89] |
| $Ni_{25}Ti_{50}Pt_{25}$ | 430 | 450 | 7.00 | 0.19 | [39] |
| $Zr_{50}Rh_{50}$ | 480 | 570 | 6.50 | 0.15 | [95] |
| $Zr_{50.59}Cu_{29.56}Ni_{19.85}$ | 497 | 597 | 7.26 | 0.21 | [91] |
| $Ti_{50}Pd_{50}$ | 537 | 577 | 7.00 | 0.20 | [96] |
| $Ti_{50}Pd_{50}$ | 544.7 | 574 | 7.00 | 0.20 | [97] |
| $Ni_{20}Ti_{50}Pt_{30}$ | 560 | 594 | 7.00 | 0.18 | [47] |
| $Ru_{43}Nb_{50}Fe_7$ | 650 | - | 6.50 | 0.16 | [98] |
| $Ni_{15}Ti_{50}Pt_{35}$ | 680 | 750 | 7.00 | 0.16 | [46] |
| $Zr_{50}Ir_{50}$ | 740 | 880 | 6.50 | 0.11 | [94] |
| $Nb_{50}Ru_{36}Fe_{14}$ | 795 | 797 | 6.50 | 0.16 | [98] |
| $Ni_{10}Ti_{50}Pt_{40}$ | 810 | 850 | 7.00 | 0.16 | [46] |
| $Nb_{50}Ru_{43}Fe_7$ | 841 | 830 | 6.50 | 0.16 | [98] |
| $Ru_{50}Nb_{50}$ | 865 | - | 6.50 | 0.15 | [99] |
| $Nb_{50}Ru_{50}$ | 887 | 890 | 6.50 | 0.15 | [98] |

| | | | | | |
|---|---|---|---|---|---|
| $Ni_5Ti_{50}Pt_{45}$ | 900 | 950 | 7.00 | 0.14 | [46] |
| $Ti_{50}Pt_{50}$ | 1020 | 1040 | 7.00 | 0.14 | [100] |
| $Ru_{50}Ta_{50}$ | 1050 | 1030 | 6.00 | 0.10 | [99,101] |
| $Ru_{46}Ta_{54}$ | 1100 | 1150 | 6.38 | 0.11 | [102] |

The alloy compositions in parentheses () are the weight percent formula of the alloys as presented in the original references.

Table 4.3: Shape memory alloys with $e_v/a>7.50$

| **Alloy Composition [at.%]** | $M_s$ [C] | $A_s$ [C] | $e_v/a$ [e atom$^{-1}$] | $c_v$ | **Ref** |
|---|---|---|---|---|---|
| **$Au_{50}Zn_{50}$** | **-206** | **-** | **11.5** | **0.21** | **[103]** |
| **$Fe_{75}Pt_{25}$** | **-188** | **-** | **8.50** | **0.22** | **[104]** |
| $Ni_{52}Mn_6Fe_{15}Ga_{27}$ | -153 | -153 | 7.63 | 0.27 | [105] |
| $Ni_{51}Fe_{22}Ga_{27}$ | -132 | - | 7.67 | 0.30 | [106] |
| $Co_{38.5}Ni_{32.5}Al_{29}$ | -131 | -113 | 7.59 | 0.33 | [107] |
| $Ni_{49.6}Mn_{27.7}Ga_{20.6}Si_{2.1}$ | -128 | -111 | 7.60 | 0.27 | [84] |
| $Ni_{52}Mn_{16}Fe_5Ga_{27}$ | -123 | -98 | 7.53 | 0.27 | [105] |
| $Ni_{49.5}Mn_{23}Ga_{24.5}Fe_3$ | -108 | - | 7.54 | 0.27 | [78] |
| $Ni_{51.7}Mn_{28.5}Ga_{15.6}In_{4.2}$ | -95 | -73 | 7.76 | 0.27 | [84] |
| $Cu_{54.74}Al_{29.75}Zn_{15.51}$ ($Cu_{72.3}Al_{6.66}Zn_{21.04}$(wt)) | -94 | -108 | 8.77 | 0.36 | [108] |
| $Co_{38}Ni_{33}Al_{29}$ | -91 | -73 | 7.59 | 0.33 | [108] |
| $Fe_{49.8}Ni_{28.11}Co_{17.35}Ti_{4.74}$ ($Fe_{50}Ni_{33}Co_{12}Ti_5$ (wt)) | -90 | 10 | 8.53 | 0.32 | [109] |
| $Ni_{50}Mn_{35}Sb_{15}$ | -88 | -128 | 8.2 | 0.27 | [110] |
| $Ni_{42}Co_2Mn_{45}Sn_{11}$ | -81 | -84 | 8.04 | 0.27 | [111] |
| $Ni_{43}Mn_{46}Sn_{11}$ | -73 | -78 | 7.96 | 0.27 | [112] |
| $Fe_{70}Pd_{24}Pt_6$ | -73 | -78 | 8.60 | 0.25 | [113] |
| $Ni_{52}Mn_{11}Fe_5Co_5Ga_{27}$ | -68 | 27 | 7.63 | 0.27 | [105] |
| $Co_{41}Ni_{32}Al_{27}$ | -54 | -85 | 7.70 | 0.33 | [114] |
| $Ni_{40}Mn_{30}Ga_{20}Fe_{10}$ | -67 | -82 | 7.74 | 0.28 | [115] |
| $Pd_{29.5}Fe_{64.25}Co_{6.25}$ | -53 | - | 8.65 | 0.27 | [116] |
| $Co_{37}Ni_{34}Al_{29}$ | -58 | -43 | 7.60 | 0.33 | [107] |
| $Ni_{43}Co_1Mn_{45}Sn_{11}$ | -53 | -52 | 8.05 | 0.27 | [111] |
| $Fe_{65.9}Mn_{12.9}Si_{4.5}Ni_{6.7}Cr_{9.5}Nb_{0.5}$ | -50 | 83 | 7.62 | 0.30 | [117] |

| | | | | | |
|---|---|---|---|---|---|
| $Fe_{71.4}Mn_{12.5}Ni_{6.2}Cr_{9.4}Ti_{0.5}$ | -50 | 69 | 7.79 | 0.30 | [117] |
| $Ni_{50}Mn_{36}Sb_{14}$ | -38 | -58 | 8.22 | 0.27 | [118] |
| $Ni_{42.5}Ti_{42.5}Cu_{15}$ | -34 | -30 | 7.60 | 0.30 | **[12]** |
| $Cu_{68.0}Al_{28.2}Ni_{3.8}$ ($Cu_{81.7}Al_{14.1}Ni_{4.2}$ (wt)) | -33 | - | 8.71 | 0.35 | [116] |
| $Ni_{51}Mn_{23}Ga_{24.5}Fe_{1.5}$ | -33 | - | 7.56 | 0.27 | [79] |
| $Ni_{41.75}Mn_{44.65}Sn_{10.65}B_{2.95}$ | -31 | -33 | 7.81 | 0.27 | [112] |
| **$Pd_{56.8}In_{25.4}Fe_{17.8}$** | **-29** | **-21** | **7.87** | **0.18** | **[120]** |
| $Cu_{70.6}Al_{25.3}Mn_{4.1}$ | -25 | -18 | 8.81 | 0.35 | [121] |
| $Fe_{62.40}Mn_{12.76}Si_{9.50}Cr_{8.84}Ni_{6.37}C_{0.13}$ ($Fe_{65.92}Mn_{13.25}Si_{5.05}Cr_{8.70}Ni_{7.05}C_{0.03}$ (wt)) | -22 | 113 | 7.43 | 0.30 | [117] |
| $Fe_{70}Pd_{28}Pt_{2}$ | -20 | -24 | 8.60 | 0.26 | [113] |
| $Co_{39}Ni_{33}Al_{28}$ | -5 | 17 | 7.65 | 0.33 | [107] |
| $Ni_{50}Mn_{29}Ga_{21}$ | -5.3 | -4.4 | 7.66 | 0.28 | [122] |
| $Ni_{40..95}Mn_{43.81}Sn_{10.47}B_{4.77}$ | 2 | -1 | 7.72 | 0.28 | [112] |
| $Cu_{70.9}Al_{20.4}Mn_{8.7}$ | 3 | 7 | 9.02 | 0.35 | [121] |
| $Pd_{29.43}Fe_{68.55}Co_{2.02}$ | 3 | - | 8.61 | 0.27 | [116] |
| $Ni_{54}Fe_{19}Ga_{27}$ | 3 | 7 | 7.73 | 0.27 | [123] |
| $Pd_{29.23}Fe_{66.67}Co_{4.10}$ | 6 | - | 8.63 | 0.27 | [81] |
| $Ni_{52}Mn_{24.5}Ga_{23.5}$ | 12 | 16 | 7.62 | 0.27 | [124] |
| $Cu_{69}Al_{27.5}Ni_{3.5}$ | 15 | 40 | 8.76 | 0.35 | [125] |
| $Fe_{70}Pd_{30}$ | 15 | 14 | 8.60 | 0.27 | [113] |
| $Ni_{50}Mn_{37}Sb_{13}$ | 17 | 2 | 8.24 | 0.28 | [118] |
| $Ni_{52}Mn_{1}Fe_{15}Co_{5}Ga_{27}$ | 17 | 297 | 7.73 | 0.27 | [105] |
| $Fe_{70}Pd_{30}$ | 17 | 14 | 8.60 | 0.27 | [126] |
| **$Au_{43.3}Cu_{31.8}Al_{24.9}$** | **17** | **70** | **9.00** | **0.19** | **[127]** |
| $Fe_{70.1}Pd_{29.9}$ | 18 | 6 | 8.60 | 0.27 | [128] |
| $Ni_{50}Mn_{28}Ga_{22}$ | 18 | 19 | 7.62 | 0.27 | [129] |
| $Co_{66.66}Ni_{28.34}Ga_{5}$ | 20 | - | 8.98 | 0.32 | [130] |
| $Co_{41}Ni_{32}Al_{24}Sb_{3}$ | 20 | 24 | 7.76 | 0.31 | [114] |
| $Fe_{72.6}Mn_{25.6}Mo_{1.8}$ ($Fe_{72}Mn_{25}Mo_{3}$ (wt)) | 21 | - | 7.71 | 0.30 | [131] |
| $Ni_{50.4}Mn_{28.8}Ga_{19.8}Si_{1}$ | 25 | -3 | 7.69 | 0.28 | [84] |
| $Ni_{49}Fe_{18}Ga_{27}Co_{6}$ | 27 | - | 7.69 | 0.27 | [132] |

| | | | | | |
|---|---|---|---|---|---|
| **$Au_{43.75}Cu_{31.25}Al_{25}$** | **27** | **-** | **9.00** | **0.19** | **[133]** |
| **$Au_{50.5}Cd_{49.5}$** | **31** | **-** | **11.50** | **0.18** | **[134]** |
| $Ni_{49.7}Mn_{28.7}Ga_{21.6}$ | 32 | 38 | 7.63 | 0.27 | [84] |
| $Fe_{80}Mn_{20}$ | 33 | 154 | 7.80 | 0.30 | [87] |
| $Cu_{73.7}Sn_{26.3}$ ($Cu_{60}Sn_{40}$ (wt)) | 37 | - | 9.16 | 0.27 | [135] |
| $Ni_{50.5}Mn_{28.2}Ga_{21.3}$ | 38 | 41 | 7.66 | 0.27 | [84] |
| $Ni_{45}Co_5Mn_{36.7}In_{13.3}$ | 39 | 37 | 7.92 | 0.27 | [136] |
| $Co_{60.7}Ni_{29.9}Si_{9.4}$ ($Co_{63.9}Ni_{31.4}Si_{4.7}$ (wt)) | 39.6 | 264.8 | 8.83 | 0.34 | [137] |
| $Ni_{50}Mn_{38}Sb_{12}$ | 42 | 17 | 8.26 | 0.28 | [118] |
| $Ni_{50}Mn_{34}In_{16}$ | 47 | - | 7.86 | 0.26 | [138] |
| **$Pd_{57}In_{25}Fe_{18}$** | **50** | **-** | **7.89** | **0.18** | **[120]** |
| $Fe_{61.96}Mn_{30.47}Co_{7.57}$ ($Fe_{62}Mn_{30}Co_8$ (wt)) | 52 | 162 | 7.77 | 0.30 | [139] |
| $Fe_{73}Mn_{24.52}Ge_{2.48}$ ($Fe_{72}Mn_{24}Ge_4$ (wt)) | 52 | - | 7.66 | 0.29 | [140] |
| $Ni_{55}Fe_{18}Ga_{27}$ | 54 | 27 | 7.75 | 0.27 | [123] |
| $Ni_{52}Fe_{18}Ga_{27}Co_3$ | 58 | - | 7.72 | 0.27 | [132] |
| $Co_{50}Ni_{23.5}Ga_{26.5}$ | 60 | - | 7.64 | 0.27 | [130] |
| $Ni_{50}Mn_{28}Ga_{21}Y_1$ | 60 | 62 | 7.62 | 0.27 | [129] |
| $Ni_{50}Mn_{30}Ga_{15}Al_5$ | 62 | -1 | 7.68 | 0.28 | [115] |
| $Co_{50}Ni_{22}Ga_{28}$ | 64 | - | 7.54 | 0.27 | [141] |
| $Cu_{67.71}Zn_{19.45}Al_{12.84}$ ([$Cu_{72.65}Zn_{21.5}Al_{5.85}$ (wt)) | 69 | 70 | 10.17 | 0.37 | [142] |
| $Ni_{50}Mn_{29}Ga_{20}Gd_1$ | 70 | 78 | 7.74 | 0.27 | [122] |
| $Ni_{50}Mn_{29}Ga_{20}Dy_1$ | 75.9 | 76.3 | 7.66 | 0.27 | [122] |
| $Cu_{68.5}Zn_{18.8}Al_{12.7}$ | 76 | - | 10.2 | 0.37 | [143] |
| $Co_{50}Ni_{22}Ga_{27}Al_1$ | 77 | - | 7.54 | 0.27 | [141] |
| $Ni_{51.4}Mn_{27.2}Ga_{21.4}$ | 78 | 80 | 7.69 | 0.28 | [31] |
| $Mn_{85}Cu_{15}$ | 80 | - | 7.60 | 0.30 | [144] |
| $Pt_{10}Ni_{40}Mn_{25}Ga_{25}$ | 82 | 77 | 8.5 | 0.34 | [145] |
| $Cu_{68.3}Zn_{20.4}Al_{11.3}$ | 85 | - | 10.3 | 0.37 | [143] |
| $Ni_{51.3}Mn_{14.4}Ga_{26.3}Fe_8$ | 86 | 88 | 7.57 | 0.27 | [84] |
| $Ni_{40}Mn_{30}Ga_{20}Co_{10}$ | 88 | 91 | 7.64 | 0.27 | [115] |
| $Fe_{69.9}Mn_{25.37}Co_{4.73}$ ($Fe_{70}Mn_{25}Co_5$ (wt)) | 97 | 177 | 7.79 | 0.30 | [139] |
| $Fe_{67}Mn_{25.41}Co_{7.59}$ ($Fe_{67}Mn_{25}Co_8$(wt)) | 100 | 175 | 7.82 | 0.30 | [139] |

| | | | | | |
|---|---|---|---|---|---|
| $Cu_{58.51}Al_{32.43}Zn_{9.06}$ ($Cu_{78.9}Al_{8.54}Zn_{12.56}$ (wt)) | 102 | 48 | 8.50 | 0.35 | [108] |
| $N_{50}Mn_{29}Ga_{19}Gd_2$ | 105 | 115 | 7.82 | 0.27 | [126] |
| $Ni_{54}Mn_{23}Ga_{23}$ | 110 | 115 | 7.70 | 0.27 | [146] |
| $Co_{86}Al_{14}$ | 112 | 236 | 8.16 | 0.32 | [141] |
| $Co_{50}Ni_{22}Ga_{26}Al_2$ | 115 | - | 7.54 | 0.27 | [141] |
| $Ni_{50}Mn_{29}Ga_{19}Dy_2$ | 126.2 | 123.7 | 7.66 | 0.27 | [122] |
| $Ni_{50}Mn_{28}Ga_{19}Y_3$ | 130 | 132 | 7.62 | 0.27 | [129] |
| $Co_{50}Ni_{22}Ga_{23}Al_5$ | 150 | - | 7.54 | 0.27 | [141] |
| $Ni_{55.6}Mn_{11.4}Fe_{7.4}Ga_{25.6}$ | 166 | 180 | 7.72 | 0.27 | [145] |
| $Co_{35}Ni_{40}Al_{25}$ | 167 | - | 7.90 | 0.33 | [148] |
| $Ni_{55}Mn_{22.5}Ga_{22.5}$ | 175 | 200 | 7.75 | 0.27 | [146] |
| $Ni_{48.75}Mn_{35.5}Ga_{15.75}$ | 175.1 | 178.7 | 7.83 | 0.28 | [149] |
| $Ni_{50}Mn_{40}In_{10}$ | 177 | - | 8.10 | 0.28 | [138] |
| $Ni_{50}Mn_{29}Ga_{18.8}Co_{2.2}$ | 223 | 224 | 7.79 | 0.28 | [31] |
| $Ni_{75}Ta_{25}$ | 250 | - | 8.75 | 0.22 | [150] |
| $Cu_{72.12}Al_{26.45}Pd_{1.43}$ ($Cu_{84.13}Al_{13.08}Pd_{2.79}$ (wt)) | 262.8 | 262.8 | 8.87 | 0.35 | [151] |
| $Cu_{79.23}Al_{20.77}$ ($Cu_{90}Al_{10}$ (wt)) | 265 | - | 9.34 | 0.36 | [152] |
| $Ni_{50.7}Mn_{34.6}Ga_{14.7}$ | 311 | 319 | 7.93 | 0.29 | [153] |
| $Ni_{50}Mn_{40}Ga_{10}$ | 347 | - | 8.10 | 0.30 | [154] |
| $Cu_{73.1}Al_{21.5}Ag_{5.4}$ ($Cu_{80}Al_{10}Ag_{10}$(wt)) | 350 | - | 9.28 | 0.35 | [152] |
| $Ni_{50}Mn_{37.5}Al_{12.5}$ | 390 | - | 8.00 | 0.32 | [154] |
| $Ni_{50}Mn_{45}Sn_5$ | 437 | - | 8.35 | 0.30 | [154] |
| $Ni_{49.6}Mn_{45.5}In_{4.9}$ | 487 | 509 | 8.29 | 0.30 | [155] |
| $Ni_{50}Mn_{50}$ | 627 | - | 8.50 | 0.32 | [155] |

The alloy compositions in parentheses () are the weight percent formula of the alloys as presented in the original references.

### 4.2.2 Dependence on valence electron concentration

The average concentration of valence electrons $c_v$ of an alloy was defined as the ratio of number of valence electrons to the total number of electrons of the alloy, (Eq. 3.2). Depending on the alloying elements, atomic fractions of elements comprising an

alloy, different $c_v$ values are resulted. These values for the alloys examined are tabulated in Tables 4.1-4.3. The variations of $M_s$ and $A_s$ temperatures versus valence electron concentration are plotted in Figure 4.2. In both cases, a main trend can be highlighted with increasing the electron concentration. For alloys within the indicated bands both $M_s$ and $A_s$ decrease consistently from temperatures as high as 1100˚C (1150˚C) down to as low as -206˚C (-153˚C) for alloys with a $c_v$ of within 0.10-0.27. The decreasing trend seems to stop around $c_v$≈0.27. By further increase of $c_v$, $M_s$ and $A_s$ remain in a relatively constant range or start to increase when the electron concentration is above 0.34-0.35. The general trends of variation of $M_s$ and $A_s$ seem to be similar.

### 4.2.3 Deviations from the main trend

Apart from the main trend which involves the majority of alloys, three other minor groups can be addressed which show some degree of deviation from the behavior of the main group. These alloys are introduced as follows.

#### 4.2.3.1 Mn-rich NiMnX Heusler alloys

When the electron concentration of the alloy is sufficiently high ($c_v$>0.27) in NiMnX (X=Ga, In, Al) Heusler alloys, by increasing the Mn content beyond a certain limit (Mn at%>30) $M_s$ and $A_s$ temperatures both increase considerably and deviate from the general trend in alloys (Figure 4.2). Figure 4.3 is a plot of transformation temperature of Mn containing Heusler alloys versus the Mn atomic fraction in the alloy. By increasing the Mn content to ~30 at.%, the $M_s$ temperatures increase.

#### 4.2.3.2 High valence electron alloys ($e_v$/a>7.50)

There are limited data points at medium or low $c_v$ values with relatively low $M_s$ temperatures as indicated by (triangle) in Figure 4.2. These data points which show some deviation from the main trend pertain to alloys with high $e_v$/a. Despite high

number of valence electrons ($e_v$/a>7.50), their $c_v$ values are low or medium (0.17-0.22). The corresponding data of these alloys have been highlighted in Table 4.3 in bold format.

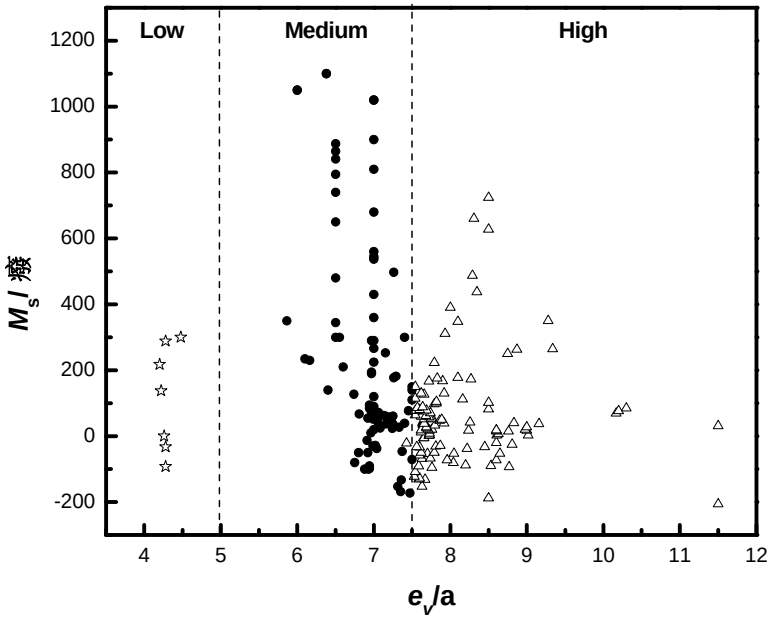


(a)

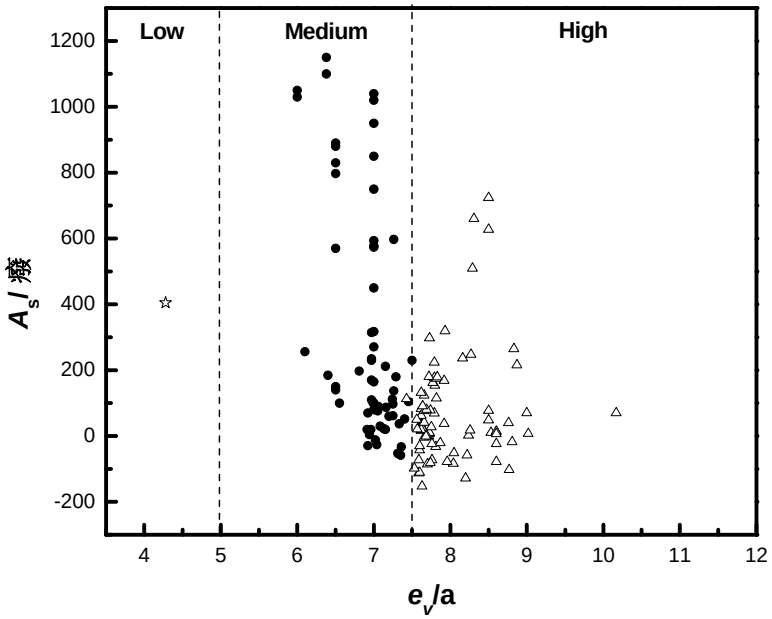


(b)

Figure 4.1: Variations of (a) $M_s$ and (b) $A_s$ with the number of valence electrons.

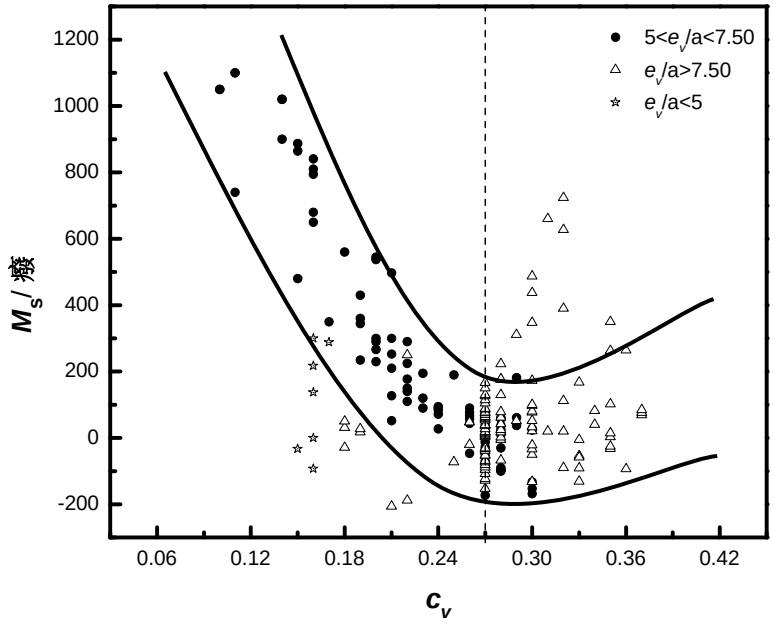


(a)

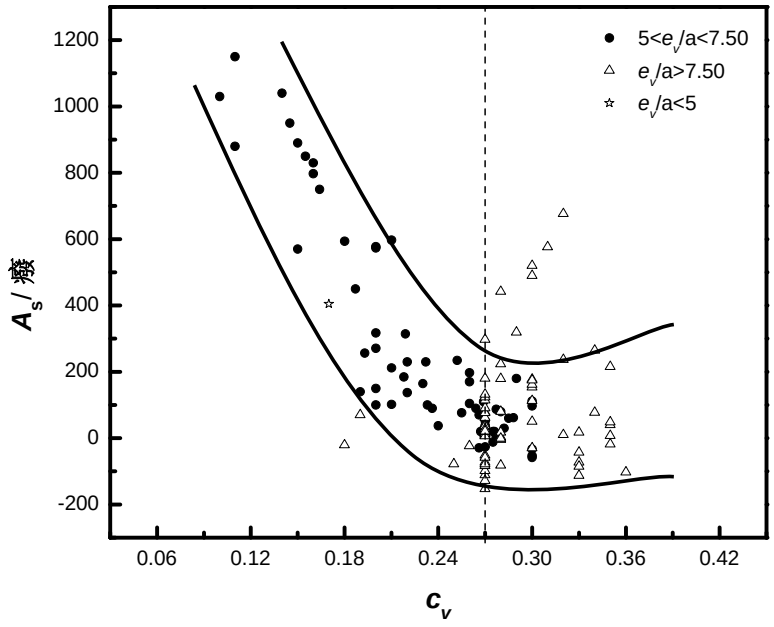


(b)

Figure 4.2: Variations of (a) $M_s$ and (b) $A_s$ with the valence electron concentration. The data in Figure 4.2 are the experimental values extracted for more than 200 alloys; each data point is very exact as is the result of precise DSC measurements which has been repeated. However, the trends of variation with $c_v$ show a scatter of data which can be represented by the $M_s$ or $A_s$ value ±100˚C.

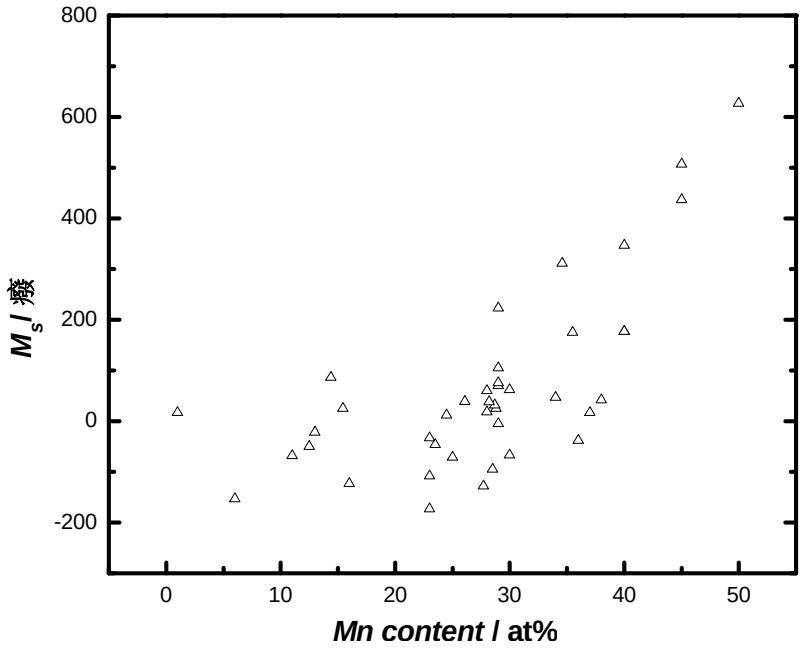


Figure 4.3: The effect of Mn content in Heusler alloys on the transformation temperatures. The data correspond to all the NiMn and NiMnX(X=Ga,In, Al,…) alloys listed in Tables 4.2 and 4.3. However it does not include NiMnGaSn or NiMnGaSb alloys in which Sb and Sn cancel the effect of antiferrmagnetism of excess Mn.

#### 4.2.3.3 Low valence electron alloys ($e_v/a<5$)

There are a limited number of TiNb-based alloys with low electron concentration (on average 0.15), and low number of valence electrons ($e_v/a<5$) which have $M_s$ and $A_s$ values lower than what is observed for ordinary alloys with similar electron concentrations. These alloys tend to have an average atomic number of around 25. These data points have been shown by stars outside the main trend in Figure 4.2.

## 4.3 Discussion

### 4.3.1 Valence electron concentration, elastic properties, and transformation temperatures

In order to understand the fundamental reason behind the influence of the main factor, $c_{v,}$ on martensitic transformation temperature of shape memory alloys, the

relationship between valence electron concentration, elastic properties and transformation temperatures of the alloys are discussed here.

In the metallic bonding the valence electrons act like 'glue', bonding non-valence electrons and ion kernels together; whereas non-valence electrons contribute to the total atomic volume of the alloy [50,181,183]. The way the strengths of particular bonds in the alloys are influenced by the change of $c_v$ remains to be investigated in detail. However, one possible explanation may be provided. Increasing valence electron concentration could mean thickening of the 'glue' bonding the ionic kernels together. In fact, an established empirical relationship between the valence electron concentration and bulk modulus of metallic materials and intermetallic compounds is known [180]. Higher valence electron concentration usually results in higher bulk and therefore shears moduli [179,180]. Bulk modulus is a measure of resistance of a solid to volume change and shear modulus is a measure of resistance to shape change [179,180]. Increasing the valence electron concentration of the alloys, results in higher elastic and shear moduli, at least in particular crystallographic directions. This has been empirically shown in transition metals and alloys [179,180]. It is thus logical to think that change of valence electron concentration is accompanied by a change in the elastic constant as the interatomic bonding is affected [50,180]. The key factor controlling the bonding is the electronic structure of the alloy. Martensitic transformation brings about a crystal shape change in different alloy systems. For instance in NiTi-based SMAs the austenite body centered cubic transforms to a monoclinic or orthorhombic shape. This shape change is resisted by the bond strength of the parent crystal at least in specific crystallographic directions. Thus, the elastic properties of the parent phase are extremely important in determining when the lattice pressure for shape change can overcome the resistance of the bonds in particular crystallographic directions for the shear to take place. The bond strengths are controlled by the density of valence electrons. Before martensitic transformation the elastic moduli decrease during cooling and reach a critical value [11]. If the elastic moduli of austenite is enhanced as a result of higher $c_v$, the cooling should continue to lower temperatures before a critical elastic constant is reached as a result of pre-martensitic softening of bulk and/or shear moduli, hence $M_s$ is decreased. On the contrary, if the alloy has lower elastic bulk and shear moduli in austenite phase, the critical elastic constant can be reached at higher temperatures and $M_s$ is increased. The decreasing trend continues until the electron concentration reaches around 0.27 and

remains in a relatively constant range for most alloys beyond this range. A possible explanation is that the 'glue' that was referred to, becomes too thick, and further increase in its thickness does not fortify the bonds, rather at very high $c_v$>0.34-0.35, high valence electron concentration may even cause antibonding and slight increase of the temperatures (Figure 4.2). $M_s$ is influenced based on the elastic constants of austenite and $A_s$ follows its variation on the basis of the degree of reversibility of transformation for each specific shape memory alloy. These explain why some of the shape memory alloy compositions have high and some others have low transformation temperatures.

Figure 4.2 which only shows the dependence of transformation temperatures on $c_v$ is formed based on the analysis of more than 200 alloys that belong to about 20 shape memory alloy systems such as NiTi, NiMnGa, NiMn, CuAlFe, etc. Although alloys of these systems, all show theroelastic shape memory behavior, however they differ from each other in many ways. This fact incorporates a number of other factors which can influence the elastic properties and transformation temperatures of the alloys. Difference between the crystal structure of parent and martensitic phases in these systems, presence or lack of magnetic properties, difference in electron orbital occupancy in alloy systems are examples of other factors that can influence the transformation temperatures even when alloys have the same $c_v$. The outcome is the scatter which has been represented by bands in the Figure 4.2. However, despite other influential factors which are not accounted for in this Figure, the influence of $c_v$ is so strong that can be observed from the Figure.

### 4.3.2 Effect of Mn

NiMnX (X=Ga, In, Al) Hesuler alloys with excess Mn and relatively high concentration of valence electrons show increased transformation temperatures (Figure 4.3) and therefore deviate from the main trend. As discussed, the concentration and number of valence electrons both play critical roles in elastic stiffness of the transition metal crystals but they do not usually act alone. The d-orbitals may become hybridized with p- and s-orbitals. Therefore, the occupancy behavior of the orbitals can also be influential. As one proceeds across one of the long rows of transition metals in the

periodic table of elements, the atomic volume changes relatively little but the elastic stiffness changes markedly, reaching a maximum near the middle of each row [180]. Mn is an exception in which the bonding is strongly affected by its anti-ferromagnetism [180]. The calculations of Moruzzi and Marcus indicate that the elastic moduli of Mn are considerably reduced due to anti-ferromagnetism [184]. In $Ni_{50}Mn_{25}Ga_{25}$, the Ni magnetic moment is much smaller than Mn moment. However, the Ni 3d state has a larger contribution to the electronic state near Fermi energy than Mn 3d state [205,206]. Therefore both elements play important roles in determining the properties of the alloy system [207]. When the Mn content of this Heusler alloy is high, it is possible that some of the anti-ferromagnetism of Mn can be maintained. This results in considerable reduction of the elastic moduli in particular direction and consequently the elevation of the transformation temperatures (Figure 4.2). Clear evidences of anti-ferromagnetism and/or negative magnetic moments on Mn atoms in NiMnGa alloys have been shown in some recent works [208,209]. It is possible that Mn-rich NiMnIn and NiMnAl alloys which also exhibit increased $M_s$ temperatures, are similarly affected by Mn antiferromagnetism. In depth clarification of the influence of Mn requires further study.

### 4.3.3 High valence electron alloys with medium or low electron concentration

In the alloys with $e_v$/a well above 7.50, the sensitivity of transformation temperature to the concentration of valence electrons is considerably reduced. This fact is evident from the plot of $M_s$-$c_v$ for these alloys (Figure 4.4). This implies that when the number of valence electrons is sufficiently high, the strength of the bonds and therefore elastic properties can be high even at medium $c_v$(0.17-0.24). This originates from the fact that higher number of valence electrons can provide sufficiently strong bonding for larger or denser ion kernels in the metallic bonds [180]. The net result is lower transformation temperature for these alloys and some degree of deviation from the main trend (Figure 4.1).

Some of the factors influencing the martensitic transformation of Cu-Zn and Cu-Zn-Al alloys have been discussed by Ahler [210]. The effect of heat treatment parameters such as cooling rate in quenching temperature and aging time prior to

quenching have been mentioned as influential. It has also been stated that in contrast to other noble alloys in Cu-Zn and CuZnAl alloys $M_s$ is not related to e/a (the number of electrons). Moreover, an interesting relationship between $M_s$ and monoclinic distoraion (c/a) in some alloys is shown. The review presented in the above pages indicates some of the factors specifically related to CuZn and CuZnAl alloy, based on alloy composition. For instance it is shown that increasing Zn content lowers $M_s$, or increasing monoclinic distortion decreases this temperature. In all of these, there is no explanation why these parameters are or are not affecting the $M_s$ temperature and the main outcome solely is that Ms temperature of the alloys is dependent on composition. Nonetheless, this type of work and the data are very valuable especially the lattice relationships data when collected in a comprehensive work may reveal some of other factors involved. From the view point of the approach presented in the current thesis which focuses on the large scale change of transformation temperature 100˚C or more, CuZn and CuZnAl alloys belong to high valence electron group of alloys. In this group the level of the dependence of the elastic properties of the parent crystals on the valence electron concentration is lower that the other alloys if the concentration of valence electrons is also high. However, elements like Zn can influence the number of valence electron which is also a factor affecting $M_s$, similarly as in these alloys s and d electrons are filled the electron occupancy in the orbitals is very influential but its effects very complex at this stage to explain and needs a number of separate studies. From the present work one important fact can be extracted and that is the influence of valence electron concentration needs to be considered in conjunction with the number of electrons and if known orbital occupancy.The lattice distortion relationship shown in some studies is an outcome of the change of composition and its effects on ion cores and lattice parameters which influence the elastic properties of the lattice and the corresponding change in the elastic properties and therefore transformation temperature.

### 4.3.4 Low valence electron alloys

The existing low valence electron alloys show $c_v$ values of 0.14-0.17, for which alloys in the main group have $M_s$ of usually more than 400˚C. In low electron alloys the $M_s$ values are significantly lower (-93-300˚C) than the main trend. These alloys contain considerable amount of Nb, and their average atomic number is nearly 25-26. The

elastic moduli of low valence electron Ti-based alloys have been studied by some researchers [211-213]. In Ti-based alloys the stability of austenite phase increases by increasing $e_v/a$ from nearly 4 by the solid solution strengthening with the addition of alloying elements near Ti group in periodic table [211].

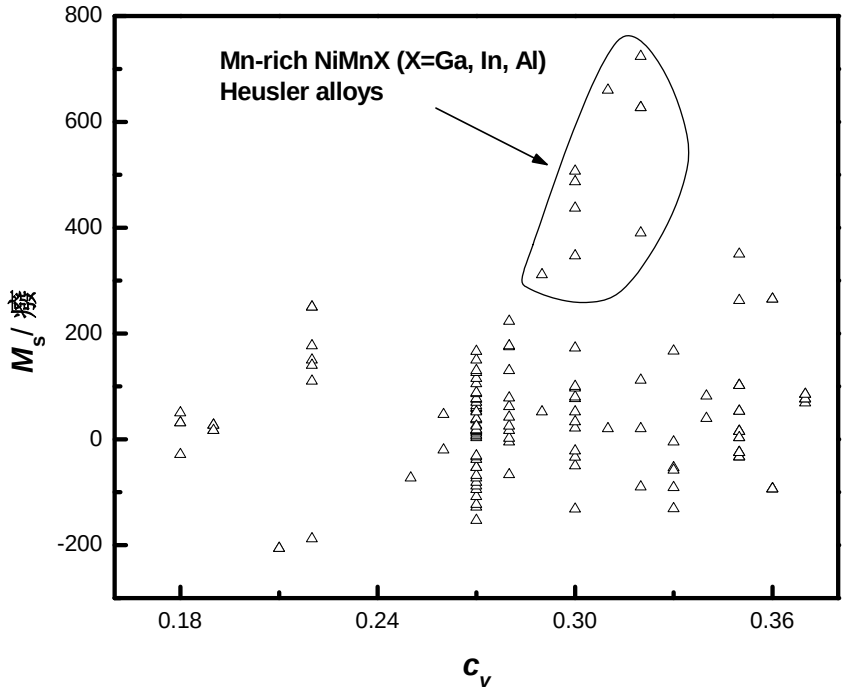


Figure 4.4: Variation of $M_s$ with valence electron concentration for high valence electron alloys.

There are reports of maximum elastic modulus of the alloy when the $e_v/a$ is in around 4.15 [212,213]. In terms of electronic structure of the alloys it is not clear why the austenite stability can be extended to lower temperatures. Apart from valence electron concentration, and the number of valence electrons per atom, the (average) atomic number of an alloy can also be influential on the mechanical and elastic properties of the material as was introduced in Chapter 2. The low valence electron alloys which are the subject of the study in this paragraph show an average atomic number of nearly 25 or 26 (the average atomic number is calculated based on the atomic fraction and atomic number of each element in the alloy). In terms of atomic number these alloys simulate a transition metal with the atomic number of almost 25 for which the electronic configuration can be written as: $1s^2 2s^2 2p^6 3s^2 3p^6 4s^2 3d^5$. In transition metals and alloys, in the condition where the d orbital is nearly half filled (d=5 or 6), usually the elastic moduli are maximum compared to higher or lower d occupancies [180]. Higher elastic

moduli of the parent phase results in lower martensitic transformation. When the alloy deviates from this maximum elastic moduli condition (higher or lower $e_v$/a), the transformation temperatures is expected to be higher. This may be indicative of the considerable influence of orbital occupancy behavior on the elastic properties and transformation temperature of the shape memory alloys with low valence electrons.

Collins has referred to the importance of $e_v$/a of Ti-based alloys as an influential factor affecting $M_s$ temperature [214]. Some empirical relationship between the e/a and elastic properties have been presented. The significance of $e_v$/a =4.15 as a specific value for the elastic properties of these alloys have been described. However, there is no explanation why $e_v$/a is influencing the elastic properties. In the present work the importance of e/a, ion core size, and orbital electron occupancy has been briefly described as important factors affecting the elastic properties of the crystals (section 2.5.1, 2.5.2). Moreover, in section 4.3 for low electron alloys it was explained that when the number of $e_v$/a is low ($e_v$/a<5) i.e. in the case of Ti-based alloys, the influence of orbital occupancy of electrons and the atomic number is considerably increased. There are reports of maximum elastic modulus of these alloys when the $e_v$/a is in around 4.15 [211,212]. In terms of electronic structure of the alloys it is not clear why the austenite stability can be extended to lower temperatures. Apart from valence electron concentration, and the number of valence electrons per atom, the (average) atomic number of an alloy can also be influential on the mechanical and elastic properties of the material as was introduced in Chapter 2. It was disscused previously that the atomic number of these alloys makes them special as it influences their elastic properties and transformation temperatures.

In general the idea of the influence of the electronic structure on the transformation temperature in Ti-based alloys have been on and off presented in the last 3 decades. Some have taken it from the Hume-Rothery rules which dates back to even older times, and some have tried to look at the influence of the number of electron per atom ($e_v$/a). In the last decade theoretical attempts to use first-principle calculations to explain the influence of electrons have been tried without any solid results. Moreover, in magnetic shape memory alloys the influence of the number of electrons per atom has been shown to affect the transformation temperatures of these alloys. However, one important point in all of these has been missing which is how the elastic properties of

the crystals are linked to the electronic structure. The key point has been introduced and demonstrated in the current work which is the relationship of valence electron concentration (density) and elastic bulk and shear moduli of the alloys and therefore transformation temperature. It is the first time that this dimension of the influence of the electronic structure has been presented.

## 4.4 Summary

Dependence of transformation temperatures of shape memory alloys on the number and concentration of valence electrons are studied. The shape memory alloys are categorized into low ($e_v$/a<5), medium (5≤$e_v$/a≤7.50), and high ($e_v$/a>7.50) valence electron groups. For majority of alloys in medium and high valence electron group, clear correlations between transformation temperatures and their valence electron concentration ($c_v$) are found. $M_s$ and $A_s$ both decrease from 1100 and 1150˚C to as low as -206˚C and -153˚C respectively, with increasing $c_v$ from 0.10 to around 0.30. When the number of valence electrons per atom is high ($e_v$/a>7.50), the transformation temperatures show much less dependence on $c_v$. High electron NiMnX (X=Ga, In, Al) Heusler alloys containing Mn (>30 at%) show high transformation temperatures at high $c_v$ values most likely due to anti-ferromagnetism of excess Mn which reduces the elastic moduli. The low valence electron group shows significantly lower transformation temperatures for their $c_v$ values compared to the main group.

# Chapter 5

# 5 Dependence of Transformation Temperatures of NiTi-based Shape Memory Alloys on the Number and Concentration of Valence Electrons

## 5.1 Introduction

Addition of various transition metals to NiTi that either elevate or lower the transformation temperatures has been studied, part of which has been reviewed by Otsuka et al. [11]. Apart from the selection of alloying elements, their replacement for Ni, Ti or both is also of paramount importance. For instance, when W is added to replace Ni, the $M_s$ temperature is above room temperature; whereas when it replaces Ti, the $M_s$ temperature drops to below room temperature [30].

Despite numerous studies on modification of the NiTi transformation temperatures by adding ternary or quaternary elements, very little work has been done to understand the fundamental reason for these changes. In shape memory alloys, prior to martensitic transformation a softening of elastic constant occurs with lowering temperature. Experimental results, mainly in Cu-based and also in NiTi-based shape memory alloys [7-10] suggest that there is a critical value of elastic constant at which transformation takes place which is not sensitive to alloy compositions [4], and is only slightly dependant on temperature [11]. Based on this, the elastic modulus of the alloy, which is dependent on both composition and temperature [11,12], is thought to influence the transformation temperatures. However, it is not clear how the addition of different alloying elements to NiTi is linked with the elastic properties and therefore the transformation temperatures.

In the present chapter, we have examined the electronic structures of various ternary and quaternary NiTi-based alloys based on the method shown in the previous chapter and correlated them to the transformation temperatures. Similarly, two parameters are paid attention to: 1) the number of valence electron per atom, and 2)

the valence electron concentration of the alloy. The correlations discovered in this study help to fundamentally understand the influence of alloying elements on the transformation temperatures of shape memory alloys, thus enabling more effective alloy design.

## 5.2 Analysis

A survey of the literature reveals that the addition of Fe, V, Mn, Co, Cu, Zr, Nb, Mo, Pd, Ag, Hf, Ta, W, Re, Pt, Au, affects the transformation temperatures of NiTi-based alloys. Particularly, addition of Fe, V, Mn, Co, Cu, and W for Ni and Re and Cu for Ti reduces the transformation temperatures; whereas addition of Hf, Zr, Ta, and W to replace Ti, or Pd, Pt, and Au to replace Ni, increases the transformation temperatures considerably. Table 5.1 lists the transformation temperatures ($M_s$, $A_s$, and hysteresis) for 50 ternary or quaternary alloys which cover nearly all the ternary and quaternary transition metals added to NiTi. In the present work only solution treated alloys have been considered to minimize the effects of precipitates and mechanical work. The possible effect of grain size or morphology has not been considered. The transformation temperature data were extracted from the relevant literature as listed in tables or presented in graphs. The variations of both the number of valence electron per atom and the valence electron concentration due to addition of alloying elements are presented in the following sections.

### 5.2.1 Number of valence electrons per atom of the alloy

The valence electrons are electrons in the outermost principal quantum level of an atom. For transition metals the valence electrons are usually considered as the number of d and s electrons for an atom. In equiatomic NiTi alloy, the electronic configurations of Ti and Ni, are, Ti: $1s^2 2s^2 2p^6 3s^2 3p^6 4s^2 3d^2$, Ni: $1s^2 2s^2 2p^6 3s^2 3p^6 4s^2 3d^8$, and the number of valence electrons, ($e_v$), of these elements are $e_v^{Ti} = 4$, $e_v^{Ni} = 10$. Therefore, the average valence electrons per atom of the alloy $e_v/a = (4+10)/2 = 7$. As a result of the addition of an alloying element, $e_v/a$ may remain constant (for replacing Ti or Ni with an element from the same group in the periodic table) or may change (by replacing Ti or Ni with an element not from the same group in the periodic table). The

valence electrons per atom of ternary and quaternary alloys can be calculated based on the atomic fraction of the elements in the alloy by Eq. 5.1:

$$\frac{e_v}{a} = f_{Ni}e_v^{Ni} + f_{Ti}e_v^{Ti} + f_T e_v^T + f_Q e_v^Q \quad (5.1)$$

Table 5.1: Ms, As, transformation hysteresis, ev/a and cv of a number of ternary and quaternary NiTi-based shape memory alloys. References show the source of transformation temperatures and hysteresis. The hysteresis values are calculated based on Ap-Mp as reported or based on the DSC or resistometry results presented in the original literature. The values designated by (*) are based on Af-Ms data, and those designated by (+) are approximated by Af-Ms estimated from the experimental curves presented in the relevant literature.

| Alloy | $M_s$ [˚C] | $A_s$ [˚C] | Hysteresis [˚C] | $e_v$/a [*e*/atom] | $c_v$ | Ref. |
|---|---|---|---|---|---|---|
| $Ni_{43}Ti_{50}Co_7$ | -100 | - | - | 6.93 | 0.278 | [11] |
| $Ni_{44}Ti_{50}Fe_6$ | -100 | - | - | 6.88 | 0.277 | [27] |
| $Ni_{47}Ti_{50}Fe_3$ | -98 | - | - | 6.94 | 0.278 | [11] |
| $Ni_{48.5}Ti_{50}Cr_{1.5}$ | -95 | - | - | 6.94 | 0.278 | [11] |
| $Ni_{48}Ti_{50}Mn_2$ | -95 | - | - | 6.94 | 0.278 | [11] |
| $Ni_{47.5}Ti_{50}Fe_2Mo_{0.5}$ | -90 | 5 | 52 | 6.94 | 0.277 | [33] |
| $Ni_{45}Ti_{50}V_5$ | -80 | - | - | 6.75 | 0.273 | [11] |
| $Ni_{46}Ti_{50}V_4$ | -50 | - | - | 6.80 | 0.274 | [11] |
| $Ni_{47.6}Ti_{46.4}Nb_6$ | -50 | -29 | - | 6.92 | 0.266 | [28] |
| $Ni_{50}Ti_{48}W_2$ | -37 | -26 | 39 | 7.04 | 0.270 | [30] |
| $Ni_{42.5}Ti_{42.5}Cu_{15}$ | -34 | -30 | 10 | 7.60 | 0.296 | This study |
| $Ni_{46}Ti_{50}Cu_3Mo_1$ | -30 | - | - | 6.99 | 0.277 | [35] |
| $Ni_{50}Ti_{49}W_1$ | -28 | -12 | 36 | 7.02 | 0.275 | [30] |
| $Ni_{48.3}Ti_{51}Mo_{0.7}$ | -13 | 20 | - | 6.91 | 0.275 | [29] |
| $Ni_{49}Ti_{50}Mo_1$ | 10 | 20 | 36 | 6.96 | 0.276 | [29] |
| $Ni_{45}Ti_{50}Pd_5$ | 20 | - | - | 7.00 | 0.270 | [11] |
| $Ni_{39.5}Ti_{49.5}Cu_{10}Cr_1$ | 25 | 30 | 14 | 7.08 | 0.282 | [38] |
| $Ni_{52}Ti_{46.74}Re_{1.26}$ | 37 | 87 | 55 | 7.16 | 0.277 | [31] |
| $Ni_{50}Ti_{45}Ta_5$ | 44 | 76 | 53 | 7.05 | 0.255 | [30] |
| $Ni_{48}Ti_{50}W_2$ | 55 | 70 | 29 | 6.92 | 0.266 | [30] |

| | | | | | | |
|---|---|---|---|---|---|---|
| $Ni_{50}Ti_{47}Ta_3$ | 58 | 90 | 48 | 7.03 | 0.264 | [22] |
| $Ni_{30}Ti_{50}Cu_{20}$ | 58 | 60 | 6 | 7.20 | 0.285 | [36] |
| $Ni_{25}Ti_{50}Cu_{25}$ | 61 | 62 | 5 | 7.25 | 0.288 | [41] |
| $Ni_{42}Ti_{49}Ag_9$ | 61 | 20 | 14* | 7.15 | 0.267 | [25] |
| $Ni_{44}Ti_{49}Ag_7$ | 63 | 23 | 14* | 7.13 | 0.270 | [25] |
| $Ni_{49.5}Ti_{45.5}Zr_5$ | 70 | 110 | 66 | 6.97 | 0.269 | [19] |
| $Ni_{44}Ti_{40}Hf_{10}Cu_6$ | 72 | 90 | 40 | 7.06 | 0.236 | [32] |
| $Ni_{48}Ti_{50}Au_2$ | 75 | - | - | 7.02 | 0.268 | [21] |
| $Ni_{29}Ti_{51}Pd_{20}$ | 85 | - | 20 | 6.94 | 0.243 | [39] |
| $Ni_{49.5}Ti_{40.5}Zr_{10}$ | 90 | 170 | 68 | 6.97 | 0.260 | [19] |
| $Ni_{30}Ti_{50}Pd_{20}$ | 90 | | | 7.00 | 0.244 | [11] |
| $Ni_{40}Ti_{50}Pt_{10}$ | 90 | 100 | 20 | 7.00 | 0.233 | [46] |
| $Ni_{26.5}Ti_{51}Pd_{22.5}$ | 95 | - | | 6.94 | 0.239 | [39] |
| $Ni_{50}Ti_{40}Hf_{10}$ | 120 | 165 | 65 | 7.00 | 0.233 | [32] |
| $Ni_{40}Ti_{50}Hf_{10}$ | 140 | 185 | 65 | 6.40 | 0.218 | This study |
| $Ni_{22.5}Ti_{52.5}Pd_{25}$ | 170 | - | 15 | 6.85 | 0.234 | [39] |
| $Ni_{49.5}Ti_{35.5}Zr_{15}$ | 190 | 235 | 41 | 6.97 | 0.252 | [19] |
| $Ni_{49.5}Ti_{35.5}Hf_{7.5}Zr_{7.5}$ | 195 | 230 | 42 | 6.97 | 0.232 | [37] |
| $Ni_{15}Ti_{50}Pd_{35}$ | 225 | - | 15 | 7.00 | 0.224 | [39] |
| $Ni_{36}Ti_{49}Hf_{15}$ | 230 | - | | 6.16 | 0.195 | [11] |
| $Ni_{35}Ti_{50}Hf_{15}$ | 235 | 256 | 55 | 6.10 | 0.193 | This study |
| $Ni_{30}Ti_{50}Pt_{20}$ | 266 | 271 | 31 | 7.00 | 0.200 | [46,47] |
| $Ni_{49.5}Ti_{30.5}Hf_{10}Zr_{10}$ | 290 | 315 | 50 | 6.97 | 0.219 | [37] |
| $Ni_{50}Ti_{30}Hf_{20}$ | 290 | 317 | 60 | 7.00 | 0.200 | This study |
| $Ni_{31}Ti_{49}Hf_{20}$ | 350 | - | - | 5.86 | 0.173 | [11] |
| $Ni_{25}Ti_{50}Pt_{25}$ | 430 | 450 | $40^+$ | 7.00 | 0.187 | [46] |
| $Ni_{20}Ti_{50}Pt_{30}$ | 560 | 594 | 55 | 7.00 | 0.176 | [47] |
| $Ni_{15}Ti_{50}Pt_{35}$ | 680 | 750 | - | 7.00 | 0.164 | [46] |
| $Ni_{10}Ti_{50}Pt_{40}$ | 810 | 850 | - | 7.00 | 0.155 | [46] |
| $Ni_5Ti_{50}Pt_{45}$ | 900 | 950 | - | 7.00 | 0.145 | [46] |

where $f_{Ni}$, $f_{Ti}$, and $f_T$ and $f_Q$ represent the atomic fractions of elements in the alloy for Ni, Ti, ternary and quaternary elements, and $e_v^{Ni}$, $e_v^{Ti}$, $e_v^T$ and $e_v^Q$ are the corresponding number of valence electrons of Ni, Ti and the ternary and quaternary elements, respectively. The calculated values for alloys in this study are within 6.10-7.20 range. Figure 5.1 illustrates the significant variations of $M_s$ and $A_s$ with the $e_v$/a ratio. For both cases, two distinct conditions are observed, i.e., $e_v$/a ≠ 7, and $e_v$/a = 7.

**$e_v$/a ≠ 7:** When $e_v$/a ≠ 7, three regions of variations are observed. 1) $e_v$/a<6.8 in which the $M_s$ and $A_s$ temperatures decrease with increasing the ratio, 2) 6.8<$e_v$/a<7.2 in which the $M_s$ and $A_s$ temperature data are scattered with no clear tendency with respect to $e_v$/a (Figure 5.1), and 3) one data point with $e_v$/a>7.2 which has slightly lower $M_s$ and $A_s$ temperatures compared to the alloys with $e_v$/a<6.8.

**$e_v$/a = 7:** At $e_v$/a = 7, $M_s$ and $A_s$ exhibit a broad range from ambient temperature to temperatures as high as 950˚C. According to Figure 1, it seems that $e_v$/a = 7 is an important condition for obtaining very high transformation temperatures. Figure 5.1 also suggests that other factors play a part in determining the transformation temperatures that will be examined in the following section.

### 5.2.2 Valence electron concentration

The average concentration of valence electrons $c_v$ of an alloy can be defined as the ratio of number of valence electrons to the total number of electrons of the alloy, $c_v = (e_v/e_t)$, which can be simply calculated as follows (Eq. 5.2):

$$c_v = \frac{e_v}{e_t} = \frac{f_{Ni}e_v^{Ni} + f_{Ti}e_v^{Ti} + f_T e_v^T + f_Q e_v^Q}{f_{Ni}Z_{Ni} + f_{Ti}Z_{Ti} + f_T Z_T + f_Q Z_Q} \qquad (5.2)$$

where $Z_{Ni}$, $Z_{Ti}$, $Z_T$, and $Z_Q$ represent the atomic numbers of Ni, Ti, ternary and quaternary elements, respectively. Depending on the alloying elements, atomic fractions and replacement sites (either for Ni or Ti, or both) different $c_v$ values are resulted. These values for NiTi-based alloys are reported in Table 5.1 and plotted in Figure 5.2. $M_s$ and $A_s$ temperatures are found to vary significantly with increasing $c_v$. By increasing the valence electron concentration $M_s$ decreases from 900˚C to -160˚C and $A_s$ also decreases with increasing $c_v$, from 950˚C down to -30˚C.

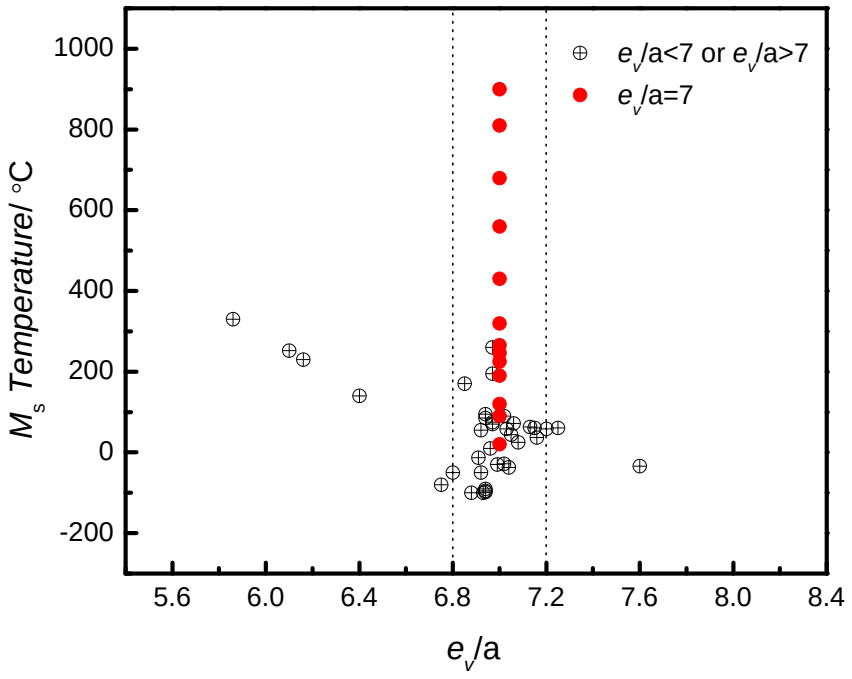


(a)

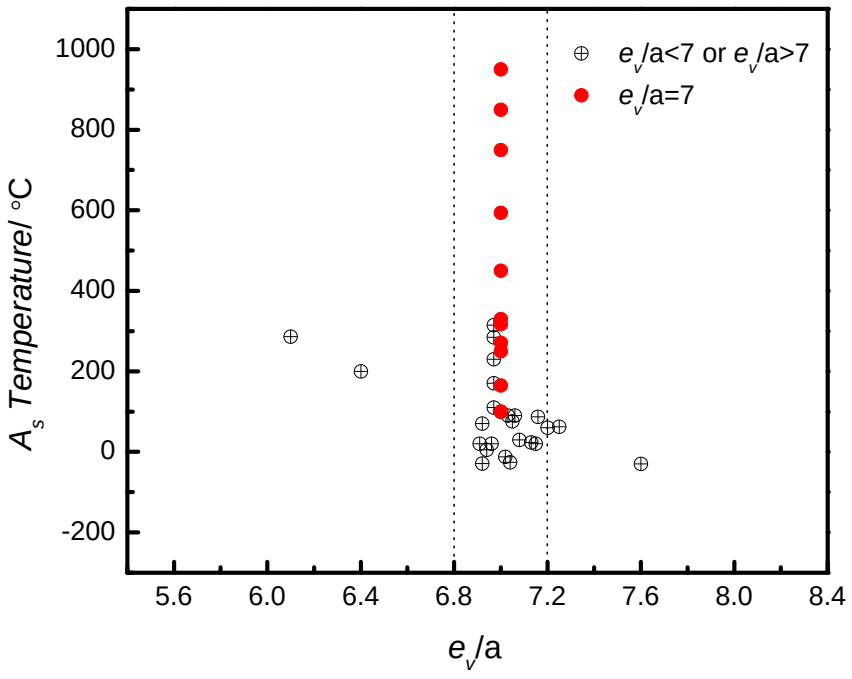


(b)

Figure 5.1: Variations of $M_s$ and $A_s$ with the number of valence electron per atom ($e_v$/a) of NiTi-based ternary and quaternary alloys, (a) Martensite start, (b) Austenite start temperatures.

### 5.2.3 Transformation hysteresis

Figure 5.3 illustrate a plot of transformation hysteresis as a function of the atomic size (radius) of the alloying elements in NiTi-based shape memory alloys. The data represent only the alloys (from Table 1) with $e_v$/a of 7 or close to 7 ($6.97 \leq e_v/a \leq 7$), and 20 at% alloying elements. For these alloys the transformation hsyteresis seems to be influenced by the atomic size of the alloying elements. By increasing the atomic size at almost constant $e_v$/a the transformation hysteresis is increased (Figure 5.3).

## 5.3 Discussion

### 5.3.1 d-d overlapping occupancies, valence electron concentration

The variation of transformation temperatures and hysteresis with $e_v$/a clearly indicates two distinct trends of variations, one corresponding to incomplete d-d overlapping electron occupancy when ($e_v$/a) ≠ 7 and, one to the complete d-d overlapping electron occupancy ($e_v$/a = 7). Overlapping orbital occupancy is the way the d orbitals of Ni, Ti and alloying elements fill up each others unoccupied orbital of very similar energies. For instance Ni atoms (d8) and Ti atoms (d2) overlap part of their d orbitals to completely fill up their common d=10 orbital. When the d–d overlapped orbital is completely filled, a broad range of transformation temperatures, which can be as high as nearly 900˚C for $M_s$, and 950˚C for $A_s$ are observed. In this condition $e_v$/a is not the controlling factor of transformation temperature (as it is constant) (Figure 5.1a). This clearly shows that the transformation temperature is very much dependant on whether or not the d-d overlapping in the alloy is complete or incomplete. This fact can be one of the useful tools for design of NiTi-based shape memory materials with expected transformation temperatures. Among the alloys with ($e_v$/a) = 7 when the total number of electrons ($e_t$) increases, the transformation temperatures increase. This indicates that not only the average valence electron but also the number of total electrons are influential. In Figure 5.2 it was shown that valence electron concentration ($c_v = e_v/e_t$) exhibits clear relationship with $M_s$ and $A_s$ temperatures. The relationships of $M_s$-$c_v$ of

$A_s$-$c_v$ may serve as useful tools for the design and approximate adjustment of the transformation temperatures of new alloys.

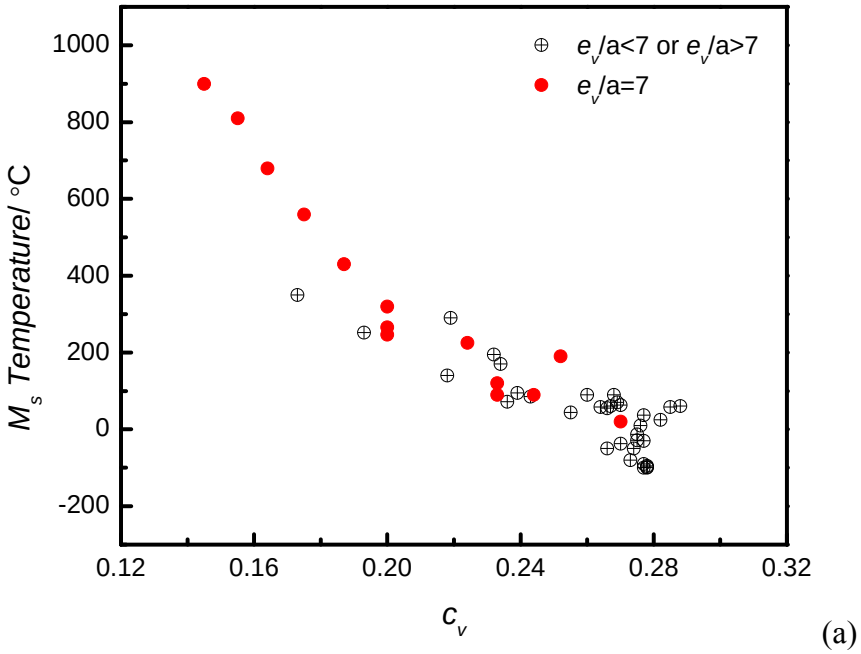


(a)

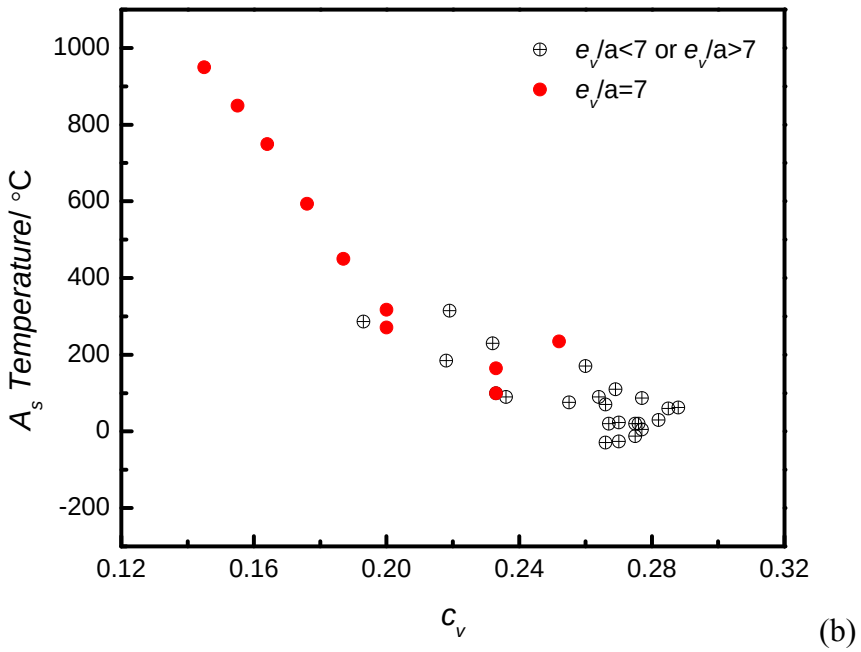


(b)

Figure 5.2: Dependence of $M_s$ and $A_s$ on valence electron concentration of NiTi-based ternary and quaternary alloys, (a) Martensite start temperature, (b) Austenite start temperature.

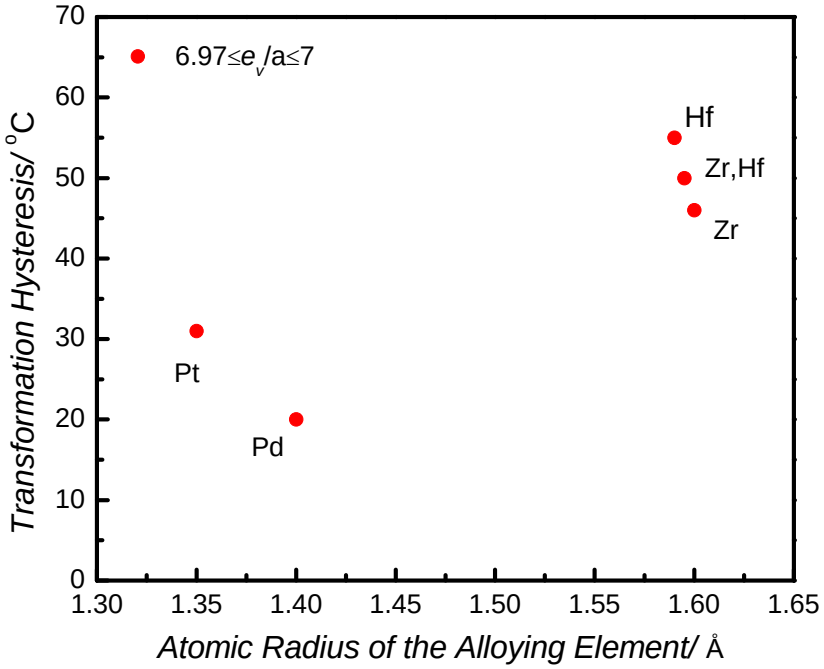


Figure 5.3: Dependence of transformation hysteresis of NiTi-based alloys on the atomic radius of the alloying elements. The alloys have $6.97 \leq e_v/a \leq 7$ ($e_v/a \approx 7$), and 20 at.% of alloying elements.

### 5.3.2 Valence electrons, elastic moduli, and transformation temperatures

Although at this stage it is difficult to comprehensively understand the fundamental reason behind the influence of the main factor, $c_{v,}$ on martensitic transformation, however, some relationships can be discussed here.

It is known that in the metallic bonding the valence electrons act like 'glue', bonding non-valence electrons and nuclei units together [50,183]; whereas non-valence electrons contribute to the total atomic volume of the alloy. There are three types of bonds in NiTi alloys (Ni-Ni, Ti-Ti and Ni-Ti) some of which are replaced by substitution of the alloying elements. The way the average strengths of these bonds are influenced by the change of $c_v$ remains to be clarified. However, one possible explanation could be the effect of valence electron densities (VED: number of valence electrons in the unit volume of the crystal). In Table 5.2 the values of VED of selected

alloys (based on availability of lattice parameters in the literature) in both austenite and martensite phases are reported along with the $c_v$ values. In general it is clear that the trend of VED in both austenite and martensite is similar to that of $c_v$ as alloys with higher $c_v$ show higher VEDs. The general decreasing trend of $M_s$ and $A_s$ temperatures with increasing VED is illustrated in Figure 5.4 which is to a large extent similar to variations of $M_s$ and $A_s$ with increasing $c_v$. Increasing $c_v$ translates into increasing valence electrons and/or decreasing atomic volume of the alloy due to less number of non-valence bonds. These in turn, can result in higher VED. On the other hand, an established relationship between the VED and bulk modulus of metallic materials and intermetallic compounds is known. Higher VED results in higher bulk and therefore shear modulus (which is usually approximated by 3/5 of bulk modulus in metals and alloys) of the alloy [179,180]. Bulk modulus is a measure of resistance of a solid to volume change and shear modulus is a measure of resistance to shape change [179,180]. Increasing valence electron concentration or in other words, valence electron density of the ternary and quaternary NiTi-based alloys therefore is expected to result in higher elastic and shear moduli. It is thus logical to think that introduction of a ternary element to NiTi is accompanied by a change in the elastic constant as the interatomic bonding is affected. The key factor controlling the bonding is the electronic structure of the alloy.

Table 5.2: Comparison of VED in austenite ($VED_a$) and martensite ($VED_m$) with $c_v$. $V_a$ and $V_m$ are the unit cell volumes of austenite and martensite, respectively. The references related to the source of $V_a$ and $V_m$ are listed.

| Alloy | $e_v$/a ($e$/atom) | $V_a$ (Å$^3$) | $V_m$ (Å$^3$) | $VED_a$ ($e$/Å$^3$) | $VED_m$ ($e$/Å$^3$) | $c_v$ | Ref. |
|---|---|---|---|---|---|---|---|
| $Ni_{25}Ti_{50}Cu_{25}$ | 7.25 | 28.37 | 57.08 | 0.255 | 0.254 | 0.285 | [37] |
| $Ni_{50}Ti_{45}Ta_5$ | 7.05 | - | 55.51 | - | 0.254 | 0.255 | [14] |
| $Ni_{50}Ti_{47}Ta_3$ | 7.03 | 27.68 | 55.79 | 0.254 | 0.252 | 0.264 | [34] |
| $Ni_{49.8}Ti_{41.7}Hf_{9.5}$ | 7.03 | 28.41 | 57.06 | 0.246 | 0.245 | 0.235 | [35] |
| $Ni_{49.5}Ti_{40.5}Zr_{10}$ | 6.97 | - | 56.90 | - | 0.245 | 0.260 | [11] |
| $Ni_{49.5}Ti_{33.5}Hf_{7.5}Zr_{7.5}$ | 6.97 | - | 58.08 | - | 0.240 | 0.232 | [35] |
| $Ni_{49.8}Ti_{35.2}Hf_{15}$ | 6.99 | 29.13 | 58.25 | 0.240 | 0.240 | 0.215 | [35] |
| $Ni_{49.5}Ti_{30.5}Zr_{20}$ | 6.97 | - | 58.57 | - | 0.238 | 0.244 | [11] |
| $Ni_{49.8}Ti_{30.2}Hf_{20}$ | 6.99 | 29.74 | 59.23 | 0.235 | 0.236 | 0.200 | [35] |
| $Ni_{49.5}Ti_{30.5}Hf_{10}Zr_{10}$ | 6.97 | - | 59.32 | - | 0.235 | 0.219 | [29] |
| $Ni_{10}Ti_{50}Pd_{40}$ | 7.00 | - | 60.87 | - | 0.230 | 0.217 | [36] |

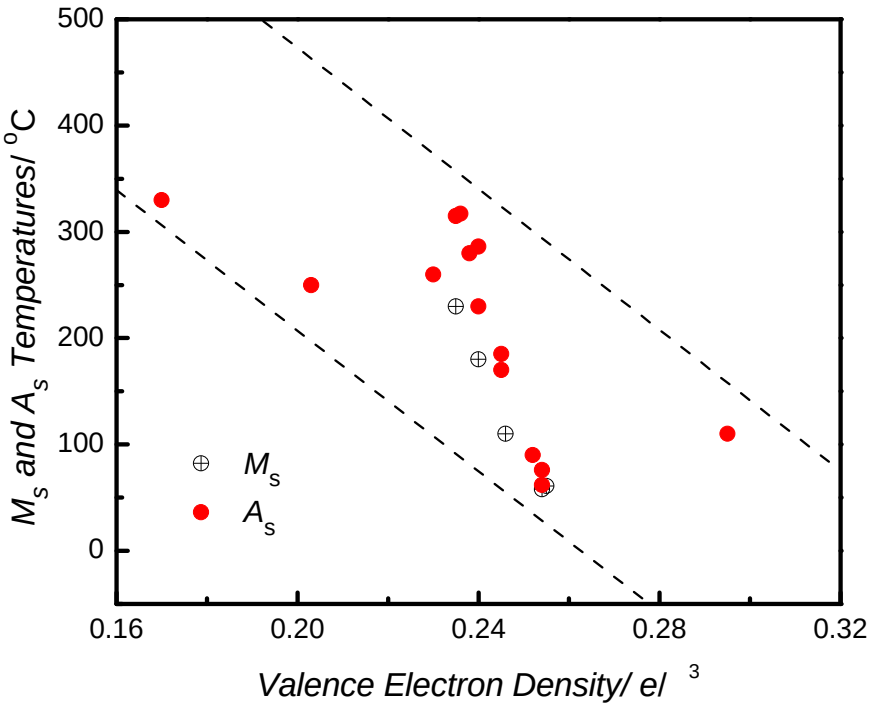


Figure 5.4: Variation of $M_s$ and $A_s$ with VED of the alloys.

The elastic moduli decrease during cooling and reaches a critical value before martensitic transformation [11]. If the modulus of elasticity of austenite becomes larger the cooling should continue to lower temperatures before a critical elastic constant is reached as a result of pre-martensitic softening of c' and $c_{44}$, hence $M_s$ is decreased. On the contrary, if the ternary or quaternary alloy has lower elastic bulk and shear moduli than binary NiTi in austenite phase, the critical elastic constant can be reached at higher temperatures and $M_s$ is increased.

A similar trend for $A_s$ is observed as it follows the variation of $M_s$ associated with transformation hysteresis. These may explain why some of the ternary and quaternary elements lower and some elevate the transformation temperatures.

The clarification of particular softening behavior of the shear moduli (c' and $c_{44}$) as a result of valence electron variations due to alloying would provide more understanding on the change of transformation temperatures and transformation routes in alloys.

### 5.3.3 Transformation hysteresis

The temperature hysteresis can have a relatively broad range of values (Table 5.1). At nearly constant $e_v/a=7$ ($6.97 \leq e_v/a \leq 7$) and constant atomic percentage of alloying element (20 at%), the effect of atomic size of the alloying elements seems to play a role (Figure 5.3). By increasing the size of the alloying elements without significant change in the number of valence electrons, the hysteresis is increased. Two energy dissipation processes in the transformation may be addressed that contribute to the hysteresis. First, energy dissipation related resistance of the interatomic bonds, and second the atomic re-arrangement and volume change associated with the transformation. It is possible that higher atomic size of the alloying elements results in more energy dissipation as volume work during transformation which leads to increased hysteresis. Variation of the valence electron combined with a change in the size of the alloying elements adds to the complexity of the phenomenon.

Ortin et al [69] have shown that in thermoelastic martensitic transformation the heat released or absorbed by specimen is due to a triple contribution: the latent heat of transformation, the reversibly stored elastic enthalpy and the irreversible work mainly spent in moving the interfaces. The thermoelastic behaviour is a condition of local balance between chemical and non-chemical forces. The condition is reached at the interfaces which are moving at a given temperature, during both the forward and reverse transformations. Chemical forces arise from the difference in Gibbs free energy between austenite and martensite, and act as a driving force promoting the phase with lower energy at each temperature. The chemical forces are a structural contribution in-the sense that their origin is the different atomic structure of austenite and martensite. Non-chemical forces can be acknowledged to arise from two main different contributions. The first one is the need to accommodate the transformational shape and volume changes. If accommodation takes place elastically; the associated elastic energy is stored in the specimen during the transformation from austenite to martensite, and reversibly recovered during the reverse transformation. Elastic accommodation of the transformational shape and volume changes is a necessary and sufficient condition for thermoelastic behaviour. The second contribution is the energy dissipated in the specimen as internal work during the transformation. The internal work is mainly devoted to overcome frictional barriers opposing interracial motion,

either during growth or during shrinkage of the martensite plates. This contribution represents the irreversible part of the non-chemical energies and is responsible for the thermal hysteresis observed in many thermoelastic transformations. Almost all the mechanical properties of the interfaces and faces including are directly related to the atomic and electronic parameters comprising it. These include size, arrangement, crystal structure, electron density and number of the atoms within the phases and on the interfaces. Increasing bond resistance by increasing electron density and in many cases by the change of the crystal structure volume through incorporation of larger atoms significantly influences the mobility of interfaces and results in a change in the internal energy dissipate and therefore alters the temperature hysteresis.

## 5.4 Summary

Dependence of transformation temperatures of NiTi-based shape memory alloys on the number and concentration of valence electrons are studied. For NiTi-based alloys, two distinct trends of transformation temperatures with respect to the number of valence electrons per atom are found depending on whether $e_v/a = 7$ or $e_v/a \neq 7$. Clear correlations between transformation temperatures and $c_v$ exist. $M_s$ and $A_s$ decrease consistently with increasing $c_v$. The possible influence of alloying elements atomic size on transformation hysteresis is also introduced.

# Chapter 6

# 6 Local Atomic Structure of Martensite and Transformation Temperature in NiTiHf Shape Memory Alloys

## 6.1 Introduction

In NiTi shape memory alloys an important aim is to elevate the martensitic transformation temperature in order to satisfy the high temperature applications of the shape memory effect, and additionof Pt, Pd, Zr or Hf to NiTi is especially effective [13–20, 216, 217]. Among the potential high temperature shape memory alloys (SMAs) those belonging to the ternary NiTiHf alloys are attractive due to their better thermal stability than NiTi and low cost [218,219]. Apart from the work of Potapov [220], most of the recent studies on NiTiHf SMAs have been related to processing, shape memory behavior, microstructure evolution and compositional modification by copper addition [32, 216–223]. Moreover, these investigations have been focused on Ni-rich alloys in which Hf is replaced for Ti. Consequently, the interaction of ternary elements such as Hf in the structure of NiTi, which promotes the change of transformation temperatures, hysteresis, and shape memory behavior in this group of SMAs requires further examination. The shape memory effect in these alloys is influenced by the characteristics of the crystallographic transformation of austenite to martensite. The role of Hf addition in modifying the martensite crystal structure is presently unclear. The crystallochemical accommodation behavior of Hf is also of paramount importance for clarification of the mechanisms by which it alters the shape memory transformation characteristics of NiTi. Fortuitously, the considerable differences in atomic numbers Hf (Z=72) with Ti (Z=22) and Ni (Z=28) results in well separated X-ray scattering factors, which underpin the determination of Hf site preference in NiTi alloys. In the present work the crystal chemistry of Ni-rich, Ti-rich and equiatomic NiTi shape memory

alloys containing Hf (5–20 at%) are studied by quantitative X-ray diffraction and the partitioning of Hf over the crystallographic sites in alloysare determined.

## 6.2 Results

### 6.2.1 Trends in unit cell constants

Austenite was present only in low amounts (less than 5 volume percent) in the specimens containing 5 at% Hf and therefore, was included in the refinement of these specimens. Figure 6.1 shows typical diffraction profiles of a number of the samples studied. The focus of this study is on the martensite crystal structure changes, thus only martensite structure is presented.

The unit cell volumes of the NiTiHf alloys expand with increasing Hf content in Ni-rich, Ti-rich and equiatomic NiTi alloys (Fig. 6.2a). At constant Hf content, Ti-rich alloys are dilated with respect to Ni-rich alloys and the equiatomic alloys have the smallest volumes. Expansion with increasing Hf is almost linear, although the rate is slightly higher in Ti-rich alloys. At Hf concentrations below 10 at%, Ti-rich and Ni-rich alloys have similar cell volumes; whereas above this concentration the differences become more significant. The origin of the changes in volume is clear when the relative changes in lattice parameters are considered. The variation of ‘c’ and ‘a’ lattice parameters with hafnium content in all the alloys is similar, increasing linearly with Hf concentration (Fig. 6.2b and 6.3c). At low Hf concentration the alloys show small differences in ‘a’ lattice parameter, but considerable extension in the ‘c’ cell edge. The ‘a’ lattice expansion becomes more significant as the Hf content of the alloys increases (Fig. 6.2c). Behavior of the ‘b’ cell edge is more complex (Fig. 6.2d), decreasing in Ni-rich alloys, but increasing linearly in Ti-rich alloys with Hf content with the latter showing smaller ‘b’ parameters compared to the former at Hf contents ≤15 at%. In equiatomic alloys ‘b’ lattice parameter expands less significantly and stabilizes around 4.10 Å.

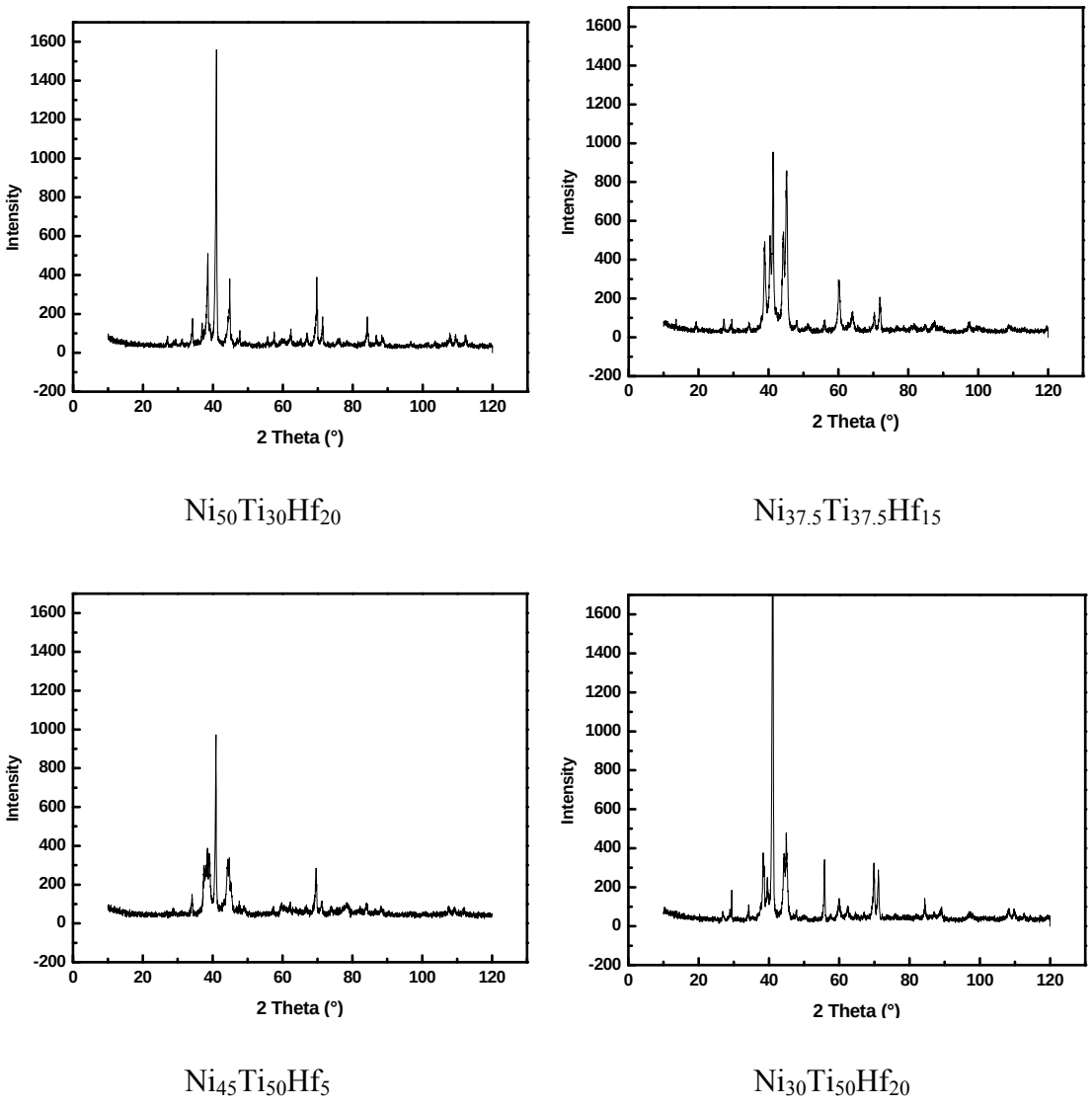


Figure 6.1: Typical diffraction patterns of NiTiHf shape memory alloys.

The monoclinic angle (b) becomes more obtuse with increasing Hf content (Fig. 6.3). In equiatomic alloys, the rate of change is small (less than 1 degree over 15 at% difference in Hf content), compared to the Ni-rich and Ti-rich alloys (more than 2 degrees over the same compositional range). The change is most pronounced at Hf concentrations above 10% in all alloys. At constant Hf compositions, Ti-rich alloys crystallize with slightly larger b angles compared to Ni-rich alloys (Fig. 6.3).

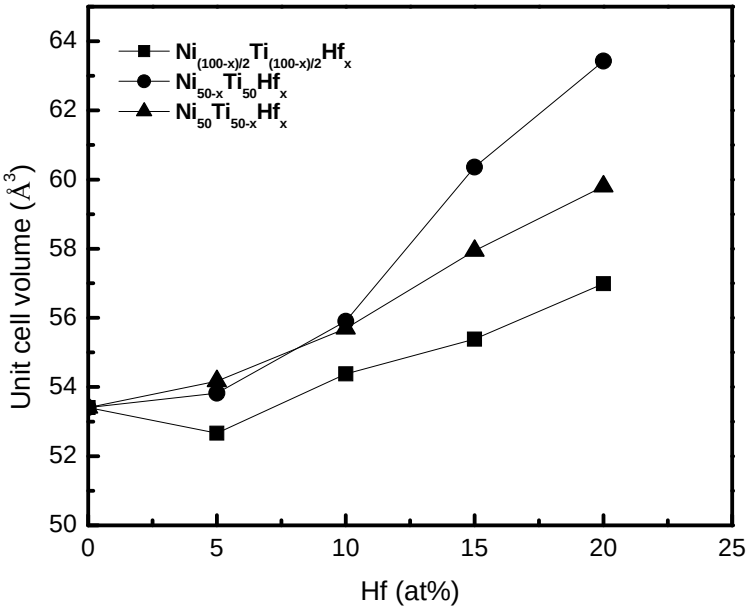


(a)

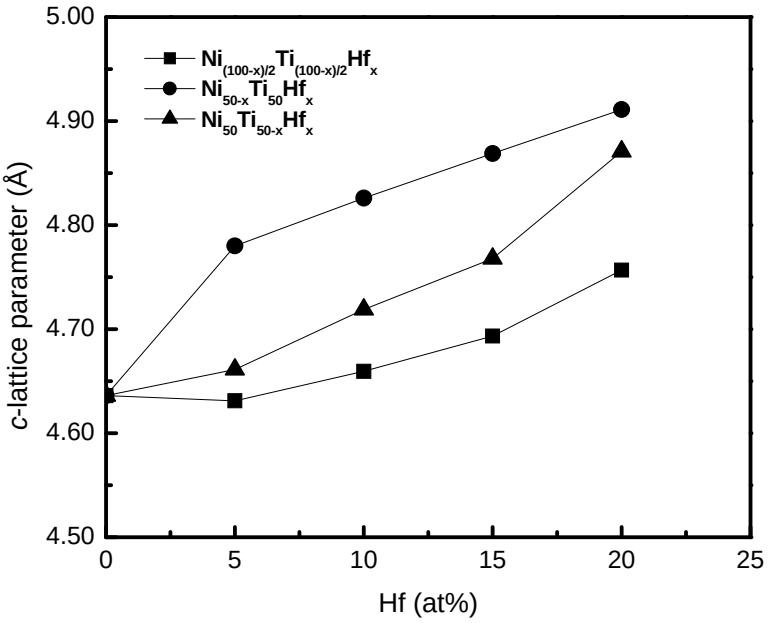


(b)

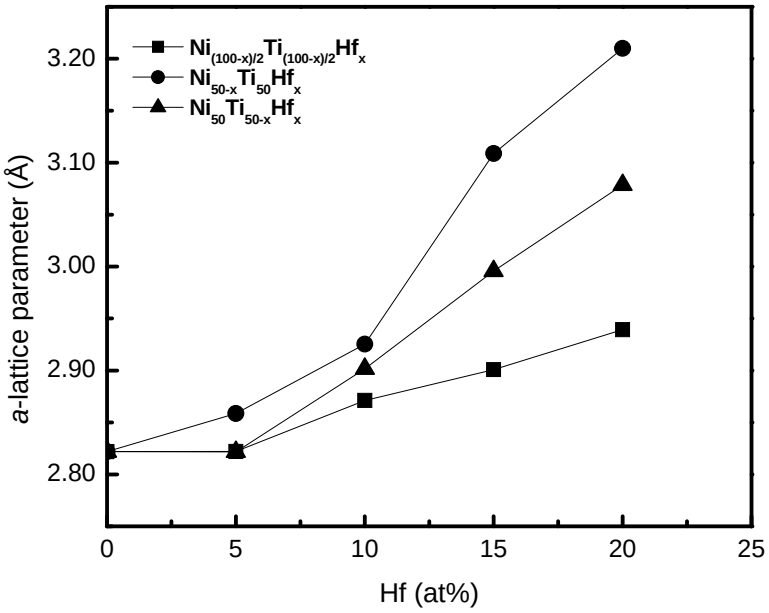


(c)

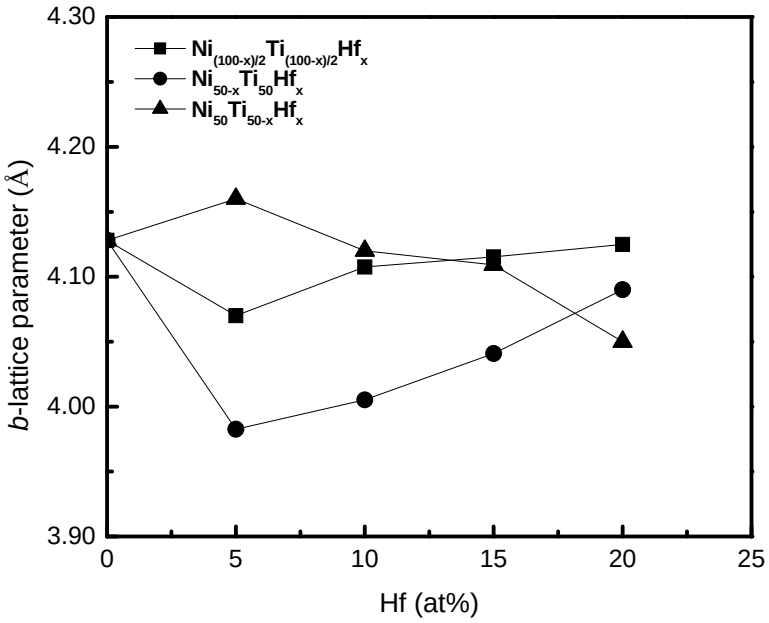


(d)

Figure 6.2: Variations of (a) unit cell volume, (b) 'c' lattice parameter (c) 'a' lattice parameter and (d) 'b' lattice parameter with Hf content of NiTiHf alloys.

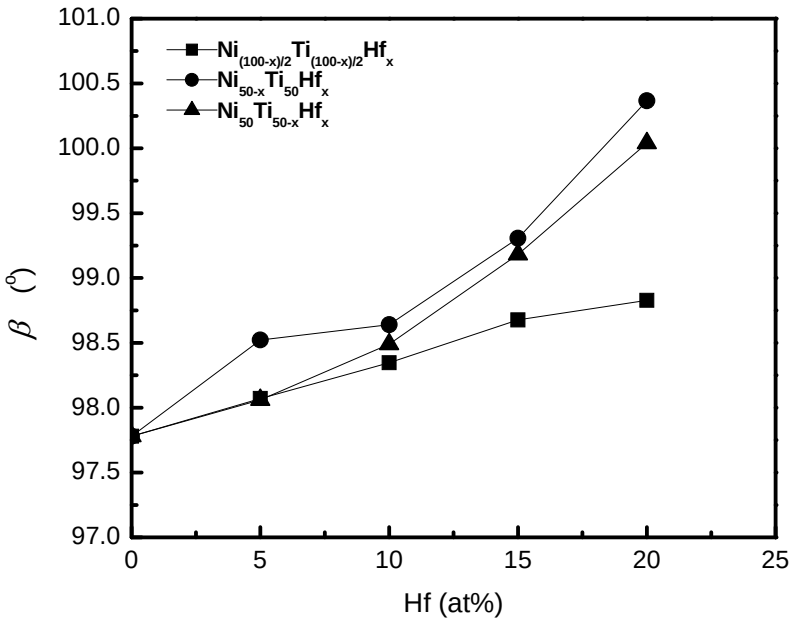


Figure 6.3: Hf content dependence of monoclinic angle of the crystal structure of B19'

## 6.2.2 Atomic site displacements

In binary NiTi, the atoms are in general parameters of Ni (0.04 0.25 0.67), and Ti (0.42 0.25 0.22) in the B19' crystal structure [200]. The change of these atomic parameters for Ti and Ni in x, y, and z directions as a result of increasing Hf concentration of the lattice are reported in Table 6.1. The change in x-parameter of Ni in equiatomic alloys is small, but becomes slightly more significant in Ni-rich and Ti-rich alloys when the Hf concentration is 20 at% (Table 6.1).

The trend of the displacement along x-axis in all three groups of the alloys is similar. The Ni displacement along y-axis is relatively very small in all alloys. The z-parameter of Ni sites in equiatomic alloys remains almost constant whereas it increases for Ni-rich and Ti-rich alloys (Table 6.1).

The displacement of Ti sites (0.42) along x-axis with increasing Hf is shown in Table 6.1. At 20 at% Hf, in equiatomic alloys, the amount of displacement is less than that observed in Ni-rich and Ti-rich alloys. The y-parameter of Ti sites in all alloys remains almost constant or changes slightly. In all the alloys the Ti z-parameter increases in a similar fashion by increasing Hf content.

Schematic projections of the crystal structures of binary $Ni_{50}Ti_{50}$, equiatomic, Ni-rich, and Ti-rich alloys containing 15 at% Hf along y-axis, are illustrated in Fig. 6.4. The typical relative average positions of Ni site (dark) and Ti site (light) along 'a' and 'c' lattice parameters with respect to the binary alloy have been indicated. In general it appears that the displacement of Ni is greater than Ti especially along z-axis, and site positions experience smaller shifts in equiatomic alloys.

Table 6.1: Refined Atomic parameters (x, y, z) of Ni and Ti sites in Ni-rich, Ti-rich and equiatomic NiTiHf alloys.

| Alloy | Composition | Atomic Parameter (Ni) | | | Atomic Parameter (Ti) | | |
|---|---|---|---|---|---|---|---|
| | | **x** | **y** | **z** | x | y | z |
| **Binary** | $Ni_{50}Ti_{50}$ | 1.04 | 0.250 | 0.67 | 0.42 | 0.250 | 0.22 |
| | $Ni_{50}Ti_{45}Hf_5$ | 0.98 | 0.246 | 0.69 | 0.47, | 0.246, | 0.15 |
| | $Ni_{50}Ti_{40}Hf_{10}$ | 1.00 | 0.236 | 0.71 | 0.50 | 0.244 | 0.18 |
| **Ni-rich** | $Ni_{50}Ti_{35}Hf_{15}$ | 1.01 | 0.239 | 0.74 | 0.55 | 0.240 | 0.22 |
| | $Ni_{50}Ti_{30}Hf_{20}$ | 1.05 | 0.241 | 0.77 | 0.57 | 0.235 | 0.26 |
| | $Ti_{50}Ni_{45}Hf_5$ | 0.96 | 0.244 | 0.71 | 0.48 | 0.234 | 0.16 |
| **Ti-rich** | $Ti_{50}Ni_{40}Hf_{10}$ | 0.98 | 0.238 | 0.75 | 0.52 | 0.237 | 0.20 |
| | $Ti_{50}Ni_{35}Hf_{15}$ | 1.04 | 0.232 | 0.80 | 0.56 | 0.244 | 0.26 |
| | $Ti_{50}Ni_{30}Hf_{20}$ | 1.08 | 0.231 | 0.84 | 0.58 | 0.247 | 0.29 |
| | $Ni_{47.5}Ti_{47.5}Hf_5$ | 0.97 | 0.239 | 0.69 | 0.48 | 0.231 | 0.15 |
| **Equiatomic** | $Ni_{45}Ti_{45}Hf_{10}$ | 0.99 | 0.237 | 0.69 | 0.49 | 0.228 | 0.18 |
| | $Ni_{42.5}Ti_{42.5}Hf_{15}$ | 1.00 | 0.234 | 0.69 | 0.48 | 0.226 | 0.21 |
| | $Ni_{40}Ti_{40}Hf_{20}$ | 0.99 | 0.231 | 0.68 | 0.46 | 0.229 | 0.23 |

### 6.2.3 Hafnium partitioning

The refined Hf site preference and fractional occupancies in the monoclinic B19' crystal structures of the alloys are presented in Table 6.2. In Ni-rich specimens Hf shows an exclusive preference for the Ti sites when Hf content of the alloy ≤15 at%, although at the highest Hf content ($Ni_{50}Ti_{30}Hf_{20}$) approximately 1/5 of the Ni is replaced.

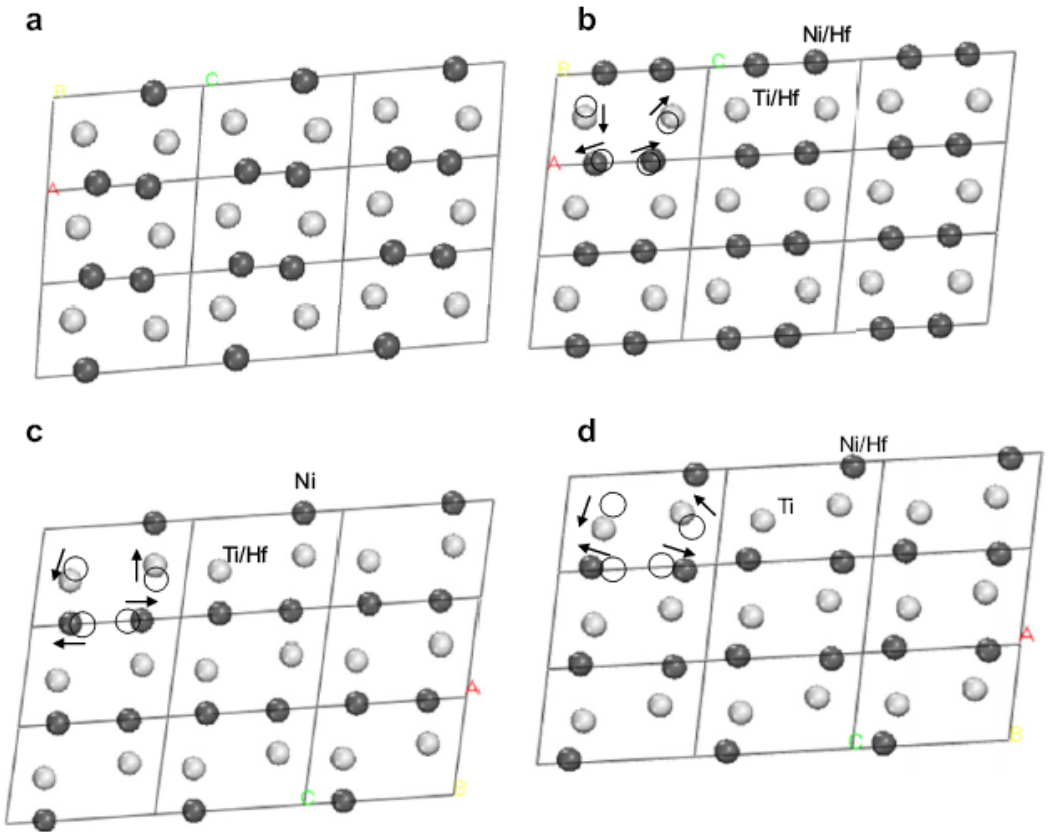


Figure 6.4: Schematic projections of the crystal structures of (a) binary Ni50Ti50, (b) Ni42.5Ti42.5Hf15, (c) Ni50Ti35Hf15, and (d) Ni35Ti50Hf15 along <010> direction, comparing the typical relative average positions of Ni site (dark) and Ti site (light) along 'a' and 'c' lattice parameters with respect to the binary alloy.

In Ti-rich specimens, Hf replaces only Ni sites at Hf concentration of 10 at%, however, above this some Hf occupies the Ti sites. By increasing the nominal Hf content of the alloy the fractional occupancy of Hf in Ni site increases; whereas the corresponding occupancy in Ti site does not increase. The refinement results show that in equiatomic alloys, Hf occupies both sites approximately equally with increasing Hf content. The total Hf at%, calculated based on the fractional occupancies of Ti and Ni sites are near

the nominal values in all the alloys. Determination of Hf site preference and occupancy in specimens containing only 5 at% Hf was inconclusive due to insufficient electron difference contrast. For Ti-rich and equiatomic alloys containing 20 at% Hf, the refinements could not converge to reliable, reproducible values probably due to higher $R_b$ values (Table 6.2).

## 6.3 Discussion

The Rietveld refinements suggest that the B19' ($P_{21}/m$) monoclinic crystal structure can be used to refine the martensite structure of NiTiHf alloys for 5≤ Hf at%≤20.

Table 6.2: Site preference and occupancy of Hf in Ni-rich, Ti-rich and equiatomic NiTiHf alloys.

| Alloy | Composition | Preferred site | Fractional site occupancy | | Refined Hf (at%) | $R_b$ (%) |
|---|---|---|---|---|---|---|
| | | | Ti | Ni | | |
| **Ni-rich** | $Ni_{50}Ti_{45}Hf_5$ | - | - | - | - | 3.4 |
| | $Ni_{50}Ti_{40}Hf_{10}$ | Ti | 0 | | 12 | 3.5 |
| | $Ni_{50}Ti_{35}Hf_{15}$ | Ti | 0.36 | 0 | 18 | 4.4 |
| | $Ni_{50}Ti_{30}Hf_{20}$ | Ti | 0.41 | 0.10 | 26 | 4.0 |
| **Ti-rich** | $Ti_{50}Ni_{45}Hf_5$ | Ni | - | - | - | 3.5 |
| | $Ti_{50}Ni_{40}Hf_{10}$ | Ni | 0 | 0.17 | 8.5 | 3.8 |
| | $Ti_{50}Ni_{35}Hf_{15}$ | Ni | 0.09 | 0.33 | 20 | 4.1 |
| | $Ti_{50}Ni_{30}Hf_{20}$ | Ni | - | - | - | 5.1 |
| **Equiatomic** | $Ni_{47.5}Ti_{47.5}Hf_5$ | - | - | - | - | 3.0 |
| | $Ni_{45}Ti_{45}Hf_{10}$ | Ti, Ni | 0.14 | 0.11 | 12.5 | 3.4 |
| | $Ni_{42.5}Ti_{42.5}Hf_{15}$ | Ti, Ni | 0.21 | 0.25 | 23 | 4.2 |
| | $Ni_{40}Ti_{40}Hf_{20}$ | Ti, Ni | - | - | - | 5.1 |

Simulated X-ray diffraction patterns showed Rb values of 3.4% to 5.1%. The fits for $Ni_{(100-x)/2}Ti_{(100-x)/2}Hf_x$ equiatomic alloys are slightly less accurate (higher $R_b$ values) which can be indicative of departure from $P2_1/m$ space group especially at Hf content of 15 and 20 at%. For samples containing10 at% or more of Hf, the presence of only a monoclinic structure with no evidence of secondary phases confirms a single phase solid solution.

### 6.3.2 Valence electrons, bond lengths and lattice dimensions

Increasing Hf concentration in the B19' structure dilates the unit cell by expansion of the 'a' and 'c' lattice parameters and opening the monoclinic angle β (Figs. 6.1 and 6.2). The 'b' cell edge behaves in a contrary fashion in Ni-rich alloys, but expands in Ti-rich alloys and to a lesser extent in the equiatomic alloys.

The arrangement of atoms and unit cell volume of an intermetallic crystal is controlled by bond lengths which in turn are dictated by both the size of the atoms and the valence electrons of the material [224]. The volume dependence of intermetallic unit cell dimensions on the size of the constituent atoms has been the subject of several studies in recent years [224–231]. These efforts have aimed to correlate the cell volume with the size, binding energy, and atomic radii of the constituent atoms. However, the complex interaction of the electronic structure of metals in different atomic environments, especially transition metals where d–d and s–d orbital behavior are not clearly understood, no general correlations have been found. The number of valence electron contributions to the atomic environment (s+d electrons), total electrons, hybridization and even electronegativity can be important factors that may have determining roles on bond length and unit cell size [224-231]. Preferential partitioning of Hf to the Ni sites results in a greater expansion in crystal lattice compared to substitution for Ti, especially at higher Hf concentrations. This can be attributed to a larger difference in atomic radius of Hf (1.58 Å) and Ni (1.29 Å) compared to that of Hf and Ti (1.45 Å). While, based on this size effect, at constant Hf, for equiatomic alloys, unit cell volumes of larger than Ni-rich and smaller than Ti-rich alloys are expected, lesser expansions observed in equiatomic alloys may reflect near equimolar partitioning of Hf over the Ni and Ti sites that leads to an enhanced packing density. In order to

clarify why the equiatomic alloys show a slightly smaller volume, an analysis of valence electrons and the bond lengths of the atoms of the alloys is useful.

The valence electrons are the electrons in the outermost principal quantum level of an atom. For transition metals the valence electrons are usually considered as the number of d and s electrons for an atom. In equiatomic NiTi alloy, the electronic configurations of Ti and Ni, are, Ti: $1s^2 2s^2 2p^6 3s^2 3p^6 4s^2 3d^2$, Ni: $1s^2 2s^2 2p^6 3s^2 3p^6 4s^2 3d^8$, and the number of valence electrons, ($e_v$), of these elements are $e_v^{Ti} = 4$, $e_v^{Ni} = 10$. The valence electrons per atom of ternary NiTiHf alloys can be calculated based on the atomic fraction of the elements in the alloy as by Eq. (6.1):

$$\frac{e_v}{a} = f_{Ni} e_v^{Ni} + f_{Ti} e_v^{Ti} + f_{Hf} e_v^{Hf} \qquad (6.1)$$

where $f_{Ni}$, $f_{Ti}$, and $f_{Hf}$ represent the atomic fractions of elements in the alloy for Ni, Ti and Hf, and $e_v^{Ni}$, $e_v^{Ti}$, and $e_v^{Hf}$ are the corresponding number of valence electrons of Ni, Ti and Hf, respectively. Since Ti and Hf ($-5d^2 6s^2$) have identical number of valence electrons,the replacement of Hf for Ti in the alloys does not affect electron ratio of the Ni-rich alloys; whereas substitution of Hf for Ni reduces the valence electron concentration in Ti-rich and equiatomic alloys to <7 depending on the Hf content. Fig. 6.5 shows the change of average refined bond lengths of atomic sites (Ni–Ni, Ti–Ti, and Ni–Ti), as a function of valence electrons per atomof the alloys for Ti-rich, Nirich, and equiatomic alloys. These lengths are the average of lengths of Ni site and Ti site with six nearest neighbors, extracted from the structure refinement. The average length of Ni–Ni site bonds increases in all the alloys with increasing Hf content (Fig. 6.5a). The increase of bond length occurs as a result of incorporation of larger Hf into the site in Ni-rich alloys. No change in the number of valence electrons per atom is resulted. In the case of Ti-rich and equiatomic alloys the increase of bond is the result of larger size of the Hf, influenced by the reduction of the valence electrons per atom. The corresponding Ni–Ni bond length averages in Ti-rich, and Ni-rich alloys are larger than equiatomic alloys (Fig. 6.5a). The Ti–Ti site average bond length increased in Ni-rich and Ti-rich alloys with increasing Hf, however,

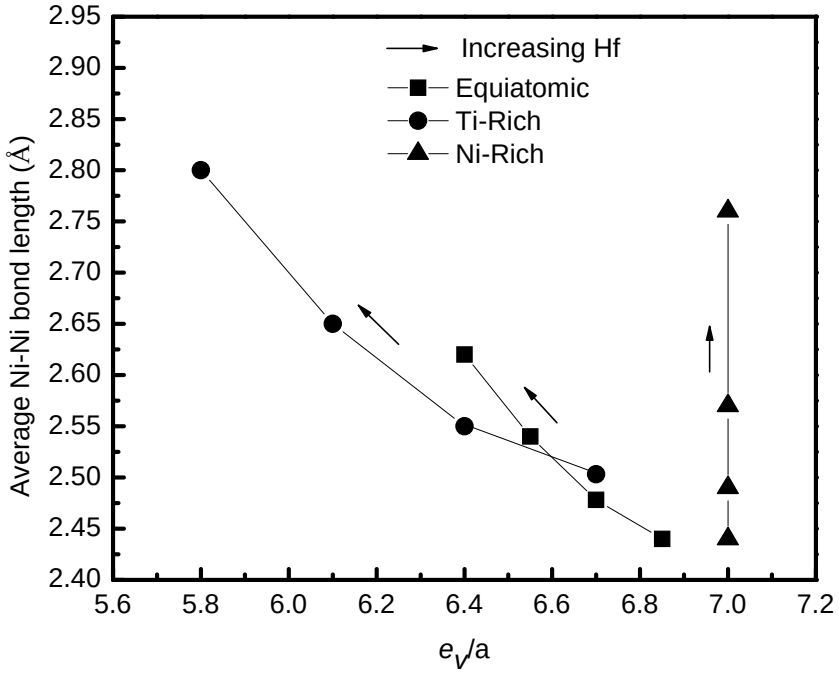


(a)

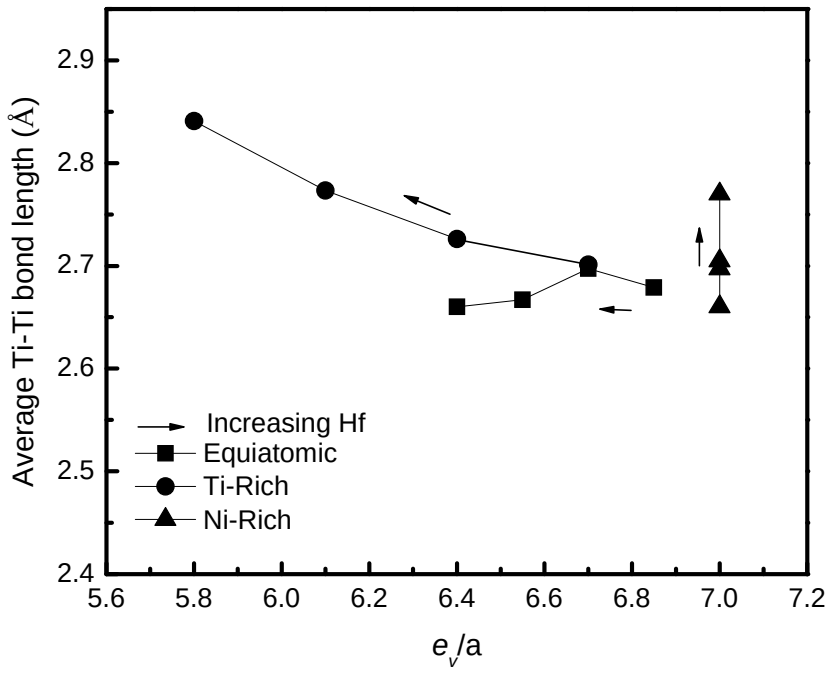


(b)

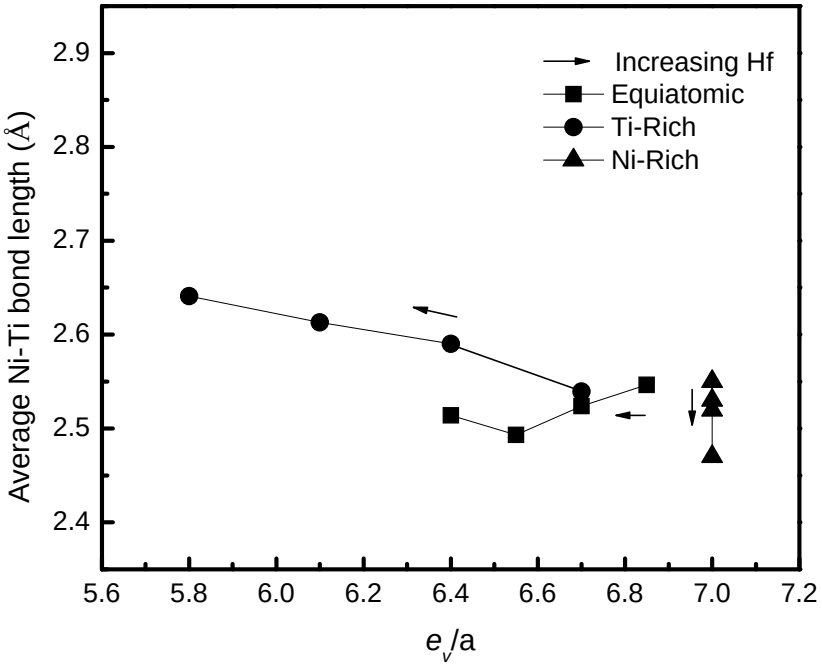


(c)

Figure 6.5: Average refined a) Ni-Ni, b) Ti-Ti, and c) Ni-Ti bond lengths variations with the number of valence electrons per atom of Ti-rich, Ni-rich and equiatomic NiTiHf alloys.

with comparatively smaller changes than Ni–Ni bonds (Fig. 6.5b). In equiatomic alloys Ti–Ti bond length remains almost constant. The Ni–Ni and Ti–Ti bond lengths changes follow the variations observed for 'a' and 'c' lattice dimensional expansion (Fig. 6.2). By increasing the Hf content, the Ni–Ti bond length remains almost constant for equiatomic alloys, slightly reduces or remains constant for Ni-rich alloys, and increases marginally for Ti-rich alloys. It seems that incorporation of Hf, mainly affects the Ni–Ni and Ti–Ti bond lengths.

A general look at the variation of all the average bond lengths as a function of $e_v$/a shows an interesting trend as is illustrated in Fig. 6.6. The average bond lengths decrease with increasing electron per atom ratio in the $e_v$/a range of 5.8 to near 7. At $e_v$/a=7 (Ni-rich group), however, where s and d orbitals are completely filled a broader range of the bond lengths is observed. In the equiatomic alloys with an $e_v$/a ratio of 6.7–6.925, the average bond lengths are in the medium to lower range of the graph therefore the unit cellvolume is smaller, in Ti-rich alloys where ev/a ratio is lower (5.8–6.7), the average bond lengths and cell dimensions are of larger dimensions. In Ni-rich alloys

($e_v$/a), a broad range of bond lengths is observed (Fig. 6.6). Different bond lengths translate into different variations along different cell axes and result in the unit cell volume of Ni-rich alloys to be larger than equiatomic alloys but smaller than Ti-rich alloys.

### 6.3.3 Atom displacements

Accommodation of Hf in the monoclinic martensite NiTi takes place by substitution of Ni and Ti atoms. One can assume that replacements are controlled primarily by the size mismatch of Hf which is larger than the parent atoms.

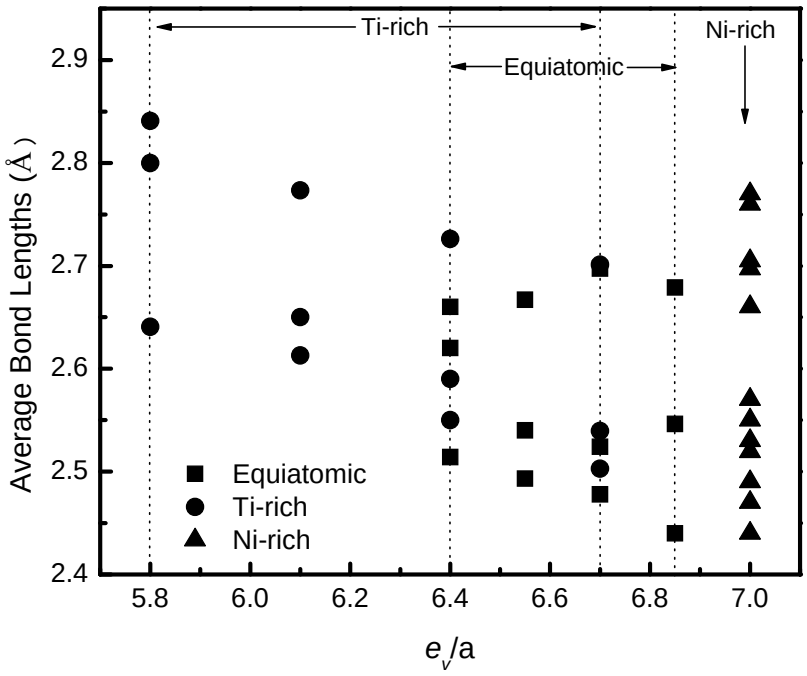


Figure 6.6: General trend of bond lengths dependence on the number of valence electrons per atom in NiTiHf alloys. All bonds (Ni-Ni, Ti-Ti, Ni-Ti) corresponding to Ti-rich specimens containing 5-20 at% Hf are shown with (circle). Similarly, the corresponding bonds for Ni-rich alloys are shown with (triangle), and the bonds for equiatomic alloys are indicated by (square). For Ti-rich and equiatomic alloys the $e_v$/a values are lower than 7 depending on the Hf content, whereas for Ni-rich alloys this ratio remains constant at 7 at all Hf compositions. At different compositions, the general picture is that the bond lengths of Ti-rich alloys are in the high value range. For Ni-rich alloys, the bond lengths show a wide range from low to high. The equiatomic alloys have bond lengths only in the low to medium range.

All atoms reside on the general position of space group $P2_1/m$ and have the freedom to be displaced in any direction during Hf incorporation. The displacements along z are larger which is consistent with greater change of 'c' lattice parameter compared to 'a' and 'b'. The atomic radii of the transition metals are environment dependant, and electron interactions determine the bond lengths and disposition of atoms. Moreover, atom displacements from original positions in binary NiTi are larger for Ni compared to Ti. Similarly, the bond lengths variation for Ni–Ni sites is more than Ti–Ti sites especially when the $e_v$/a ratio is smaller. When Hf replaces both Ni and Ti, as in equiatomic alloys, the displacement of atoms is significantly less, in line with small increase of unit cell volume. In equiatomic alloys, Ni–Ni, Ti–Ti and Ni–Ti bond lengths are all comparatively closer to each other than Ni-rich and Ti-rich alloys (Fig. 6.5). Isotropic bonding translates to higher packing density and therefore atoms occupy a smaller cell.

### 6.3.4 Hafnium site preference

From the refined Hf site occupancy results (Table 6.2) it can be concluded that Hf prefers to occupy the available sites in NiTi monoclinic structure as its tendency towards the Ni and Ti sites at equally available sites (equiatomic alloys) is almost similar. Bozzolo et al. have reported the absolute site preference of elements in NiTi, PdTi, and PtTi systems based on atomistic modeling [187,188]. In NiTi the atomistic modeling predicts an energy gap of 6.21 and 4.26 eV for substitution of Hf in Ni and Ti sites, respectively [187]. Based on this criterion, the tendency of Hf for Ni and Ti is near each other with more inclination towards Ni sites. In the present work we have experimentally shown that Hf preference of Ni and Ti sites are almost similar.

### 6.3.5 Transformation temperature

The martensite start temperatures ($M_s$) of selected NiTiHf alloys are reported in Table 6.3. As discussed, the addition of Hf to NiTi structure results in changes of bond lengths, lattice parameters and unit cell volumes. It may also result in reduction of the

number of valence electrons of the alloys (in equiatomic and Ti-rich alloys). These two variations cause the valence electron density (VED), the number of valence electrons per unit cell of the crystal, to change.

Table 6.3: Transformation temperatures and valence electron concentration of selected NiTiHf alloys.

| Alloy | $M_s$ | $e_v/a$ | $c_v$ |
|---|---|---|---|
| NiTi | 60 | 7.00 | 0.280 |
| $Ni_{50}Ti_{40}Hf_{10}$ | 120 | 7.00 | 0.233 |
| $Ni_{50}Ti_{35}Hf_{15}$ | 200 | 7.00 | 0.215 |
| $Ni_{42.5}Ti_{42.5}Hf_{15}$ | 215 | 6.55 | 0.204 |
| $Ni_{35}Ti_{50}Hf_{15}$ | 235 | 6.10 | 0.193 |

The average ratio of valence electrons, $c_v$, over total electrons of the alloy (average number of valence electrons divided by average atomic number of the alloy as discussed in the previous chapters) also changes. As was shown, the valence electron density and valence electron concentration ($c_v$) variations follow a similar trend in NiTi-based shape memory alloys. The values of this parameter for the alloys are reported in Table 6.3. By increasing the Hf content of the alloy, $c_v$ is decreased. There is an established relationship between bulk moduli of the alloys and their valence electron density or concentration. By increasing the VED or $c_v$, the bulk and shear moduli increases [179,180]. Hence increasing Hf content in Ni-rich alloys which is accompanied by unit cell expansion (Fig. 6.2) and reduction of $c_v$ (Table 6.3) results in the elastic moduli of NiTi crystal to decrease and shear to occur at higher temperatures. The net result is the elevation of the martensitic transformation temperature (Table 6.3). For the purpose of comparison, the $M_s$ of specimens containing 15at% Hf, in Ni-rich, equiatomic and Ti-rich condition are reported (Table 6.3). The difference in Ms in these alloys is similarly related to their slight difference in $c_v$. The lower the $c_v$ the higher the transformation temperature. A more comprehensive understanding of the dependence of martensitic transformation temperature on valence electron concentration (density) in NiTi-based shape memory alloys was introduced in Chapter 5.

## 6.4 Summary

Local atomic structure investigation of a number of NiTiHf shape memory alloys are carried out using quanititative X-ray diffraction (XRD). At the same Hf content, Ti-rich alloys exhibit larger cell volumes than Ni-rich alloys. The equiatomic alloys show smaller unit cell volumes than Ti-rich and Ni-rich groups possibly due to more isotropic bonding. The $e_v$/a and $c_v$ of the alloys influence the atomic bond lengths and unit cell dimensions. The similar tendency of Hf towards occupancy in Ni and Ti sites, results in its preference for available sites in the structure.

# Chapter 7

# 7 Transformation Temperature Changes due to Second Phase Precipitation in NiTi-Based Shape Memory Alloys

## 7.1 Introduction

Control of transformation temperatures of shape memory alloys has been an important research subject to enhance the reliability and applicability of these functional materials [4,7,9-11]. Factors influencing the $M_s$ temperature are believed to be the elastic properties of the parent austenite crystal and certain microstructural features such as precipitates [11,48-49]. The dependence of transformation temperatures on the number and concentration of valence electrons in the quenched NiTi-based and NiTiHf shape memory alloys was demonstrated in Chapters 5 and 6. It was shown that in NiTi-based shape memory alloys the transformation temperature is distinctly related to whether the number of valence electrons per atom of the alloy is ($e_v$/a) = 7 or ($e_v$/a) ≠7. More importantly, it was shown that by increasing the valence electron concentration ($c_v$) of the as quenched NiTi-based alloys, the transformation temperatures decrease as a result of higher elastic constants of the crystal which influence the resistance against shear, responsible for martensitic transformation. Chapter 4 also introduced a similar dependence of transformation temperatures on the valence electron concentration for nearly all transition-metal-based shape memory alloys. Increasing valence electron concentration is closely related to the increase of particular elastic constants of the parent phase (austenite) which in turn can influence the resistance against shape and volume change of the crystal [179,180]. The higher the elastic constants of the austenite; the lower the transformation temperatures, as more pre-martensitic elastic softening is required by cooling before the transformation occurs.

As reported in a number of studies [11,46,194,232-250], in order to improve the shape memory and mechanical properties, the alloys are usually aged at an appropriate

temperature that may give rise to the precipitation of second phases from the supersaturated matrix. Although the focus of the majority of these studies has been the shape memory effect, considerable amount of data have been made available on the change of $M_s$ temperature as a result of aging. The temperature alterations are suggested to be affected by the effect of precipitation hardening and change of the matrix composition [11]. However, no satisfactory explanation on how the compositional change of the matrix influences the $M_s$ temperature has been offered.

In the present chapter, we further examine the NiTi-based alloys in the as-quenched and aged conditions. The number and concentration of valence electrons of the matrix of these alloys before and after aging are compared to understand the intrinsic effect of precipitation on the transformation temperature. It is shown that the direction of change of $M_s$ temperature mainly inversely follows the electron concentration of the matrix (which ias altered as a result of precipitation). The extrinsic effect of the precipitate particles on $M_s$ change is also discussed.

## 7.2 Analysis

### 7.2.1 Precipitation and change of $M_s$

It has been shown that as a result of aging, of NiTi-based alloys, the martensitic transformation temperatures can be changed [46,194,232-250]. Tables 7.1 and 7.2 list the martensitic transformation temperatures of a number of solution-treated, and aged NiTi-based alloys that experience considerable change of $M_s$ temperature (>15°C). The data are accompanied by the corresponding type of the precipitates formed. These two groups of alloys are categorized with respect to the direction of the change of $M_s$ due to precipitation, which are described as follows.

In the first group, precipitation is accompanied by an increase of $M_s$. In NiTi [11,239], Ni-rich NiTiHf [245] and NiTiPt [46], precipitation of $Ni_4Ti_3$, $Ni_4(Ti,Hf)_3$, and NiTiPt compounds, respectively, results in a considerable increase of $M_s$ (Table 7.1). In contrast, in the second group of NiTi-based alloys, precipitation results in a decrease of the $M_s$ temperature. Precipitation of $Ti_2Pd$ from the $Ni_{21.8}Ti_{51.2}Pd_{27.0}$ alloy matrix causes the $M_s$ to decrease considerably [249]. Similarly, formation of a

$(Ti,Hf)_2Ni$ phase leads to a considerable decrease of the $M_s$ temperature in NiTiHf alloys [236] (Table 7.2).

Table 7.1: $M_s$, $c_v$ , $e_v$/a, type and/or measured or estimated quantity of the precipitate and the resulting composition of aged matrix for shape memory alloys in which precipitation leads to a considerable increase of transformation temperature. The references show the source of transformation temperatures or/and precipitate quantity.

| **Matrix (Quenched)** | **$c_v$ ($e_v$/a)** | **$M_s$ (°C)** | **Precipitate** | **Matrix (Aged)** | **$c_v$ ($e_v$/a)** | **$M_s$ (°C)** | **Ref.** |
|---|---|---|---|---|---|---|---|
| $Ni_{50.8}Ti_{49.2}$ | **0.281** (7.05) | -20 | (~10%)$Ni_4Ti_3$ | $Ni_{50.0}Ti_{50.0}$ | **0.280** (7.00) | 0 | [239] |
| $Ni_{50.80}Ti_{49.20}$ | **0.281** (7.05) | -10 | (15%)$Ti_{44.10}Ni_{55.90}$ | $Ni_{49.90}Ti_{50.10}$ | **0.279** (6.99) | 15 | **[243]** |
| $Ni_{50.8}Ti_{49.2}$ | **0.281** (7.05) | -3 | (15%)$Ni_4Ti_3$ | $Ni_{49.67}Ti_{50.33}$ | **0.279** (6.98) | 27 | [161] |
| $Ni_{50}Ti_{40}Hf_{10}$ | **0.233** (7.00) | 120 | (~10%)$Ni_4(Ti_{0.85},Hf_{0.15})_3$ | $Ni_{49.2}Ti_{40.4}Hf_{10.4}$ | **0.230** **(6.95)** | 144 | this study |
| $Ni_{50.6}Ti_{29.4}Hf_{20}$ +$(Ti,Hf)_2Ni$ | **0.201** (7.04) | ~145 | (15%)$Ni_4(Ti_{0.85},Hf_{0.15})_3$ +$(Ti,Hf)_2Ni$ | $Ni_{49.3}Ti_{28.1}Hf_{22.6}$ | **0.191** (6.96) | ~225 | [245] |
| $Ni_{50}Ti_{35}Hf_{15}$ | **0.215** (7.00) | 200 | (~15%)$Ni_4(Ti_{0.85}Hf_{0.15})_3$ | $Ni_{48.7}Ti_{34.7}Hf_{16.6}$ | **(0.208)** (6.92) | 247 | this study |
| $Ti_{48.52}Ni_{31.03}Pt_{20.45}$ ($Ti_{50}Ni_{30}Pt_{20}$) | **0.201** (7.09**)** | ~244 | $Ti_{39.44}Ni_{38.67}Pt_{21.89}$ | $Ti_{46.46}Ni_{29.01}Pt_{24.53}$ | **0.192** (7.21**)** | 307 | [46] |
| $Ni_{50}Ti_{30}Hf_{20}$ | **0.200** (7.00**)** | 290 | (15.6%)$Ni_4(Ti_{0.85},Hf_{0.15})_3$ | $Ni_{48.7}Ti_{30}Hf_{21.3}$ | **0.195** (6.92) | 315 | This study |
| $Ti_{52.58}Ni_{22.35}Pt_{24.49}$ | **0.184** (6.79) | ~360 | $Ti_{66.6}Ni_{1.67}Pt_{31.74}$ | $Ti_{49.76}Ni_{21.11}Pt_{29.13}$ | **0.177** **(7.01)** | 402 | [46] |
| $Ti_{47.79}Ni_{20.79}Pt_{30.79}$ | **0.175** (7.07) | ~530 | $Ti_{39.16}Ni_{29.46}Pt_{31.38}$ | $Ti_{46.53}Ni_{17.79}Pt_{35.69}$ | **0.167** (7.20) | 605 | [46] |

Table 7.2: $M_s$, $c_v$ , $e_v$/a, type and/or measured or estimated quantity of the precipitate and the resulting composition of aged matrix for shape memory alloys in which precipitation results in a considerable decrease of transformation temperature. References show the source of transformation temperatures or/and precipitate quantity.

| Matrix (Quenched) | $c_v$ ($e_v$/a) | $M_s$ (°C) | Precipitate | Matrix (Aged) | $c_v$ ($e_v$/a) | $M_s$ (°C) | Ref. |
|---|---|---|---|---|---|---|---|
| $Ni_{21.8}Ti_{51.2}Pd_{27.0}$ | **0.232** (6.93) | 190 | (15%)$Ti_2Pd$ | $Ni_{25.6}Ti_{48.5}Pd_{25.9}$ | **0.238** (7.09) | 147 | [249] |
| $Ni_{48.5}Ti_{36.5}Hf_{15}$ | **0.213** (6.91) | 200 | (15%) $NiTi_{0.6}Hf_{0.4}$ | $Ni_{48.3}Ti_{37.6}Hf_{14.1}$ | **0.216** (6.90) | 170 | [246,247] |
| $Ni_{49}Ti_{36}Hf_{15}$ | **0.214** (6.94) | 179 | (15%)$(Ti,Hf)_2Ni$ | $Ni_{51.8}Ti_{36.5}Hf_{11.7}$ | **0.229** (7.11) | 127 | [236] |

## 7.2.2 Little or no change of $M_s$

In a number of alloys (third group), little or no change has been reported after aging. The available data are presented in Table 7.3. The precipitation of TiCu or $Ti_2(Cu,Ni)$ in NiTiCu alloys [192,234,237] and (TiNi+Nb)+$(Ti,Nb)_2Ni$ in NiTiNb alloys, formation of (Ti,V)Ni+$V_9$(Ti,Ni) in NiTiV alloys [232], and precipitation of $(Ti,Zr)_2Ni$ in NiTiZr alloys [14, 16] lead to little (<15°C) or no variation of the $M_s$. Aging $Ni_{49}Ti_{51}$ alloy has also been reported [238] to show almost no change in the $M_s$ temperature due to the presence of considerable amount of stable $Ti_2Ni$ precipitate in the as-quenched alloy (Table 7.3).

The majority of the transformation temperature data presented here have been extracted from the relevant literature as listed in tables or presented in graphs. In order to understand why $M_s$ temperature may or may not change after aging, two main areas need to be considered: first, how the change of matrix composition affects the phase transformation, and second, what the direct effect of the precipitate can be on this transformation. For analysis of the former, the variations of the valence electron concentration of the matrix due to precipitation are presented while for the latter the effect of coherency strain and defect population are discussed in the following sections.

Table 7.3: $M_s$, $c_v$ , $e_v$/a, type and/or measured or estimated quantity of the precipitate and the resulting composition of aged matrix, for shape memory alloys in which precipitation leads to little or almost no change of transformation temperature. References show the source of transformation temperatures or/and precipitate quantity.

| **Matrix (Quenched)** | **$c_v$ ($e_v$/a)** | **$M_s$ (°C)** | **Precipitate** | **Matrix (Aged)** | **$c_v$ ($e_v$/a)** | **$M_s$ (°C)** | **Ref.** |
|---|---|---|---|---|---|---|---|
| $Ti_{45}Ni_{45}Nb_{10}$ | **0.255** (6.80) | -40 | (TiNi+Nb)+ $(Ti,Nb)_2Ni$ | ~$Ti_{45}Ni_{45}Nb_{10}$ | **~0.255** (6.80) | -52 | [241] |
| $Ni_{50.8}Ti_{49.2}$ | **0.281** (7.05) | -20 | (10%)$Ni_4Ti_3$ | $Ni_{50.0}Ti_{50.0}$ | **0.280** (7.00) | -10 | [251] |
| $Ni_{51.3}Ti_{48.7}$ | **0.282** (7.08) | -20 | (10%)$Ni_4Ti_3$ | $Ni_{50.65}Ti_{49.35}$ | **0.281** (7.04) | -5 | [252] |
| $Ni_{50.7}Ti_{49.3}$ | **0.281** (7.04) | -5 | (10%)$Ni_4Ti_3$ | $Ni_{49.99}Ti_{50.01}$ | **0.280** (7.00) | 10 | [201] |
| $Ti_{47.25}Ni_{48.75}V_4$ | **~0.28** (6.97) | 19 | $(Ti,V)_2Ni$+ $V_9(Ti,Ni)$ | $Ti_{46.40}Ni_{50.69}V_{2.91}$ | **~0.28** (7.07) | 26 | [232] |
| $Ni_{25}Ti_{50}Cu_{25}$ | **0.287** (7.25) | 60 | (11%)TiCu | $Ni_{28}Ti_{50}Cu_{22}$ | **0.287** (7.22) | 64 | [193,232] |
| $Ni_{25}Ti_{50}Cu_{25}$ | **0.287** (7.25) | 60 | (9%)TiCu +(7%)$Ti_2(Cu,Ni)$ | $Ni_{28.4}Ti_{48.6}Cu_{23}$ | **0.288** (7.31) | 64 | [193,232] |
| $Ni_{25}Ti_{50}Cu_{25}$ | **0.287** (7.25) | 60 | (9%)$Ti_2(Cu,Ni)$ | $Ni_{25.8}Ti_{48.4}Cu_{25.8}$ | **0.289** (7.35) | 61 | [193,234] |
| $Ni_{49}Ti_{51}$+ some($Ti_2Ni$) | **0.278** (6.94) | 81 | $Ti_2Ni$ | $Ni_{49}Ti_{51}$+some ($Ti_2Ni$) | **0.278** (6.94) | 81 | [238] |
| $Ti_{40.81}Ni_{49.01}Zr_{10.18}$ | **0.259** (6.94) | 100 | $(Ti,Zr)_2Ni$ | $Ti_{40.81}Ni_{49.01}Zr_{10.18}$ | **0.259** (6.94) | 100 | [235] |
| $Ni_{20.5}Ti_{49.5}Pd_{30.0}$ | **0.230** (7.03) | 183 | (15%)$Ti_2Ni$ | $Ni_{18.3}Ti_{46.4}Pd_{35.3}$ | **0.229** (7.21) | ~183 | [248] |
| $Ti_{51}Pd_{30}Ni_{19}$ | **0.229** (6.94) | ~235 | $Ti_{64.72}Ni_{22.46}Pd_{12.82}$ | $Ti_{46.8}Pd_{34.7}Ni_{18.5}$ | **0.229** (7.19) | ~222 | [250] |
| $Ti_{26.5}Ni_{48.5}Zr_{25}$ | **0.229** (6.91) | 385 | $(Ti,Zr)_7Ni_{10}$ or $(Ti,Zr)_2Ni_7$ or NiZr | - | **~0.229** **(-)** | 385 | [233] |

### 7.2.3 Change of composition and electron concentration of the matrix

Depending on the type of the precipitates, the chemical composition of the matrix is altered. Change of matrix composition may vary the number and concentration of valence electrons. The number of valence electron can be calculated based on the contributions of s+d electrons of the transition metals or s+p electrons of the non-transition metals. The contribution of each element present in the crystal corresponds to the atomic fraction of that element in the alloy (Eq. 7.1) :

$$\frac{e_v}{a} = f_{Ni}e_v^{Ni} + f_{Ti}e_v^{Ti} + f_T e_v^T + f_Q e_v^Q \qquad \text{(Eq. 7.1)}$$

where $f_{Ni}$, $f_{Ti}$, and $f_T$ and $f_Q$ represent the atomic fractions of elements in the alloy for Ni, Ti, ternary and quaternary elements, and $e_v^{Ni}$, $e_v^{Ti}$, $e_v^T$ and $e_v^Q$ are the corresponding number of valence electrons of Ni, Ti and the ternary and quaternary elements, respectively. With the valid assumption (in most cases) that quenching avoids precipitation of second phases from the matrix, valence electron concentration is defined as the number of valence electrons of the alloy divided by the total electrons of the alloy (Eq. 7.2),

$$c_v = \frac{e_v}{e_t} = \frac{f_{Ni}e_v^{Ni} + f_{Ti}e_v^{Ti} + f_T e_v^T + f_Q e_v^Q}{f_{Ni}Z_{Ni} + f_{Ti}Z_{Ti} + f_T Z_T + f_Q Z_Q} \qquad \text{(Eq. 7.2)}$$

where $Z_{Ni}$, $Z_{Ti}$, $Z_T$, and $Z_Q$ represent the atomic numbers of Ni, Ti, ternary and quaternary elements, respectively. Upon aging, the second phase precipitation causes the alteration of the atomic fractions of the elements in the matrix due to the exit of the elements required for precipitation. Thus, the atomic fraction of the elements in the matrix must be calculated by knowing the corresponding atomic fractions of the elements and measurement or an estimation of the weight fraction of the precipitate, according to the Eqs. 7.3-7.11:

$m_x = f_x A_x$ ($x$=Ni, Ti, ternary element, quaternary element…) (Eq. 7.3)

$$w_x = \frac{m_x I}{m_{Ni} + m_{Ti} + m_T + m_Q} = \frac{m_x I}{M_{Alloy}} \qquad \text{(Eq. 7.4)}$$

where $m_x$ is the weight of the element $x$ in the alloy formula, $f_x$ is its atomic fraction in the alloy, $A_x$ is the corresponding atomic weight of the element, $I$ is the total weight of the sample, and $M_{Alloy}$ is the molecular weight of the alloy. To calculate the weight of each element in the matrix after precipitation, the weight of elements that comprise the precipitate must be deducted from the corresponding $w_x$ values. Assuming a weight fraction of $P$ for the precipitate, and $f_x^{'}$ as the atomic fraction of element $x$ in the precipitate, the weight of elements in the precipitate is calculated as follows:

$$m_x^{'} = f_x^{'} A_x \qquad \text{(Eq. 7.5)}$$

$$w_x^{'} = IA_x \frac{m_x^{'} P}{m_{Ni}^{'} + m_{Ti}^{'} + m_T^{'} + m_Q^{'}} = \frac{m_x^{'} IP}{M_{\Pr ecipitate}} \qquad \text{(Eq. 7.6)}$$

where $m_x^{'}$ is the weight of the element $x$ in the precipitate formula, $w_x^{'}$ is its weight in the precipitate, and $M_{\Pr ecipitate}$ is the molecular weight of the precipitate. Hence, the weight of element $x$ in the matrix after precipitation, $w_x^{''}$, is calculated as follows:

$$w_x^{''} = w_x - w_x^{'} \qquad \text{(Eq. 7.7)}$$

Substituting for the terms on the right side yields:

$$w_x^{''} = IA_x \left(\frac{f_x}{M_{Alloy}} - \frac{f_x^{'} P}{M_{\Pr ecipitate}}\right) \qquad \text{(Eq.7.8)}$$

The number of moles of element $x$ in the matrix, $f_x^{*}$ is calculated by Eq. 7.9,

$$f_x^{*} = \frac{w_x^{''}}{A_x} \qquad \text{(Eq.7.9)}$$

and the atomic fraction of the element $x$ in the matrix after precipitation, $f_x^{''}$ is calculated from Eq. 7.10:

$$f_x^{''} = \frac{I\left(\frac{f_x}{M_{Alloy}} - \frac{f_x^{'} P}{M_{\Pr ecipitate}}\right)}{f_{Ni}^{*} + f_{Ti}^{*} + f_T^{*} + f_Q^{*}} \qquad \text{(Eq.7.10)}$$

The corresponding quantities of the precipitates are reported in Tables 7.1-7.3. Therefore, the aged valence electron concentration of the matrix can be calculated using Eq. 7.11:

$$(c_v)_{aged} = \frac{f''_{Ni}e_v^{Ni} + f''_{Ti}e_v^{Ti} + f''_T e_v^T + f''_Q e_v^Q}{f''_{Ni}Z_{Ni} + f''_{Ti}Z_{Ti} + f''_T Z_T + f''_Q Z_Q} \qquad \text{(Eq.7.11)}$$

where $f''_{Ni}$, $f''_{Ti}$, $f''_T$ and $f''_Q$ represent the atomic fractions of the elements of the matrix crystal after precipitation. In some cases, the chemical composition of the matrix before and after precipitation has been directly reported in the original reference without a need for measurement of the quantity of second phases formed. In most other cases, the second phase fractions are measured values, and in very few were estimated at 15wt% (Tables 7.1-7.3).

Comparisons between the matrix chemical composition and transformation temperature in solution-treated and aged conditions, together with the precipitates formed during aging, are presented in Tables 7.1-7.3 for a number of NiTi-based alloys. The data are accompanied by the calculated $c_v$ and $c_{v(\text{aged})}$ values based on Eqs. 7.2 and 7.11, the quantity of the precipitates, and the resulting aged matrix composition. The variation of $M_s$ of as-quenched and aged alloys with the valence electron concentration of the matrix is illustrated in Figure 7.1. In general, $M_s$ temperature decreases with increasing $c_v$. Figure 7.2 depicts the alteration of $M_s$ temperature ($\Delta M_s$) versus the change of valence electron concentration of the matrix after aging ($\Delta c_v$). It is evident that when $\Delta c_v = c_{v(\text{aged})} - c_v \approx 0$, the $\Delta M_s = M_{s(\text{aged})} - M_s$, is small (<15°C). However, if $\Delta c_v > 0$ then $\Delta M_s < 0$, whereas in the cases where $\Delta c_v < 0$, then $\Delta M_s > 0$ and the absolute value is $|\Delta M_s| > 15$°C (Figure 7.2). The absolute value of temperature change increases with increases in the absolute value of $\Delta c_v$. Aging can also alter the number of valence electrons ($e_v$/a) of the matrix. The $M_s$ temperature variation versus the change in the number of valence electrons of the matrix is illustrated in Figure 7.3. It is evident that for the alloys experiencing no change in $c_v$ after aging, the $M_s$ variation is small regardless of the value of $\Delta e_v$/a.

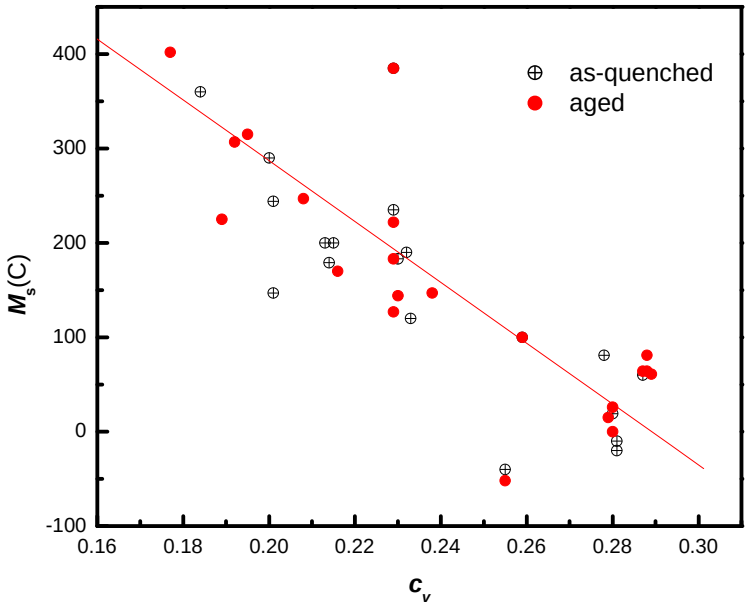


Figure 7.1: Variation of $M_s$ temperature of as-quenched and aged alloys with valence electron concentration of the matrix.

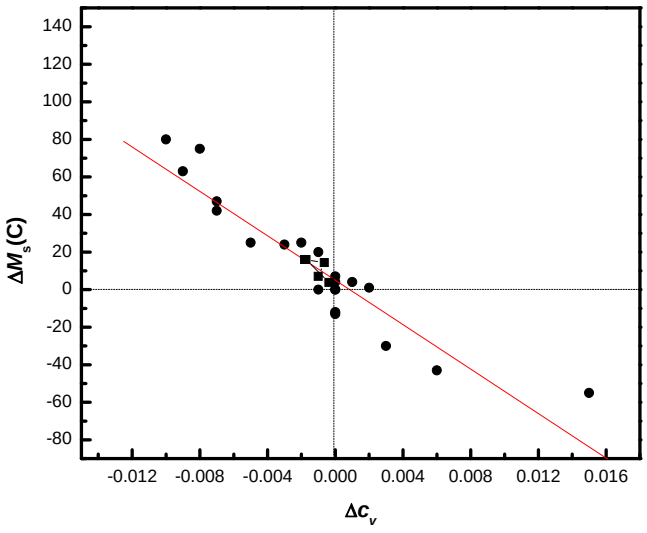


Figure 7.2: Influence of variation of valence electron concentration of the matrix after aging on the change of $M_s$ temperature.

The absolute value of temperature change increases with increasing the absolute value of $\Delta c_v$. Aging can also alter the number of valence electrons ($e_v$/a) of the matrix. The $M_s$ temperature variation versus the change in the number of valence electrons of

the matrix is illustrated in Figure 7.3. It is evident that for the alloys experiencing no change in $c_v$ after aging, the $M_s$ variation is small regardless of the value of $\Delta e_v/a$.

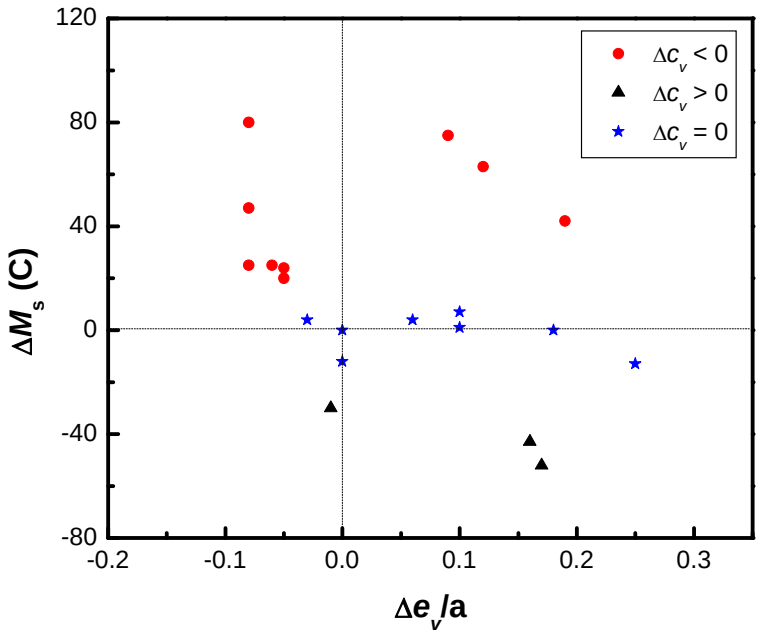


Figure 7.3: Influence of variation of the number of valence electron of the matrix after aging on the change of $M_s$ temperature.

## 7.3 Discussion

As indicated in Table 7.1-7.3, precipitation gives rise to two phenomena: first, the formation of the precipitate with coherent/incoherent relationship with the matrix, second, the chemical composition change of the matrix brought about by this formation. Both phenomena may influence the $M_s$ temperature as is discussed in the following.

### 7.3.1 Matrix (chemical composition, electron concentration and elastic constants)

The $M_s$ temperature is decreased with increasing $c_v$ in the aged alloys (Figure 7.1). This is consistent with our previously shown $M_s$-$c_v$ correlation for the as-quenced alloys with $M_s$ temperatures within the range -100 to 900 °C, part of which is presented

in Figure 7.1. Based on the data presented in Table 7.1 and 7.2, it is clear that as a result of precipitation, the change of matrix chemical composition alters the average electron concentration of the matrix. When $c_v$ is decreased, $M_s$ increases In contrast, when precipitation leads to an increase of $c_v$, $M_s$ is decreased (Figure 7.2). Depletion of Ni in the matrix of NiTiHf and NiTiPt and NiTi alloys dilutes the valence electron concentration (Table 7.1); whereas the exit of Ti and Pd from the matrix of the NiTiPd alloy and Ti and Hf from the NiTiHf alloys (Table 7.2) enriches the valence electron concentration of the matrix. Elastic bulk and shear moduli of transition metals and intermetallic crystals are dependent on and enhanced by increasing electron concentration [179,180]. Hence, in NiTi-based alloys an increase of $c_v$ translates into strengthening of bonds and therefore an increase of the elastic constants of austenite *B2* crystal. It has been shown that in transformation of *B2* to B19' martensite, the monoclinic shear and basal plane shear moduli, ($c_{44}$ and c'), play very crucial roles [11]. On the other hand, it is known that before the transformation occurs, during cooling a pre-martensitic softening of *B2* lattice takes place until a critical value is reached [2,48,49]. Hardening of $c_{44}$ and/or c' necessitates further cooling before transformation can occur. The net result is the decrease of transformation temperature which applies to the alloys in the (Table 7.2). In contrast, for NiTi, NiTiHf, and NiTiPt the electron concentration ($c_v$) is reduced as a result of composition change due to precipitation (Table 7.2). Reduction of $c_v$ in the matrix translates to lower shear and bulk moduli of the *B2* crystal. This leads to less resistance of the crystal against shape or volume change. Consequently less cooling for pre-martensitic softening is required before the martensitic transformation starts, and thus $M_s$ is elevated.

In the NiTiCu, NiTiZr, and other alloys listed in Table 7.3, after precipitation, the $c_v$ does not change significantly, although the matrix experiences some chemical composition alteration. It is evident that in these cases the change of $M_s$ is considerably smaller (Table 7.3). This is because the elastic constants which are the measures of resistance against transformation change insignificantly.

The $|\Delta M_s|$ increases by increasing $|\Delta c_v|$ as shown in Figure 7.2. This is indicative of the occurrence of more change in elastic constants as $|\Delta c_v|$ increases. The $\Delta M_s$-$\Delta c_v$ correlation in the NiTi-based SMAs is an almost linear relationship (Figure 2) which can be approximately represented by the Eq. 7.12:

$$\Delta M_s \approx -6000\ \Delta c_v \qquad \text{(Eq. 7.12)}$$

This empirical equation can also show the difference in $M_s$ of the quenched alloys with different valence election concentrations. A difference of 1000°C in $M_s$ exists between an alloy having $c_v$=0.10 ($M_s$=900°C) and another alloy of $c_v$=0.27 ($M_s$=-100°C reported in Chapter 5), which can be estimated satisfactorily by Eq. 7.12. Although the number of valence electrons of the matrix ($e_v$/a) are changed after precipitation, nonetheless Figure 7.3 shows that the dominant parameter is $\Delta c_v$ regardless of any positive or negative $\Delta e_v$/a.The change in the elastic constants in particular directions ($c_{44}$ and c') may also influence the energetics of *B2* phase change phenomenon and lead to the formation of intermediate phases requiring less strain energy such as B19 and R phase [11] which is not discussed here.

The discussion above indicates that the direction of variation of transformation temperature ($M_s$) as a result of precipitation in NiTi-based shape memory alloys is mainly influenced by how the resistance of *B2* lattice against transformation is affected by change of matrix valence electron concentration. An increase of $c_v$ results in a decrease in $M_s$ and its decrease leads to elevation of the transformation temperature of aged alloys. This is also a confirmation of the importance of the intrinsic elastic constants of the matrix in phase transformation which are closely related to electron concentration of the crystal.

### 7.3.2 Precipitate (coherency strain energy, amount, and distribution)

In the analysis of variations of $M_s$ due to precipitation, the extrinsic influence of precipitates should also be considered as is discussed in this section.

As indicated, in some NiTi-based alloys, second phase precipitation does not alter the valence electron concentration and therefore the elastic constants of the *B2* matrix (Table 7.3). It is logical to think if no change in the matrix elastic constants are brought about by precipitation, the direct influence of the strain induced by the precipitate into the matrix can be observed more clearly. This is the case of the alloys listed in Table 7.3. In these alloys, there is almost no change in matrix valence electron concentration, and this leads to only little change of $M_s$. Available evidence also

suggests that the influence of induced strain energy to the *B2* lattice, on the transformation temperature may be less pronounced than that of the change in elastic properties of the matrix (Tables 7.1-7.3). More detailed work is required to clarify the effect of coherency. The small but significant variation of the $M_s$ temperature is indicative of the influence of the interaction between precipitate and the matrix. However, if the number of valence electrons per atom becomes very close to 7, even in the absence of any change in the valence electron concentration, an elevation of the transformation may be observed due to specific overlapping occupancy of electrons at this value. This is consistent with what was reported in earlier chapters. The $Ni_{50.80}Ti_{49.20}$ alloy represents this condition (Table 7.1).

The precipitation of fine particles, when coherent with the matrix, induces additional energy to affect the relative stability of B2, B19', or intermediate phases such as R phase in NiTi-based alloys. This is the coherency strain energy associated with the lattice distortion during martensitic transformation [11]. During martensitic transformation *B2* is distorted into martensite lattice. However, the precipitates do not transform and do not follow such a shape change. Hence, strain energy increases, which is thought to be proportional to the square of transformation strain (η), $E = K\eta^2$, where K is related to elastic constants and distribution density of the precipitate particles and E represents the strain energy [11]. It is this additional energy that may also influence the transformation temperature and/or path.

Intuitively, it can be thought that the extent to which this additional energy is influential on the phase transformation temperature, is related to the characteristics of the precipitate such as its level of coherency with the matrix, the difference in its amount in the as-quenched and aged microstructures, and more importantly the level of the resistance it imposes against the shape change in matrix crystal in particular directions.

Higher degrees of coherency should result in an enhanced influence on the matrix through higher strain energies induced to the lattice. The interesting work of Rösner et al in the comparison of the coherent and incoherent precipitates confirms this fact [241].

The amount and distribution of the precipitates are dependent on the degree of supersaturation of the matrix and the microstructural defect populations [11,23,240].

Higher degree of supersaturation of the matrix with respect to Ni, Ti or alloying elements, gives rise to a higher amount of homogeneous distribution of precipitates during aging. However, when the degree of supersaturation is low, the precipitation occurs in less quantity and is favored by the presence of defects such as dislocations and grain boundaries [240]. The outcome is a preferred distribution of precipitates along these defects [11,239,240]. A unified model for explaining the microstructure evolution at low and high supersaturation which explains both three-stage and two-stage transformation behavior of supersaturated NiTi has been presented [11,240].

The change of $M_s$ can also be related to the amount of precipitate prior to aging. Figure 7.4 schematically illustrates the possible scenarios for precipitation when considering the quantity and type of precipitates before and after aging. Quenched samples are usually expected to have negligible amount of precipitates which upon aging produce considerable amount of precipitates (Figure 7.4, Scenario 7.4). Alternatively, they may include small but significant quantity of precipitates and aging increases the amount of these precipitates (Figure 7.4, Scenario 2). In some cases the quenched microstructure includes considerable amount of precipitates which do not significantly change as a result of aging (Figure 7.4, Scenario 3). It is also possible that a certain amount of precipitates in the quenched microstructure alter in type, size and quantity after aging (Figure 7.4, Scenario 4). Therefore, the direct influence of precipitation due to aging is also dependent on the quantity and type of precipitates in the quenched microstructures.

Any change in distribution pattern, size, or amount of precipitates can potentially influence the overall resistance to shape change of matrix crystal and therefore transformation temperature.

In summary, precipitation may exert both intrinsic and extrinsic effects. Intrinsic changes to the elastic constants of the matrix seem to cause larger transformation temperature variations than extrinsic strain energy induced by precipitate particles. However futher detailed study is required. The intrinsic energy is governed by lattice dynamics (elastic softening), while the extrinsic energies arise from resistance to lattice distortion (transformation) by precipitates or dislocations.

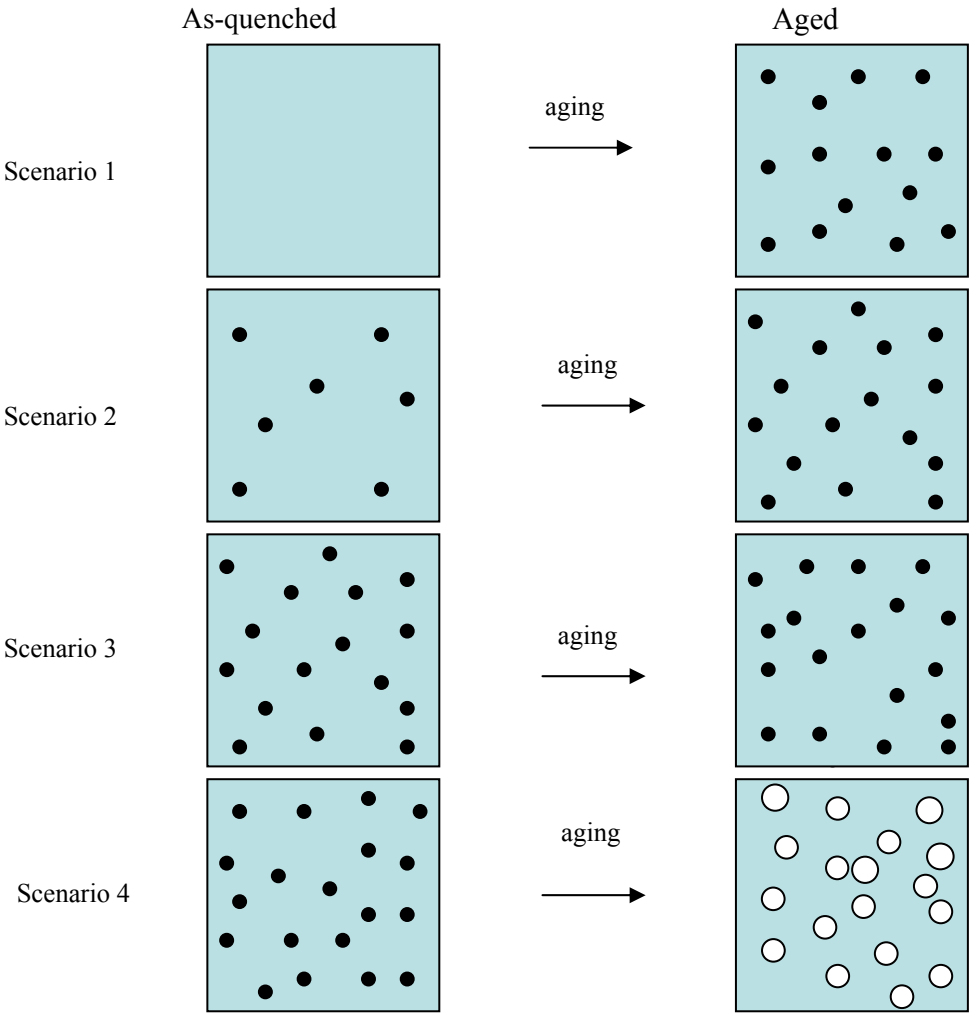


Figure 7.4: Schematic representation of the effect of aging on the type and quantity of precipitates. Scenario 1 depicts a condition where after quenching negligible amounts of precipitates exist and in the aged sample large quantity of the precipitate are formed from the supersaturated matrix. Scenario 2 illustrates the presence of some precipitate in the as-quenched samples. Aging increases the quantity of this precipitate. Scenario 3 shows the presence of large quantity of a precipitate in the as-quenched matrix which does not change in type or quantity significantly after aging. In Scenario 4 a quenched matrix having including a precipitate is shown which as a result of aging changes in type, and/or distribution pattern and/or quantity.

## 7.4 Summary

For NiTi-based shape memory alloys, the changes of martensite start temperature ($M_s$) as a result of second phase precipitation are studied. The alteration of $M_s$ as a result of precipitation is mainly due to the change of electron concentration of the matrix because of its composition change. The extrinsic effect of the precipitates on $M_s$ is also discussed on the basis of their quantity in the as-quenched and aged microstructures.

# Chapter 8

# 8 Evolution of Local Atomic Structure and Change of Transformation Temperature in a Melt-Spun $Ni_{25}Ti_{50}Cu_{25}$ Shape Memory Alloy during Crystallization

## 8.1 Introduction

NiTi-based alloys that exhibit a thermoelastic martensitic transformation are practically the most useful shape memory alloys [195]. Substitution of Cu for Ni in NiTi lowers the transformation hysteresis [196,252-255]. Crystalline $Ni_{25}Ti_{50}Cu_{25}$ is an attractive shape memory alloy with a small transformation hysteresis that may prove especially useful in actuating systems. When the Cu content is high (>10 at %) the bulk alloy embrittles considerably and workability is reduced which limits its applicability [253-256]. Melt-spinning is a technique that permits the fabrication of thin amorphous NiTiCu ribbons of high ductility [252-258], that should be crystallized to exhibit shape memory properties, with the effect of annealing on microstructure, texture, maretensitic transformation and shape memory properties of NiTiCu ribbon the subject of many studies [253-265]. To understand the structure-property relationships it is essential to know the atomic scale nature of the as-melt-spun ribbon, and the subsequent local chemical and bond evolution during crystallization. The NiTiCu alloy undergoes a martensitic transformation with onset around 335 K, and consequently, is in its martensitic state at room temperature if crystallized, adopting an orthorhombic structure (B19, *Pmmb*) [196].

The nature of metallic glasses is of considerable interest from both a fundamental viewpoint and to regulate functionality [266-268], and amorphous materials must possess some short-range order at atomic length scales to satisfy the requirements of chemical bonding. However, the applicability of several proposed structural models for metallic glasses (MGs) such as (i) Bernal's dense random packing of hard spheres [269,270], (ii) the stereochemically defined model, which stipulates that

nearest neighbors have the same structure as crystalline equivalents of similar composition [271,272], (iii) the medium-range order (MRO) description [273], and (iv) the face-centered cubic (f.c.c.) packing of overlapping clusters depiction [274] remain subjects for debate. Over the last decade, a body of evidence that includes experimental [275-280] and computational [280-282] investigations supports the existence of icosahedral atomic structures in some metallic glasses. The important work of Sheng et al has recently suggested that in general, Kasper polyhedron short range order is the main underlying topological SRO in MGs [283]. Based on this model, not only can the important role of the relative size between the solute and solvent atoms in MGs be validated [274,285,286], but the packing topologies for various coordination numbers specified [284]. Furthermore, the free volume (FV) has been widely adopted to explain the thermodynamic and mechanical behaviors of MGs, such as the rate of atomic diffusion and shear deformation localization, but deeper structural knowledge of MGs of different alloy systems will be essential to understand their crystallization mechanisms and properties.

An ideal tool to directly investigate local structures is X-ray absorption spectroscopy (XAS), with analysis of the extended X-ray absorption fine structure (EXAFS) providing information about nearest neighbor coordination, bond lengths, degree of disorder, and the chemistry of surrounding species. In this work, XAS was used to study the structure of melt-spun $Ni_{25}Ti_{50}Cu_{25}$ and its crystallochemical evolution in conjuction with thermal analysis through differential scanning calorimetry (DSC). Specifically, we explore the presence of short range order in a $Ni_{25}Ti_{50}Cu_{25}$ melt-spun ribbons and the evolution of chemical bonding during annealing.

## 8.2 Results

### 8.2.1 XRD

The XRD patterns of the as-prepared $Ni_{25}Ti_{50}Cu_{25}$ melt-spun alloy and some of the annealed samples exhibit a broad peak located at $2\theta \approx 42°$, being characteristic of the amorphicity (Fig. 8.1). Several additional peaks, located at $2\theta \approx 29°$, 38°, 40°, 42°, 45°, 60°, and 65°, were detected after annealing for 1, 3, 5 and 10 minutes which can be

indexed by a B19 (*Pmmb*) martensite phase. The emergence of peaks even at 1 min at 500ºC annealing indicates a short incubation and fast crystallization. For the longest annealing (5 and 10-min) narrow Bragg reflections indicate substantial or complete crystallization of the alloy.

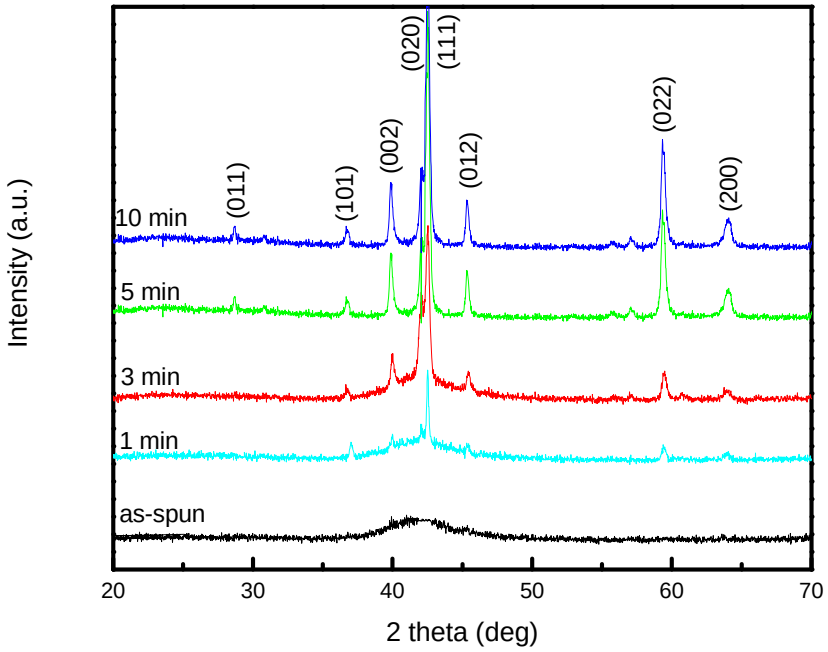


Figure 8.1: XRD patterns of $Ni_{25}Ti_{50}Cu_{25}$ of melt-spun ribbon, and annealed samples for 1, 3, 5 and 10 minutes.

## 8.2.2 DSC

Differential scanning calorimetry (DSC) shows the crystallization onset is near 500ºC when the heating rate is high (200ºC/min) (Fig. 8.2a). During isothermal heating at 500ºC, it is evident that prior to the sharp exothermic peak, a weak and diffuse exothermic peak (as indicated) is observed prior to attaining the hold temperature (Fig. 8.2b). This diffuse peak spans from nearly 1 min before reaching the isothermal temperature and terminates immediately before the evolution of the sharp crystallization peak around 1 minute into isothermal annealing, that is complete after 3-4 min (Fig. 8.2b). The melt-spun sample contains a very small quantity of a crystalline phase which exhibits reversible martensitic transformation. The corresponding enthalpy, in

comparison to the fully crystalline ribbon, suggests the presence of around 1-2% crystalline material in the as-spun sample (Fig. 8.3). Figure 8.4(a-b) shows the DSC cooling and heating curves of the martensitic transformation of the as-spun and annealed ribbon, respectively. The martensite start temperature ($M_s$) of the small amount of crystalline phase in this ribbon (52°C) rises with increasing annealing time and stabilizes around 63°C in fully crystalline sample (Fig 8.3, 8.4). The presence of shoulders on the martensite and reverse transformation peaks or even emergence of small separate peaks at intermediate annealing times is clearly observed (Fig. 8.4). As the annealing time for crystallization increases the amount of transformation heat released or absorbed increases, whereas the transformation hysteresis ($A_p$-$M_p$) of the ribbon decreases and stabilizes around 5°C after full crystallization (Fig. 8.4).

### 8.2.3 EXAFS

A direct comparison between the X-ray absorption fine structure (XAFS) data in wave vector (k) space for the as-prepared material and the samples treated for < 5 min shows small changes, while the longer annealing (> 10 min) yields more significant spectral changes for all K-edge spectra (Fig. 8.5). The Fourier transforms (FT) of the $k^3$ $\chi(k)$ data of Ni, Ti and Cu K-edge show clear structural differences as a function of annealing time (Fig.8.6). It is clear that these changes are much more pronounced for the Ti-K and the Cu-K edges compared to the Ni-K edge. The structural data obtained by fitting the first coordination shell are presented in Table 8.1 for the three elements. The interatomic distances either increase or are essentially constant following crystallization, where the overall coordination numbers increased. During isothermal annealing the relative fraction of Cu-Cu and Ti-Ti bonds in the ribbon initially increases (up to 3 min annealing) and is then reduces considerably by further annealing (10 min), whereas the Ni-Ni bond fraction progressively grows during crystallization. The R-space fitting of Cu edge data of as-prepared and 10 min treated (crystallized) samples show enhancement of Ti-Cu and suppression of Cu-Cu bond intensities (Fig. 8.7).

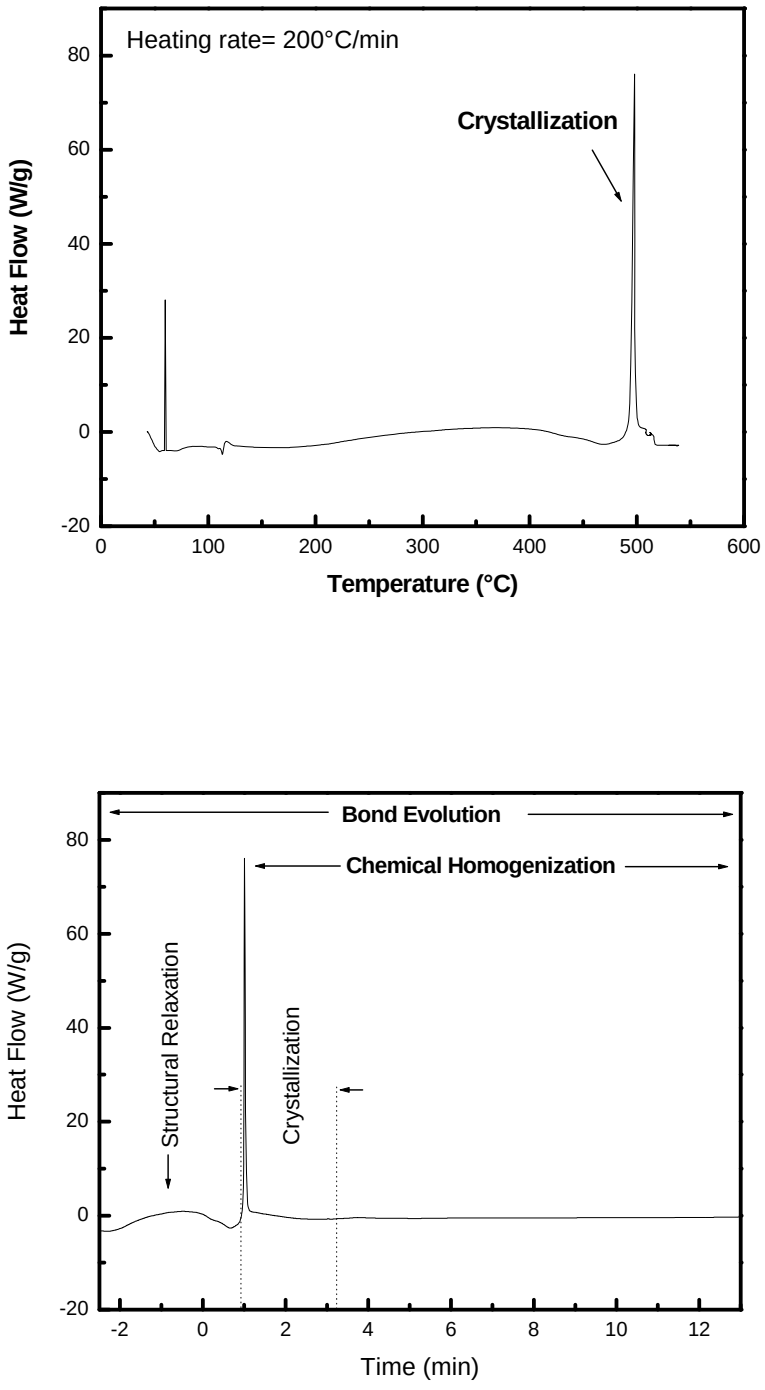


Figure 8.2: (a) DSC curve of as-melt spun $Ni_{25}Ti_{50}Cu_{25}$ ribbon measured at a constant heating rate of 200ºC /min and (b) the isothermal DSC curves of the as-spun $Ni_{25}Ti_{50}Cu_{25}$ ribbon measured at isothermal annealing temperature of 500°C.

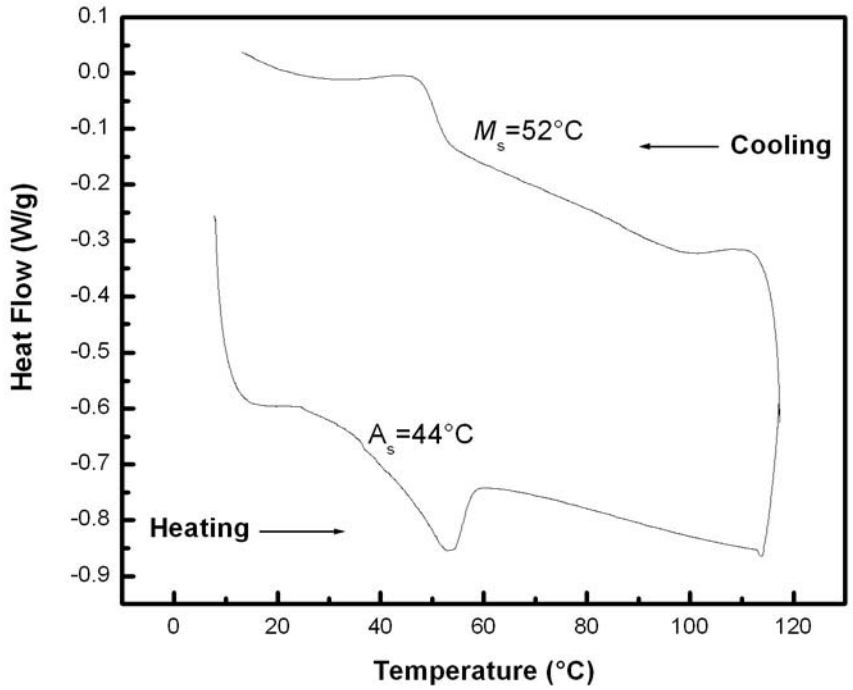


Figure 8.3: Thermoelastic martensitic transformation in the as-spun ribbon.

## 8.3 Discussion

### 8.3.1 Local atomic structure of the amorphous ribbon

Kasper polyhedron can describe the main underlying topological SRO in MGs [284]. In the as-prepared $Ni_{25}Ti_{50}Cu_{25}$ ribbon, the atoms show coordination numbers of ~10 for Ti, and ~12 for Cu and Ni atoms (Table 8.1).The similarity of bond lengths for Cu-Ti and Cu-Cu, and also Ni-Ti and Ni-Ni (Table 8.1) is indicative of a rather uniform local structure around Ni and Cu atoms in the as-prepared ribbon. For Ti atoms, evidence of segregation (between two phases) can be observed as the Ti-Ti interatomic distance is considerably larger than Ti-Ni in the as-prepared sample (2.88 vs. 2.55Å). The role of the relative size between the solute and solvent atoms in MGs has been validated [273,285,286] and the packing topologies for various coordination numbers

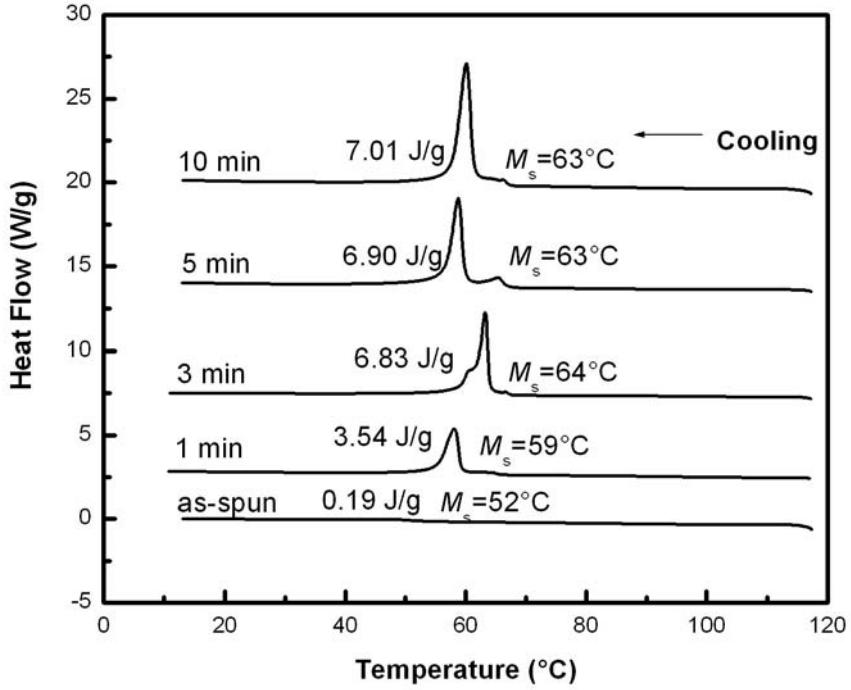


a

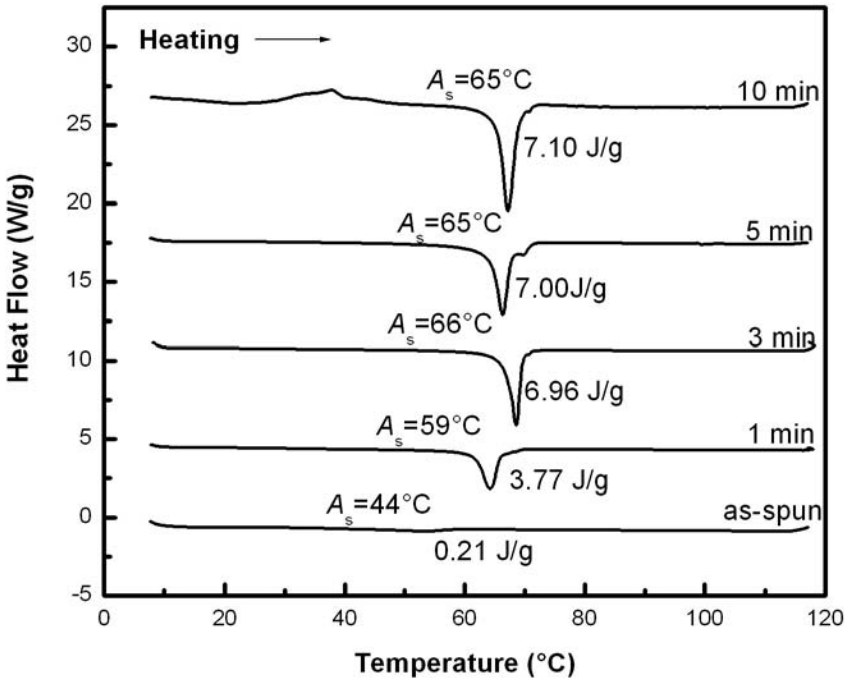


b

Figure 8.4: Thermal analysis of martensitic transformation

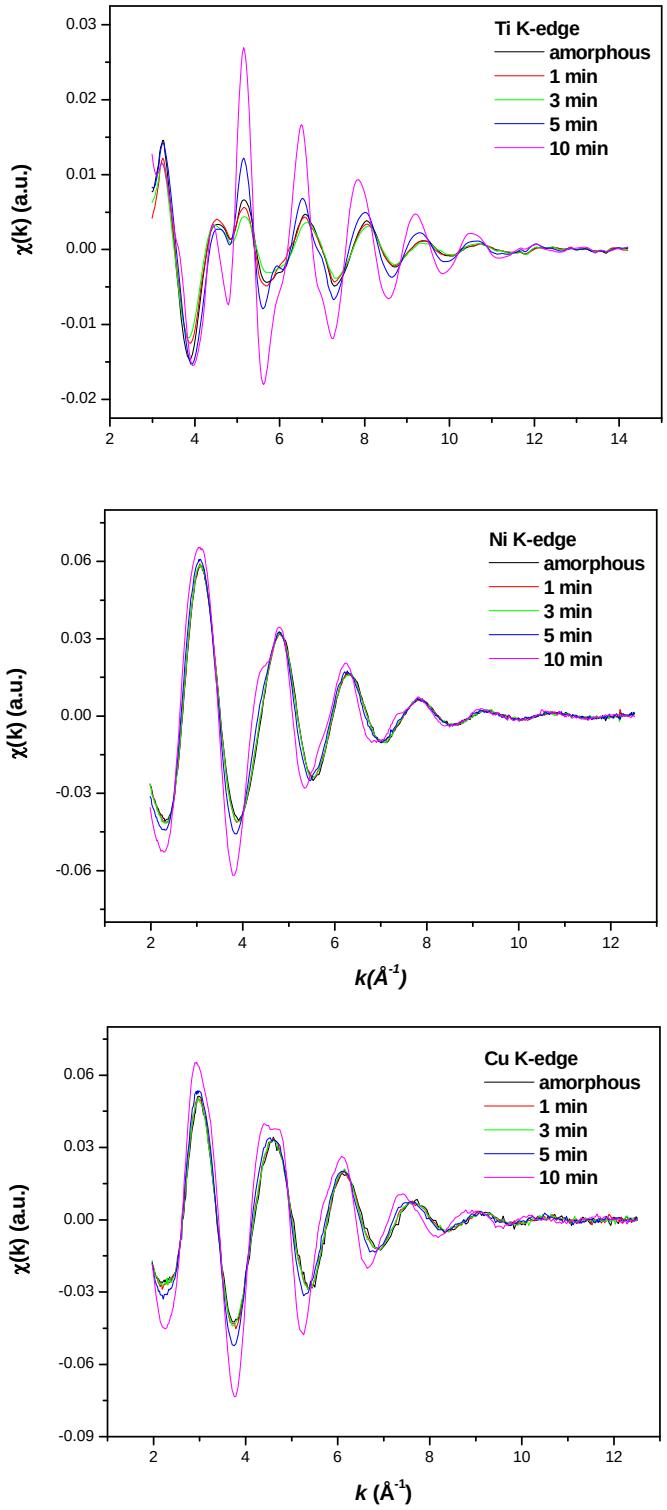


Figure 8.5: XAFS spectra at the Ti, Ni and Cu K-edges of $Ni_{25}Ti_{50}Cu_{25}$ ribbon, showing the differences due to changes of structural environment of the amorphous and annealed samples.

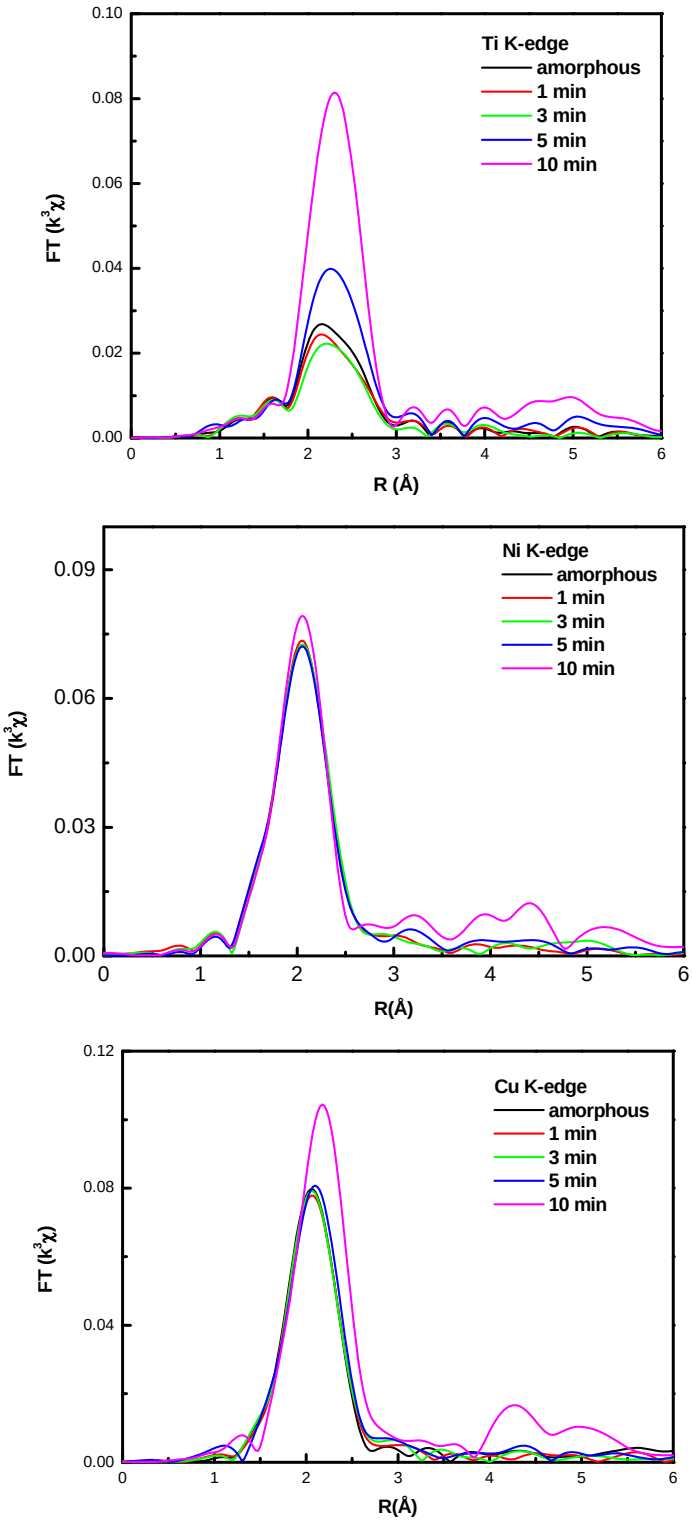


Figure 8.6: Fourier transforms of $k^3\,\chi(k)$ of (a) Ti K-edge, (b) Ni K-edge, and (c) Cu K-edge for $Ni_{25}Ti_{50}Cu_{25}$. Phase shift was not corrected.

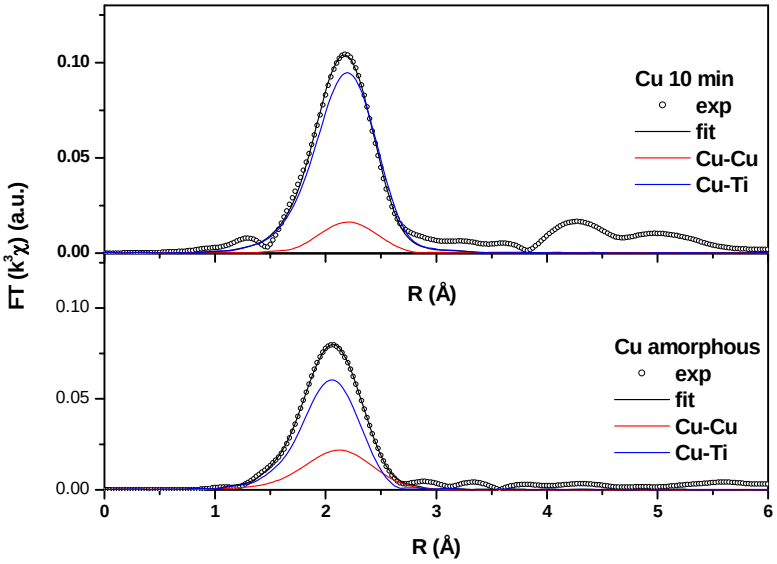


Figure 8.7: Experimental and the fit to the first shell of Cu K-edge FT at the amorphous and 10 min annealed states by employing two coordinations, Cu-Cu and Cu-Ti.

specified [284]. In this system, Ti is the solvent, Ni and Cu are the solutes, the effective atomic size ratios between the solutes and the solvent are $R^*_{Ni}\approx0.85$- $R^*_{Cu}\approx0.87$ and the interatomic distances of Ni-Ti and Cu-Ti are distinct from Ti-Ti (Table 8.1). Hence, the presence of two dominant types of Kasper polyhedra or distorted polyhedral clusters [284], centered with the solute species i.e Ni and Cu, could be deduced, with majority of polyhedra shell atoms being Ti.

The dense random packing model has proven to be inadequate to describe the atomic structures of real multi-component amorphous alloys [284,287,288]. Based on the theory of Turnbull and Cohen [289] and the concept of Egami *et al.* [290] the free volume (FV) around an atom originates from the breaking bonds between an atom and its neighbors. The overall coordination number of all species in as-prepared ribbon increases to some extent during annealing (Table 8.1). It has been shown that statistically, FV decreases with increasing coordination number of the atoms [284]. Moreover, the diffuse peak that appears before the main crystallization peak in the

Table 8.1: Structural parameters *N* (coordination number), *R* (interatomic distance), σ (relative displacement of atoms) and relative fraction of homo- and hetero-bonds, obtained from Ni, Ti, and Cu K-edge spectra analyzed by the EXAFS technique for as-prepared $Ni_{25}Ti_{50}Cu_{25}$ glassy alloy and the samples annealed at 773 K for 1, 3, 5 and 10 min.

**Ti edge**

| Annealing time | Number of Shells | *R* (Å) ± 0.02 | | *N* ± 1 | | $\sigma^2$(Å) ± 0.002 | | Relative fraction* |
|---|---|---|---|---|---|---|---|---|
| | | Ti-Ni | Ti-Ti | Ti-Ni | Ti-Ti | Ti-Ni(Cu) | Ti-Ti | |
| 0 min | 2 | 2.55 | 2.88 | 6.5 | 4.1 | 0.016 | 0.013 | 0.36 |
| 1 min | 2 | 2.56 | 2.88 | 6.1 | 4.2 | 0.017 | 0.014 | 0.37 |
| 3 min | 2 | 2.55 | 2.87 | 6.1 | 3.8 | 0.019 | 0.010 | 0.45 |
| 5 min | 2 | 2.59 | 2.91 | 7.2 | 4.7 | 0.012 | 0.011 | 0.32 |
| 10 min | 2 | 2.57 | 2.96 | 6.7 | 2.2 | 0.009 | 0.003 | 0.18 |

**Cu edge**

| Annealing time | Number of Shells | *R* (Å) ± 0.02 | | *N* ± 1 | | $\sigma^2$(Å) ± 0.002 | | Relative fraction* |
|---|---|---|---|---|---|---|---|---|
| | | Cu-Ti | Cu-Cu | Cu-Ti | Cu-Cu | Cu-Ti | Cu-Cu | |
| 0 min | 2 | 2.52 | 2.53 | 5.3 | 5.1 | 0.009 | 0.018 | 0.30 |
| 1 min | 2 | 2.52 | 2.56 | 4.6 | 5.8 | 0.009 | 0.017 | 0.35 |
| 3 min | 2 | 2.52 | 2.55 | 3.4 | 10.9 | 0.006 | 0.023 | 0.50 |
| 5 min | 2 | 2.55 | 2.57 | 4.6 | 9.3 | 0.008 | 0.026 | 0.42 |
| 10 min | 2 | 2.64 | 2.53 | 11.5 | 1.5 | 0.013 | 0.005 | 0.16 |

| Ni edge | | | | | | | | |
|---|---|---|---|---|---|---|---|---|
| Annealing time | Number of Shells | $R$ (Å) ± 0.02 | | $N$ ± 1 | | $\sigma^2$(Å) ± 0.002 | | Relative ratio* |
| | | Ni-Ti | Ni-Ni | Ni-Ti | Ni-Ni | Ni-Ti | Ni-Ni | |
| 0 min | 2 | 2.53 | 2.45 | 7.8 | 4.6 | 0.015 | 0.008 | 0.33 |
| 1 min | 2 | 2.54 | 2.45 | 7.6 | 5.9 | 0.016 | 0.010 | 0.42 |
| 3 min | 2 | 2.54 | 2.45 | 7.4 | 4.9 | 0.015 | 0.010 | 0.42 |
| 5 min | 2 | 2.53 | 2.46 | 8.1 | 4.7 | 0.017 | 0.010 | 0.40 |
| 10 min | 2 | 2.60 | 2.47 | 9.9 | 4.4 | 0.022 | 0.006 | 0.47 |

*The relative fraction indicates the fractions of the homo-bonds such as Ti-Ti, Cu-Cu and Ni-Ni. The relative ratios of the hetero-bond are (1 - corresponding value of the fraction of the homo-bond for each element).

isothermal DSC curve of crystallization at 500°C (Fig. 1) is a consequence of a structural relaxation that occurs to lower the energy of the alloy system [254,291,292].

Structural relaxation has been associated with the annihilation of the free volume (FV) which is characterized by a wide and diffuse exothermal peak in the DSC curve (Fig. 8.1). Tong et al have previously explained this phenomenon in the same alloy ribbon [195]. The excess energy available from a higher internal stress field associated with the free-volume provides additional driving force for crystallization [195]. These two evidences confirm the reduction of FV in $Ni_{25}Ti_{50}Cu_{25}$ as a result of crystallization and support the idea that the structure of as-prepared samples initially includes some free volume in addition to ordered structures.

### 8.3.2 Crystallization

Using calorimetric data (Fig. 8.8) the change of enthalpy in the martensitic transformation as a function of annealing time for the ribbons can be determined. As crystallization is fast at 500°C, the transformation enthalpy is considerable (3.54 J/g) even after 1 min annealing. Upon further annealing the enthalpy increases and approaches 7.01 J/g, indicating that about 50% of the material crystallizes within the first minute while the remaining volume orders more slowly prolonged ribbon annealing does not change the martensitic transformation enthalpy as reported recently by the Chang et al. [254]. The emergence and development of characteristic diffraction reflections corresponding to B19 martensite after 1 min annealing (Fig. 8.1) is consistent with the measured enthalpy that suggests partial crystallization and the coexistence of amorphous phase that exhibits a broad maximum. The characteristic crystalline peaks develop after 3 min annealing, leading to sharp and narrow Bragg reflections indicative of complete alloy crystallization after 10 min at 500°C (Fig. 1). Changes of all the K-edge absorption spectra confirm that crystallization becomes more significant with increasing annealing times (Fig. 8.5,8.6). The structural data obtained by fitting the first coordination shell for the three elements (Table 8.1) show that the local atomic structures in the as-prepared alloy are substantially altered by crystallization and include variations in interatomic distances, coordination numbers, and relative percentages of each pair component (Table 8.1). Although the structural (phase) change from amorphous to crystalline proceeds rapidly within the first 3 min of annealing (around 90% crystallized), changes in local atomic structure continue to the end of the annealing period (10 min), as the relative ratioes of each bond pair component and/or coordination numbers change considerably (Table 8.1). While there is some error for relative pair ratio due to multiple parameter correction, it is evident that the Ni-K edge is little altered, but Ti and Cu undergo significant changes after 10 min annealing. Hence, during crystallization, the local structures of Ni changes slightly, whereas those of Ti and Cu are modified to a remarkable extent. Ti tends to neighbor with Ni and Cu as the Ti-Ni, Ti-Cu, and Ni-Ti fractions increase, consistent with the preferential formation of stable Ni-Ti bonds during crystallization. Ni prefers to associate with Ni or Cu as crystallization proceeds (Table 8.1). It is important to note that at intermediate annealing times, the relative abundance of Cu-Cu and Ti-Ti bonds increases up to 3 minutes, then subsequently decreases with the formation of hetero-

bonds. To explain the enhancement of homo-bonds of Cu and Ti at initial and intermediate annealing times, the recent finding of Chang et al [254] are instructive.

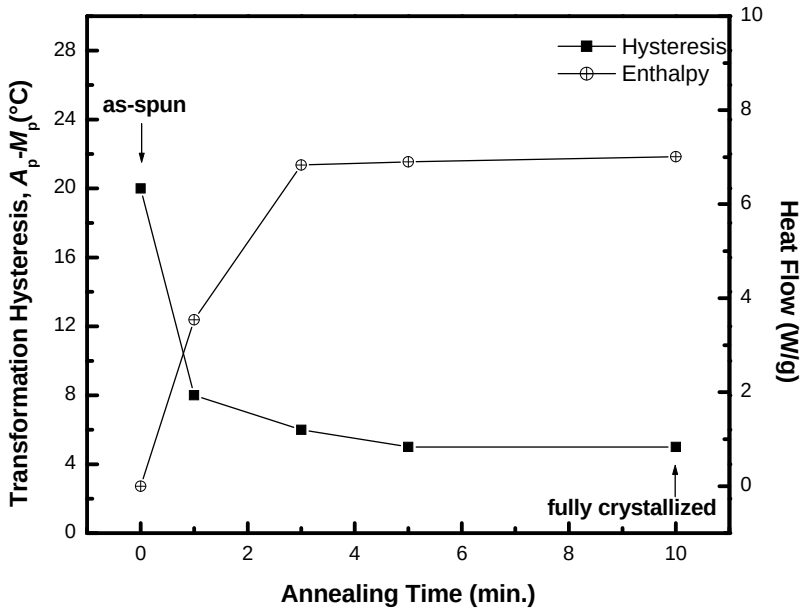


Figure 8.8: Change of transformation hysteresis of the crystalline phase of the ribbon by annealing

Semi-quantitative electron dispersive spectroscopy (EDS) shows the formation of Ti-rich and Cu-poor crystalline grains from early to intermediate crystallization times that by mass balance implies that the remaining amorphous phase is enriched in Cu and Ti-poor [254]. This interpretation is consistent with the bond evolution results of the current study. Figure 8.9 illustrates the variations of the relative homo-bonds fractions with respect to the hetero-bonds versus the annealing time. It is clear that the fractions of homo-bonds increase by annealing for up to 3 min, especially for Cu and Ti. As the formation of a Cu-rich amorphous phase increases the fraction of Cu-Cu bonds and crystallization of Ti-rich grains enhances the fraction of Ti-Ti bond. The emergence of shoulder-like features or separate peaks on the martensitic transformation DSC curves of the materials annealed for (1-5 min) (Fig 8.4), together with the change of transformation temperatures (Fig. 8.4), support the formation of martensite crystals of discrete chemical composition. Crystallization is substantially complete within the first 4 min with around 90% progress in the three minute. However, as is evident from Fig. 8.9, bond evolution continues for longer annealing times and is mainly related to formation of more Cu and Ti hetero-bonds (Fig. 8.9) that reduces the chemical

inhomogeniety by diffusion. The introduction of 25 at% Cu in NiTi crystals through replacement of Ni reduces the transformation hysteresis to around 5°C. Because crystals formed in the initial stages of crystallization are Cu-poor they exhibit a thermoelastic martensitic transformation with high hysteresis (>5°C) (Fig. 8.8). Increasing the annealing time lead to further diffusion of Cu into the crystallites and the transformation hysteresis is considerably reduced (Fig. 8.8), which confirms the decrease of the inhomogeniety of elements especially Cu and Ti in the microstructure.

Further annealing (10 min) considerably enhances the formation of Ti and Cu hetero-bonds indicative of the formation of TiCu clusters that cannot be detected by XRD. Cu K-edge FT reveals the formation of a long bond length component (Fig. 8.6), and Ti K-edge FT and fitting reveals that Ti tends to neighbor with Cu or Ni. Precipitation of the stable Ti(Cu, Ni) phase in the ribbon as a result of annealing has been indicated in several studies including the work of Tong et al [234].

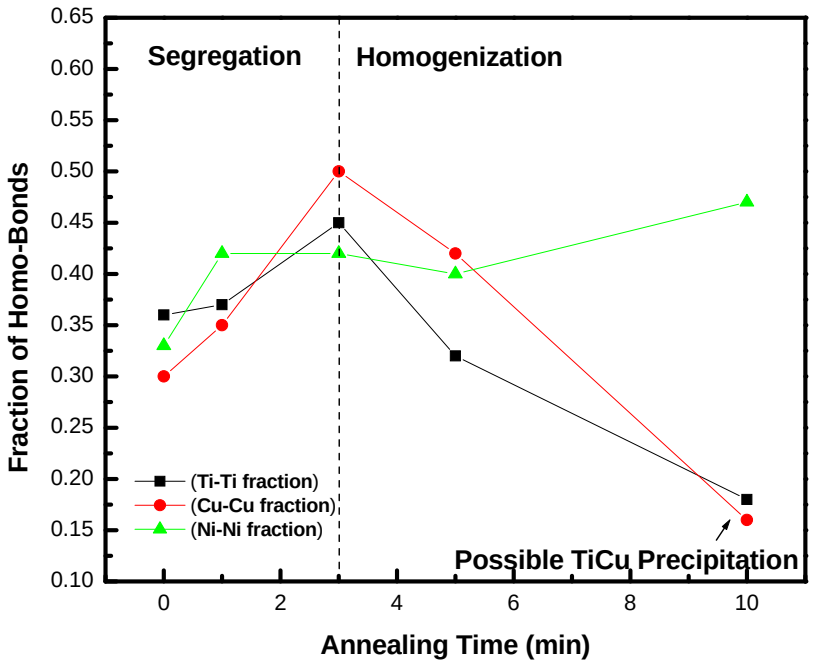


Figure 8.9: Bond evolution in $Ni_{25}Ti_{50}Cu_{25}$ ribbon during crystallization annealing.

By further annealing (10 min.) considerable reduction of relative fractions of Cu, and Ti homo-bonds which indicates the formation of Ti and Cu hetero-bonds can be

indicative of the formation of Ti Cu clusters, not detectable by XRD. From Cu K-edge FT, the formation of a long bond length component is evident (Fig. 8.6), moreover, Ti K-edge FT and fitting results indicate that at 10 min annealing, Ti tends to neighbor with Cu or Cu. Precipitation of the stable Ti(Cu, Ni) phase in the ribbon as a result of annealing has been indicated in several studies including the work of Tong et al [234].

In summary, crystallization of the $Ni_{25}Ti_{50}Cu_{25}$ ribbon is preceded by structural relaxation, that gives rise to segregation of Cu and Ti, and is followed by chemical homogenization of elements in the microstructure and formation of Ti(Cu,Ni) precipitates.

## 8.4 Summary

The local atomic environment of an amorphous $Ni_{25}Ti_{50}Cu_{25}$ met-spun ribbon and bond evolution during its crystallization were studied as an example of the change of local chemistry and its effect on transformation temperature of the alloy, by extended x-ray absorption fine structure (EXAFS) spectroscopy and differential scanning calorimetry (DSC). In the amorphous alloy the interatomic distances of Ni-Ti and Cu-Ti are distinct from Ti-Ti and can be indicative of the formation of two types of dominant polyhedra or distorted polyhedral clusters centered with Ni and Cu, with majority of shell atoms being Ti. The overall increase of the coordination numbers of Ni, Ti, and Cu by crystallization and an evidence for structural relaxation suggest the melt-spun alloy ribbon contains a combination of ordered structures and free volume prior to the heat treatment. Crystallization continues by a short-range Ti and Cu diffusion dominated process, as the near-neighbor structures of Ti and Cu change considerably more than Ni during annealing to homogenize the microstructure followed by possible precipitation of a TiCu compound. The segregation of Cu and Ti results in the change of chemical composition of the crystalline phase and brings about the varaiation of transformation temperature of the alloy during crystallization.

# Chapter 9

# 9 Conclusions

**Shape memory alloys, chemical composition and transformation temperatures**

The main correlations shown in this work introduce the most influencing factors, i.e. $e_v$/a and $c_v$, and antiferromagnetic effect of Mn, responsible for the changes of transformation temperatures in transition metal shape memory alloys. Shape memory alloys can be divided into low ($e_v$/a<5), medium (5≤$e_v$/a≤7.50), and high ($e_v$/a>7.50) electron groups with majority of the alloys in these groups following a relatively similar tendency of transformation temperature change. The valence electron concentration ($c_v$) is found to be an important parameter influencing the transformation temperatures for the majority of the shape memory alloys (main trend). $M_s$ and $A_s$ both decrease with increasing $c_v$ from 0.10 to around 0.27, remain almost constant beyond that and start to increase beyond 0.34-0.35. Increasing $c_v$ translate into increasing elastic moduli of the alloys which explains the transformation at lower temperatures. Three minor groups of alloys deviate from the main trend, 1) NiMnX (X=Ga, In, Al) Heusler alloys containing high Mn content (Mn≥ 30 at.%) show higher transformation temperatures most likely due to anti-ferromagnetism effect of this element and the consequent reduction of elastic properties, 2) high valence electron alloys having low or medium $c_v$ as a result of sufficient bonding provided by high number of valence electrons, and 3) low valence electron alloys with lower transformation temperatures possibly due to electron occupancy behavior of the d orbital.

**NiTi-based shape memory alloys, chemical composition and transformation temperatures**

The way the transformation temperatures of the alloys changes is distinctly related to whether their number of valence electrons per atom $e_v$/a = 7 or $e_v$/a ≠ 7. The valence electron concentration, $c_v$, is found to be an important parameter influencing the transformation temperatures. $M_s$ decreases with increasing $c_v$; whereas $A_s$ decreases with

increasing $c_v$ when $c_v \leq 0.27$, and increases with $c_v$ beyond this value. Transformation hysteresis is influenced considerably by the number of electrons per atom, ($e_v$/a), the d-d band electron occupancy, and atomic size of the alloying elements. The proposed correlations introduce probably the most influencing factors, i.e. $e_v$/a and $c_v$, responsible for the changes of transformation temperatures in NiTi-based ternary and quaternary alloys.

**NiTi-based shape memory alloys, precipitation and transformation temperatures**

The relationship between electron concentration and elastic properties was used to explain the change of $M_s$ temperature as a result of second phase precipitation in aged NiTi-based shape memory alloys. The following conclusions can be drawn:

The $M_s$ temperature of NiTi-based SMAs changes as a result of the change of valence electron concentration of the *B2* matrix due to second phase precipitation. The direction of the change in $M_s$ is mainly related to how the valence electron concentration of the matrix changes. Increase of $c_v$ results in a decrease of transformation temperature and vice versa. The change in the transformation temperature ($|\Delta M_s|$) increases with increasing absolute value of change of valence electron concentration$|\Delta c_v|$.

If precipitation does not change the average valence electron concentration of the matrix significantly, the slight transformation temperature change might be related to the extrinsic coherency energy induced by the precipitates particles. Futher work is required for clarification.

**NiTiHf shape memory alloys, local structure and transformation temperatures**

As a result of Hf addition to NiTi structure, the *'a'* and *'c'* lattice parameters, monoclinic angle (β), and unit cell volume increase; whereas *'b'* contracts in Ni-rich alloys and expands in Ti-rich and equiatomic alloys. The average Ni-Ni, Ti-Ti and Ni-Ti site bond lengths in NiTiHf alloys decrease by increasing the valence electrons per atom ratio ($e_v$/a) of the alloy when $e_v/a \neq 7$ (Ti-rich and equiatomic alloys). At $e_v/a = 7$ (Ni-rich alloys), increasing Hf content results in expansion of Ni-Ni and Ti-Ti site bonds

and contraction of Ni-Ti site bonds. Unit cell variations are influenced not only by the atomic radius of Hf but also by changes to the electronic structure of the alloy. In the present study it was found that at constant Hf content the unit cell volume could be ranked as Ti-rich>Ni-rich>equiatomic alloys. The partitioning of Hf across the Ni and Ti sites is similar, with a slight preference for the latter in line with the atomic radii considerations. The transformation temperatures of these alloys increase by reduction of valence electron concentration of the alloys.

**$Ni_{25}Ti_{50}Cu_{25}$ melt-spun shape memory alloy, local atomic structure**

The local atomic structures of Ti, Ni, and Cu in amorphous melt-spun $Ni_{25}Ti_{50}Cu_{25}$ alloy and annealed crystalline samples were probed by Ti, Ni, and Cu, K-edge EXAFS and DSC measurements. The formation of local coordination polyhedra is a manifestation of short range order in the amorphous alloy. From the thermal evidence for structural relaxation and an increase of overall coordination number of atomic species after annealing it is deduced that the alloy ribbons are composed of ordered structure and free volume prior to the heat treatment. After short and intermediate annealing times chemical inhomogeneity influences the overall bond evolution and enhances the frequency of Ti-Ti and Cu-Cu homo-bonds. This results in the formation of Ti-poor crystals and Cu enrichment of the remaining amorphous phase. Crystallization is rapid and the evolution of short range order during annealing arises mainly from variations of Ti and Cu local atomic structures as diffusion leads to homogenization of the microstructure. The structural relaxation, crystallization and chemical homogenization is followed by TiCu phase precipitation that results in a considerable increase of Ti, Cu hetero-bonds in the later stages of annealing.

# Original Contributions to Knowledge

1. In an original work, the relation between the transformation temperatures and valence electron concentration of the alloys is introduced and explained for the first time.
2. The influence of the number of valence electrons on the transformation temperatures in shape memory alloys in general and for NiTi-based intermetallics was shown by categorization of the alloys based on this parameter.
3. The intrinsic effect of precipitation in NiTi-based shape memory alloys was shown by the analysis of the change of electron concentration of the matrix of the alloys.For the first time the dependence of the direction of the alteration of transformation temperature as a result of aging was shown.
4. The crystal chemistry and local atomic structure of NiTiHf alloys were analyzed for the first time. The site occupancy of Hf in NiTi lattice was also experimentally determined and its influence of the transformation temperature was shown.
5. The local atomic structure and bond evolution of a melt-spun $Ni_{25}Ti_{50}Cu_{25}$ shape memory alloy during crystallization were shown for the first time.

# Recommendations for Future Work

Based on the knowledge achieved in this work, measurements of specific elastic constants of the shape memory alloys at temperatures before the corresponding martensitic transformation start temperatures are recommended.

Detailed study on the effect of Mn antiferroganetism on the elastic constants of the shape memory alloys and its effect of the transformation temperatures are recommended.

The influence crystal structure of austenite and martensite on the transformation temperature is an important area which needs to be studied in detail.

Since valence electron occupancy of the orbitals is an important factor in determining the elastic properties of the transition metal crystals a thorough study (first principle calculation study) is required.

# Author's Vita

Mehrdad Zarinejad has been involved in research work on development, and structure-property relationship in metallic and ceramic materials since 1995. He studied and worked at Sharif University of Technology (Iran), the University of Tehran (Iran), McGill University (Canada), Massachusetts Institute of Technology (USA), and University of Southern California (USA). Before joining Nanyang Technological University in 2007 the author served as the manager of materials development program for ThermicEdge-PrecisionH2 (Canada) during 2002-2004 and manager of science and technology for British Council (UK, Iran) from 2004-2006.

# References


1. K.N. Melton, 'Ni-Ti based shape memory alloys' in Engineering Aspects of Shape Memory Alloys, T. W. Duerig, K. N. Melton, D. Steckel, and C. M. Wayman, eds. 1990, Butterworth-Heinemann, Boston, MA, USA, 21–33.
2. G.B. Olson, W. Owen, eds, Martensite, 1992 ASM International, Materials Park, OH, USA.
3. E.K.H. Salje, Phase Transitions in Ferroelastic and Co-elastic Crystals 1993, Cambridge University Press, Cambridge, UK.
4. K. Otsuka, C. M. Wayman, Shape Memory Materials 1998, Cambridge University Press, Cambridge, UK.
5. C.S. Barrett, T.B. Massalski, Structure of Metals, Pergamon, Oxford, UK 1987.
6. K. Bhattacharya, S. Conti S, G. Zanzotto, J. Zimmer, Nature 2004, 428, 55.
7. A. Planes, L. Manosa, D. Rioa-Jara, J. Ortin, Phys Rev B 1992, 45, 7633.
8. L. Manosa, J. Zarestky, T. Lograsso, D.W. Dalaney, C. Stassis, Phys. Rev. B 1993, 48, 15708.
9. L. Manosa, M. Jurado, A. Planes, J. Zarestky, T. Lograsso, C. Stassis, Phys. Rev. B 1994, 49, 9969.
10. X. Ren, N. Miura, J. Zhang, K. Otsuka, K. Tanaka, M.A. Koiwa, Mater. Sci. Eng. A 2001, 312, 196.
11. K. Ostuka, X. Ren, Prog. Mater. Sci. 2005, 50, 511.
12. X. Ren, K. Taniwaki, K. Otsuka, T. Suzuki, K. Tanaki, Y.I. Chumlyakov, T. Ueiki, Phil Mag. A 1999, 79, 31.
13. G. Firstov, J. Van Humbeeck, Y.N. Koval, J. Intel. Mat. Syst. Str. 2006, 17, 1041.
14. S.F. Hsieh, S.K. Wu, J. Alloy. Compd. 1998, 266, 276.
15. Y. Suzuki, Y. Xu, S. Morito, K. Otsuka, K. Mitsoe, Mater. Lett. 1998, 36, 85.
16. M.K. Panuranga, D.D. Shin, G.P. Carman, Thin Solid Films 2006, 515, 1938.

17. Y. Xu, S. Shimizu, Y. Suzuki, K. Otsuka, T. Ueki, K. Mitose, Acta Mater. 1997, 45, 1503.
18. W. Cai, K. Otsuka, M. Asai, Mater. T. JIM 1999, 40, 895.
19. S.F. Hsieh, S.K. Wu, J. Alloy. Compd. 1998, 270, 237.
20. E. Cesari, P. Ochin, R. Portier, V. Kolomystsev, Y. Koval, A. Pasko, V. Soolshenko, Mater. Sci. Eng. A 1999, 273-275, 738.
21. K.H. Eckelmeyer, Scripta Metall. Mater. 1976, 10, 667.
22. C.W. Gong, Y.N. Wang, D.Z. Yang, J. Alloy. Compd. 2006, 419, 61.
23. D.R. Angst, P.E. Thoma, M.Y. Kao, J. Phys. IV 1995, 5, 747.
24. H. Hosoda, S. Hanada, K. Inoue, T. Fukui, Y. Mishima, T. Suzuki, Intermetallics 1998, 6, 291.
25. C. Zamponi, M. Wuttig, E. Quandta, Scripta Mater. 2007, 56, 1075.
26. H.C. Lin, K.M. Lin, S.K. Chang, C.S. Lin, J. Alloy. Compd. 1999, 284, 213.
27. S. Miyazaki, K. Otsuka, Phil. Mag. A 1984, 50, 393.
28. T. Takagi, Y. Suto, R. Kainuma, K. Yamauchi, K. Ishida, Appl. Biomater. B 2006, 76, 179.
29. T.H. Nam, D.W. Chung, J.S. Kim, S.B. Kang, Mater. Lett. 2002, 52, 234.
30. S.F. Hsieh, S.K. Wu, H.C. Lin, C.H. Yang, J. Alloy. Compd. 2005, 387, 121.
31. H. Steckmann, V. I. Kolomytsev, A. V. Kozlov, Ultrasonics 1999, 37, 59-62.
32. K. Chastaing, P. Vermaut, P. Ochin C. Segui J. Y. Laval, R. Portier, Mater. Sci. Eng. A 2006, 438-440, 661.
33. F.S. Liu, Y. Li, Y. Li, H. Xu, Mater. Sci. Eng. A 2006, 438-440, 896.
34. F. Liu, Z. Ding, Y. Li, H. Xu, Intermetallics, 2005, 13, 357.
35. G.B. Cho, T.Y. Kim, C.A. Yu, Y. Liu, T.H. Nam, J. Alloy. Compd. 2008, 449, 317.
36. Y.H. Li, L.J. Rong, Z.T. Wang, G.X. Qi, C.Z. Wang, J. Alloy. Compd. 2005, 400, 112.
37. S.F. Hsieh, S. K. Wu, J. Alloy. Compd. 2000, 312, 288.
38. H.C. Lin, C.H. Yang, K.M. Lin, G.K. Hsu, J. Alloy. Compd. 2005, 386, 157.

39. R. Zarnetta, A. Savan, S. Thienhaus, A. Ludwig, Appl. Surf. Sci. 2007, 254, 743.
40. K. Mohanchandra, K. Panduranga, D.D. Shin, G.P. Carman, Thin Solid Films 2006, 515, 1938.
41. Y. Tong, Y. Liu, Z. Xie, J. Alloy. Compd. 2007, 456, 170.
42. C. Gong, F. Guo, D.Z. Yang, J. Alloy. Compd. 2006, 426, 144.
43. P.L. Potapov, A.V. Shelyakov, A.A. Gulyaev, E.L. Svistunova, N.M. Mateveena, D. Hodgson, Mater. Lett. 1997, 32, 247.
44. P.K. Kumar, D.C. Lagoudas, in Proc. of SPIE, Vol. 6526: Behavior and Mechanics of Multifunctional and Composite Materials (Ed: J. Dapino), SPIE, 2007.
45. H. Rösner, P. Shloßmacher, A.V. Shelyakov, A.M. Glezer, Acta Mater. 2001, 49, 1541.
46. O. Rios, R. Noebe, T. Biles, A. Garg, A. Palczer, D. Scheiman, H.J. Seifert, M. Kaufman, in Proc. of SPIE Vol. 5761: Smart Materials and Structures (Ed: W.D. Armstrong), SPIE, 2005.
47. R. Noebe, D. Gaydosh, S. Padua II, A. Garg, T. Biles, M. Nathal, in Proc. of SPIE Vol. 5761: Smart Materials and Structures (Ed: W.D. Armstrong), SPIE, 2005.
48. P.C. Clapp, Phys Stat Sol B 1973, 57, 561.
49. P.C. Clapp, Met Trans A 1981, 12, 589.
50. W.D. Callister, Materials Science and Engineering: An Introduction, John Wiley and Sons, Asia 2007.
51. K. Parlinski, M. Oarlinska-wojtan, Phys. Rev. B, 2002, 66, 64307.
52. S.E. Kulkova, D.V. Valujsky, J.S. Kim, G. Lee, Y.M. Koo, Solid State Commun. 2001, 119, 619.
53. C.M. Wayman, T.W. Duerig, 'An introduction to martensite and shape memory' Engineering aspects of shape memory alloys, T. W. Duerig, K. N. Melton, D. Steckel, and C. M. Wayman, eds. 1990, Butterworth-Heinemann, Boston, MA, 3-20.
54. J.P. McCormick, PhD thesis, Georgia Institute of Technology 2006.
55. T. Tamaki, K. Otsuka, K. Shimizu, 'Shape memory alloys' Ann. Rev. Mater. Sci. 1988, 18, 25.

56. T.W. Duerig, G. Zane, 'An engineer's perspective of pseudo elasticity' Engineering aspects of shape memory alloys, T. W. Duerig, K. N. Melton, D. Stocked, and C. M. Wayman, eds. 1990, Butterworth-Heinemann, Boston, MA, 369–393.
57. R. DesRoches, J. McCormick, M. Delemont, J. Struc. Eng. 2004, 130, 38.
58. T.W. Duerig, K.N. Melton, D. Stockel, C.M. Wayman, Engineering aspects of shape memory alloy, 1990 Butterworth-Heinemann, Boston, MA, USA.
59. M. Asai, Y. Suzuki, 'Applications of shape memory alloys in Japan' Mater. Sci. Forum 2000, 327, 17.
60. S.E. Hsu, M.T. Yeh, I.C. Hsu, S.K. Chang, Y.C. Dai, J.Y. Wang, Mater. Sci. Forum 2000, 327, 119.
61. C.H. Beauchamp, R.H. Nadolink, S.C. Dickinson, L.M. Dean, in Proc. of the First European Conference on Smart Structures and Materials 1992, Glasgow, UK.
62. R. Chandra, Smart Mater. Struc. 2001, 10, 1018.
63. D.J. Hard, D.C. Lagoudas, Proceedings of the Institution of Mechanical Engineers, Part G: Journal of Aerospace Engineering 2007, 221, 535.
64. J.L. Ericksen, Arch. Ration. Mech. Anal. 1989, 107, 23.
65. P. Tole´dano, V. Dmitriev, Reconstructive Phase Transitions 1996, World Scientific, Singapore.
66. L.M. Barker, R.E. Hollenbach, J. Appl. Phys. 1974, 45, 4872.
67. K. Otsuka, K. Shimizu, Scripta Met. 1977, 11, 757.
68. T. Maki, I. Tamura, in Proc. Int. Conf. on Martensitic Transformations 1986, The Japan Institute of Metals, Nara, Japan.
69. J. Ortin, L. Delaey, Intl. J. Non-Linear Mech. 2002, 37, 1275.
70. R.J. Salzbrenner, M. Cohen, Acta Metall. 1979, 27, 739.
71. A. Planes, J.L. Macqueron, J. Ortin, Philos. Mag. Lett. 1988, 57, 291.
72. J. Ortin, A. Planes, J. Phys. IV 1991, 4, 4.
73. J. Ortin, J. Appl. Phys. 1992, 71, 1454.
74. S. Miyazaki, H.Y. Kim, H. Hosoda, Mater. Sci. Eng. A 2006, 438-440,18.
75. H.Y. Kim, S. Hashimoto, J.I. Kim, T. Inamura, H. Hosoda, S. Miyazaki, Mater. Sci. Eng. A 2006, 417, 120.
76. H.Y. Kim, Y. Ohmatsu, J.I. Kim, H. Hosoda, S. Miyazaki, Mater. Trans. 2004, 45, 1090.

77. D.H. Ping, Y. Mitarai, F.X. Yin, Scripta Mater. 2005, 52, 1287.
78. D.E. Soto-Parra, F. Alvarado-Hernandez, O. Ayala, R.A. Ochoa-Gamboa, H. Flores-Zuniga, D. Rios-para, J. Alloy. Compd. 2008, 464, 288.
79. M. Valeanu, G. Filoti, V. Kuncser, F. Tolea, B. Popescu, A. Galatanu, G. Schinteie, A.D. Jianu, I. Mitelea, D. Schinle, C.M. Craciunescu, J. Magne. Magne. Mater. 2008, 320, e164.
80. P.J. Webster, K.R.A. Ziebeck, S.L. Town, M.S. Peak, Phil. Mag. B 1984, 49, 295.
81. P. Zhao, L. Dai, J. Cullen, M. Wuttig, Metall. Mater. Trans. A 2007, 38, 745.
82. B.C. Maji, C.M. Das, M. Krishnan, R.K. Ray, Corrosion Sci. 2006, 48, 937.
83. J. Liu, H.X. Zheng, M.X. Xia, J.G. Li, Scripta Mater. 2005, 52, 955.
84. I. Glavatskyy, N. Glavatska, O. Söderberg, S.P. Hannula, J.U. Hoffmann, Scripta Mater. 2006, 54, 1891.
85. F. Dalle, V. Kolomytsev, P. Ochin, R. Portier, Scripta Mater. 2001, 44, 929.
86. Y. Tong, Y. Liu, Z. Xie, J. Alloy. Compd. 2007, 456, 170.
87. A. Sato, E. Chishima, Y. Yamaji, T. Mori, Acta Metall. 1984, 32, 539.
88. Y.N. Koval, G.S. Firstov, L. Delaey, J.V. Humbeeck, Scripta Metall. Mater. 1994, 31, 799.
89. T. Hoshiya, K. Inoue, K. Enami, in the Proc. of mechanical properties and phase transformations of multiphase intermetallic alloys 1994, TMS, USA, 99-106.
90. Y.N. Koval, G.S. Firstov, A.V. Kotko, Scripta Metall. Mater. 1992, 27, 1611.
91. G.S. Firstov, J. Van Humbeeck, Y.N. Koval, Mater. Sci. Eng. A 2004, 378, 2.
92. J.H. Zhang, W.Y. Peng, J.J. Zhang, X. Zuyao (T.Y. Hsu), Mater Sci Eng A 2008, 481-482, 326.
93. E.L. Semenova, V.M. Petyukh, Y.V. Kurdryavstev, J. Alloy. Compd. 1995, 230, 115.
94. E.L. Semenova, Y.V. Kudryavstev, J. Alloy. Compd. 1994, 203, 165.

95. G.S. Firstov, Y.N. Koval, J. Van Humbeeck, R. Portier, P. Vermaut, P. Ochin, Mater. Sci. Eng. A 2006, 438-440, 816.

96. T. Yamamuro, Y. Morizono, J. Honjyo, M. Nishida, Mater. Sci. Eng. A 2006, 438-440, 327.

97. K. Otsuka, K. Oda, Y. Ueno, M. Piao, Scripta Mater. 1993, 29, 1355.

98. X. Gao, W. Cai, Y.F. Zheng, L.C. Zhao, Mater. Sci. Eng. A 2006, 438-440, 862.

99. R.W. Fonda, H.N Jones, R.A. Vandermeer, Scripta Mater. 1998, 39, 1031.

100. T. Biggs, M.B. Cortie, M.J. Witcomb L.A. Cornish, Metall. Mater. Trans. A 2001, 32, 1881.

101. R.W. Fonda, R.A. Vandermeer, Phil. Mag. A 1997, 76, 119.

102. B.H. Chen, H.F. Franzen, J. Less-Common Metals, 1990, 157, 37.

103. R.D. McDonald, P.A. Goddard, J. Lashley, N. Harrison, C.H. Mielke, J. Singleton, H. Harima, M. Suzuki, J. Phys. Chem. Solids 2006, 67, 2100.

104. T Sakomoto, T. Fukuda, T. Kakeshita, Mater. Sci. Eng. A 2006, 438-440, 1036.

105. K. Tsuchiya, Y. Sho, T. Kushima, Y. Todaka, M. Umemoto, J. Magne. Magne. Mater. 2007, 310, 2764.

106. Y. Murakami, Appl. Phys. Lett. 2008, 92, 102512-1.

107. Z. Liu, S. Yu, H.Yang, G. Wu, Y. Liu, Intermetallics 2008, 16, 447.

108. J.M. Guilemany, F.J. Gil,. Thermochimica Acta, 1990, 167, 129.

109. L. Jian, C.C. Chou, C.M. Wayman, Mater. Chem. Phys. 1993, 34, 14.

110. S. Chatterjee, S. Giri, S. Majumdar, A.K. Deb, S.K. De, V. Hardy, J. Phys: Condens. Matter. 2007, 19, 346213-1.

111. H.S. Liu, C.L. Zhang, Z.D. Han, H.C. Xuan, D.H. Wang, Y.W. Du, J. Alloy. Compd. 2009, 467, 27.

112. H.C. Xuan, D.H. Wang, C.L. Zhang, Z.D. Han, B.X. Gu, Y.W. Du, Appl. Phys. Lett. 2008, 92, 102503-1.

113. T. Wada, T. Tagawa, M. Taya, Scripta Mater. 2003, 48, 207.

114. G.F. Xu, Z.M. Yin, S.Z. Mou, F.H. Lou, K. Oikawa, Trans. Nonferrous. Met. Soc. China 2006, 16, 776.

115. R.P. Mathur, R.K. Singh, V. Chandrasekaran, S. Ray, P. Ghosal, Metall. Mater. Trans. A 2007, 38, 2076.

116. D. Vokoun, Y.W. Wang, T. Goryczka, C.T. Hu, Smart. Mater. Struct. 2005, 14, S261.

117. N. Stanford, D.P. Dunne, B.J. Monaghan, J. Alloy. Compd. 2007, 430, 107.

118. J. Du, Q. Zheng, X. Ren, W.J. Feng, X.G. Liu, Z.D. Zhang, J. Phys. D: Appl. Phys. 2007, 40, 5523.

119. Y. Zhang, J. Gui, R. Wang, L. Gao, Y. Wu, Y. Tang, J. Phys.: Condens. Matter. 1993, 5, 2719.

120. H. Ishikawa, Y. Sutou, T. Omori, K. Oikawa, K. Ishida, A. Yoshikawa, R.Y. Umetsu, K. Kainuma, Appl. Phys. Lett. 2007, 90, 261906-1.

121. N. Zarubova, V. Novak, Mater. Sci. Eng. A 2004, 378, 216.

122. L. Gao, Z.Y. Gao, W. Cai, L.C. Zhao, Mater. Sci. Eng. A 2006, 438-440, 1077.

123. C. Segui, J. Pons, E. Cesari, J. Dutkiewicz, J. Mater. Sci. Eng. A 2006, 438-440, 923.

124. W.H. Wang, G.H Wu, J.L. Chen, S.X. Gao, W.S. Zhan, Appl. Phys. Lett. 2001, 79, 1148.

125. M. Landa, P. Sedlak, P. Sittner, H. Seiner, V. Novak, Mater. Sci. Eng. A 2007, 462, 320.

126. V. Recarte, C. Gomez-Polo, V. Sanchez-Alarcos, J.I. Perez-Landazabal. J. Magne. Magne. Mater. 2007, 316, e614.

127. L. Battezzati, G. Fiore, M. Massazza, J. Alloy. Compd. 2007, 434–435, 264.

128. D. Vokoun, T. Goryczka, C.T. Hu, J. Alloy. Compd. 2004, 372, 165.

129. W. Cai, L. Gao, A.L. Liu, J.H. Sui, Z.Y. Gao, Scripta Mater. 2007, 57, 659.

130. M. Wuttig, J. Li, C. Craciunescu, Scripta Mater. 2001, 44, 2394.

131. K. Tsuzaki, Y. Natsume, Y. Tomota, T. Maki, Scripta Metall. Mater. 1995, 33, 1087.

132. H. Morito, A. Fujita, K. Oikawa, K. Ishida, K. Fukamichi, R. Kainuma, Appl. Phys. Lett. 2007, 90, 062505-1.

133. S. Urbano, A. Mancaa, S. Besseghini, G. Airoldia , Scripta Mater. 2005, 52, 317.

134. Y. Murakami, T. Ohba, T. Morii, S. Aoki, K. Otsuka, Acta Mater. 2007, 55, 3203.

135. M. Kamal, Radia. Effec. Defec. Sol. 2006, 161, 189.

136. Y. Murakami, T. Yano, D. Shindo, R. Kainuma, K. Oikawa, K. Ishida, Scripta Mater. 2006, 55, 683.

137. W. Zhou, Y. Liu, B. Jiang, P. Zhou, Mater. Sci. Eng. A 2006, 438-440, 468.

138. X. Moya, Ll. Manosa, A. Planes, S. Aksoy, M. Acet M, E.F. Wassermann, T. Krenke, Phys. Rev. B 2007, 75, 184412-1.

139. A.A.H. Hamers, C.M. Wayman, Scripta Metall. 1991, 25, 2723.

140. X. Lu, B. Zhang, Z. Qin, Y. Zhang, B. Ding, Z. Hu, Mater. Sci. Eng. A 2003, 347, 258-264.

141. P.N. Zhang, J. Liu, J. Alloy. Compd. 2008, 462, 225.

142. Z.G. Wang, X.T. Zu, H.J. Yu, X. He, C. Peng, Y. Huo, Thermochimica Acta 2006, 448, 69.

143. V. Asanovic, K. Delijic, N. Jaukovic, Scripta Mater. 2008, 58, 599.

144. Q. Tian, F. Yin, T. Sakaguchi, K. Nagai, Acta Mater. 2006, 54, 1805.

145. Y. Kishi, Z. Yajima, K. Shimizu, M. Wuttig, Mater. Sci. Eng. A 2004, 378, 361.

146. G. Feng, C. Jiang, T. Liang, H. Xu, J. Magne. Magne. Mater. 2002, 248, 312.

147. H.B. Wang, C. Liu, Y.C. Lei, W. Cai, J. Alloy. Compd. 2008, 465, 458.

148. W. Maziarz, J. Alloy. Compd. 2008,448, 223.

149. Y. Liu, F. Ai, B. Jiang, Y. Liu, X. Qi, Mater. Sci. Eng. A 2006, 438-440, 999.

150. G.S. Firstov, Y.N. Koval, J. Van Humbeeck, P. Ochin, Mater. Sci. Eng. A 2008, 481-482, 590.

151. Z.C. Lin, W. Yu, R.H. Zee, B.A. Chin BA, Intermetallics 2000, 8, 605.

152. R.A.G. Silva, A. Cuniberti, M. Stipcich, A.T. Adorno, Mater. Sci. Eng. A 2007, 456, 5.

153. Y. Ma, C. Jiang, Y. Li, H. Xu, C. Wang, X. Liu, Acta Mater. 2007, 55, 1533.

154. T. Krenke, X. Moya, S. Aksoy, M. Acet, P. Entel, Ll. Manosal, A. Planes, Y. Elerman, A. Yucel, E.F. Wassermann, J. Magne. Magne. Mater. 2007, 310, 2788.

155. X. Moya, L. Manosa, A. Planes, T. Krenke, M. Acet, E.F. Wassermann, Mater. Sci. Eng. A 2006, 438–440, 911.

156. T.B. Massalski, H. Okamoto, P.R. Subramanian, L. Kacprzak, Binary alloy phase diagrams, 2nd edition 1990, vol. 3. ASM International, Materials Park, OH USA.T.H. Nam, T. Saburi, K. Shimizu, Trans. JIM 1990, 31, 959.

157. K. Otsuka, T. Kakeshita, MRS Bulletin 2002, 27, 91.

158. M. Bram, A. Ahmad-Khanlou, A. Heckmann, B. Fuchs, H.P. Buchkremer, D. Stover, Mater. Sci. Eng. A 2002, 337, 254.

159. K. Gall, K.H. Sehitoglu, Intl. J. Plasticity 1999, 15, 69.

160. K. Gall, H. Sehitoglu, Y.I. Chumlyakov, I.V. Kireeva, H.J. Maier, J. Eng. Mater. Tech. 1999, 121, 19.

161. X. Huang, G.J. Ackland, K.M. Rabe, Nature Materials 2003, 2, 307.

162. T.H. Nam, T. Saburi, K. Shimizu, Trans. JIM 1990, 31, 959.

163. G.R. Barsch, Mater. Sci. Forum 1999, 327–328, 367.

164. Z. Nishiyama, Martensitic Transformations. New York: Academic Press; 1978.

165. X. Ren, N. Miura, K. Otsuka, T. Suzuki, K. Tanaki, Y.I. Chumlyakov, Mater. Sci. Eng. A 1999, 273–275, 190.

166. J. Zhang, X. Ren, K. Otsuka, K. Tanaki, Y.I. Chumlyakov, M. Asai, Mater. Trans. JIM 1999, 40, 385.

167. X. Ren, K. Otsuka, Scripta Mater. 1998, 38, 1669.

168. A. Prasetyo, F. Reynaud, H. Warlimont, Acta Metall. 1976, 10, 789.

169. K. Otsuka, T. Sawamura, K. Shimizu, C.M. Wayman, Metall. Trans. 1971, 2, 2583.

170. G. Guenin, M. Morin, P.F. Gobin, W. Dijonghe and L. Delaey, Scripta Metall. 1977,11, 1071.

171. N. Nakanishi, Y. Murakami, S. Kachi, Scripta Metall. 1971, 5, 433.

172. S. Zirinsky, Acta Metall. 1956, 4, 164.

173. K. Enami, J. Hasunuma, A. Nagasawa, S. Nenno, Scripta Metall. 1976, 10, 879.

174. O. Mercier, K.N. Melton, G. Gremaud, J. Hagi, J. Appl. Phys. 1980, 51, 1833.

175. V.N. Khachin, S.A. Muslov, V.G. Pushin, Y.I. Chumlyakov, Sov. Phys. Dokl 1987, 32, 606.T. Honma, M. Matsumoto, Y. Shugo, M. Nishida, I. Yamazaki, in Proc. 4th Intl Conf. on Titanium, H. Kimura, O. Izumi eds. 1980, AIME; Kyoto, Japan.

176. T.M. Brill, S. Mittelbach, W. Assmus, M. Müllner, B. Lüthi, J .Phys.: Condens. Matter 1991, 3, 9621.

177. W. Tang, Metall. Trans. A 1997, 28, 537.

178. Y. Nakata, T. Tadaki, K. Shimizu, Mater. Trans. JIM 1991, 32, 580.

179. J. Gilman, R.W. Cuberland, R.B. Kaner, Int. J. Refract. Met. H. 2006, 24, 1.

180. J. Gilman, Electronic Basis of the Strength of Materials, Cambridge University Press, Cambridge, UK 2003.

181. C. Kittel, Introduction to Solid State Physics 8$^{th}$ Ed. John & Wiley Sons, USA, 200.

182. H. Ledbetter, Z. Metallkd. 1991, 82, 820.

183. W. Pfeiler (Ed.), Alloy Physics: A Comprehensive Reference vol. 1, 2007 Wiley-VCH Verlag GmbH & Co. KGaA, Weinheim**.**

184. V.L. Moruzzi, P.M. Marcus, Phys. Rev. 1993, 48, 7665.

185. Y. Nakata, T. Tadaki, K. Shimizu, Mater. Trans. JIM 1991, 32, 1120.

186. Y. Nakata, T. Tadaki, K. Shimizu, in Proc. of Displacive phase transformations and their applications in materials engineering, K. Inoue, K. Mukherjee, K. Otsuka, H. Chen, eds. 1998, TMS, USA.

187. G. Bozzolo, R.D. Noebe, H.O. Mosca, J. Alloys. Compd. 2005, 389, 80.

188. G. Bozzolo, H.O. Mosca, R.D. Noebe, Intermetallics 2007, 15, 901.

189. X. Ju, Y. Su, J. Synchrotron Rad. 2001, 8, 520.

190. P.A. Bhobe, K.R. Priolkar, P.R. Sarode, Phys. Rev. B 2006, 74, 224425-1.

191. A. Mehta, V. Imbeni, R.O. Ritchie, T.W. Duerig, Mater. Sci. Eng. A 2004, 378, 130-137.

192. M. Fuyuma, M. Matsumoto, H. Kimura, K. Aoki, M. Masumoto, Marter. Trans. JIM, 1990, 31, 504.

193. Y.X. Tong, PhD Thesis, Nanyang Technological University 2008.

194. T.M. Nam, S.M. Park, T.Y. Kim, Y.W. Kim, Smart Mater. Struc. 2005, 14, s239.

195. Y.X. Tong, Y. Liu, J. Alloys Compd. 2008, 449, 152.

196. Y.W. Kim, T.H. Nam, Scripta Mater. 2004, 51, 653.

197. H. Rösner, A.V. Shelyakov, A.M. Glezer, P. Schloßmacher, Mater. Sci. Eng. A 2001, 307, 188.

198. P.E. Thoma, J.J. Boehm, Mater. Sci. Eng. A 1999, 273–275, 385.

199. R.W. Cheary, A. Coelho, J. Appl. Crystallogr. 1992, 25, 109.

200. Y. Kudoh, M. Tokonami, S. Miyazaki, K. Otsuka, Acta Metall. 1985, 33, 2049.

201. J. Khalil-Allafi, W.W. Schmahl, M. Wagner, H. Sitepu, D.M. Toebbens, G. Eggeler, Mater. Sci. Eng. A 2004, 378, 161.

202. T. Liu, X. Gao, A.T.S. Wee, Y. Ping, H.O. Moser, Adv. Sync. Radiat. 2008, 1, 79.

203. H.O. Moser, Nucl. Instru. Mthds. Phys. Res. Sec. B 2005, 235, 83.

204. T.J. Ressler, J. Synchrotron Radiat. 1998, 5, 118.

205. A.L. Ankudinov, B. Ravel, J.J. Rehr, S.D. Conradson, Phys. Rev. B 1998, 58, 7565.

206. P.J. Brown, J. Phys. Condens. Matter. 1999, 11, 4715.

207. S. Fujii, J. Phys. Soc. Japan 1989, 58, 3657.

208. S. Imada, A. Yamasaki, T. Kanomata, T. Muro, A. Sekiyama, S. Suga, J. Magne. Magne. Mater. 2007, 310, 1857.

209. C. Jiang, Y. Muhammad, L. Deng, W. Wu, H. Xu, Acta Mater. 2004, 52, 2779.

210. M. Ahler, Prog. Mater. Sci. 1986, 30, 135.

211. F. Albertini, L. Pareti, A. Paoluzi, L. Morellon, P.A. Algarabel, M.R. Ibarra, Appl. Phys. Lett. 2002, 81, 4032.

212. E.W. Collings, H.L. Gegel, Scripta Metall 1973,7,437.

213. C.A. Luke, R. Taggart, D.H. Polonis, Trans. ASM 1964, 57, 142.

214. E.W. Collings, The physical metallurgy of Titanium Alloys, ASM, 1986.

215. H.L. Hao, S.J. Li, S.Y. Sun, C.Y. Zheng, R. Yang, Acta Biomater 2007, 3, 277.

216. X.L. Meng, W. Cai, F. Chen, L.C. Zhao, Scripta Mater. 2006, 54, 1599.

217. B. Kockar, I. Karaman, J.I. Kim, Y.A. Chumlyakov, Scripta Mater 2006, 54, 2203.

218. S. Sanjabi, Y.Z. Cao, Z.H. Barber, Sensors and Actuators A 2005, 121, 543.

219. D.S. Grummon, JOM 2003, 55, 24.

220. P.L. Potapov, A.V. Shelyakov, A.A. Gulyaev, E.L. Svistunova, N.M. Mateveena, D. Hodgson, Mater. Lett. 1997, 32, 247.

221. X.L. Meng, Y.X. Tong, K.T. Lau, W. Cai, L.M. Zhou, L.C. Zhao, Mater. Lett. 2002, 57, 452.

222. S. Besseghini, E. Villa, A. Tuissi, Mater. Sci. Eng. A 1999, 273–275, 390.

223. X.L. Meng, W. Cai, Y.F. Zheng, L.C. Zhao, Mater. Sci. Eng. A 2006, 430–440, 666.

224. A. Simon, Angew. Chem. Int. Ed 1983, 22, 95.

225. M.L. Bhatia, R.W. Cahn, Intermetallics 2005, 13, 474.

226. R.W. Cahn, Intermetallics 1999, 7, 1089.

227. M.L. Bhatia, A.K. Singh, T.K. Nandy, Intermetallics 1997, 6, 141.

228. H.J. Weber, J. Non-Cryst. Solids 1999, 243, 220.

229. I. Bakonyi, Acta Mater. 2005, 53, 2509.

230. O. Coreno-Alonso, Intermetallics 2006, 14, 475.

231. A.O. Mekhrabov, M.V. Akdeniz, Acta Mater. 1999, 47, 2067.

232. H.C. Lin, C.H. Yang, M.C. Lin, C.S. Lin, K.M. Lin, L.S. Chang, J. Alloys Compds. 2008, 449, 119.

233. S.F. Hsieh, S.K. Wu, Mater. Charac. 1998, 41, 151.

234. Y.X. Tong, Y. Liu, Z. Xie, M. Zarinejad, Acta Mater. 2008, 56, 1721.

235. S.K. Wu, S.F. Hsieh, J. Alloy. Compds 2000, 297, 294.

236. X.L. Meng, Y.F. Zheng, Z. Wang and L.C. Zhao, Scripta Mater. 2000, 42, 341

237. H. Rösner, P. Schloßmacher, A.V. Shelyakov, A.M. Glezer, Scripta Mater. 2000, 43, 871.

238. H.C. Lin, S.K. Wu, J.C. Lin, Mater. Chem. Phys. 1994, 37, 184.

239. J. Khalil-Allafi, G. Eggeler, W.W. Schmahl, D. Sheptyakov, Mater. Sci. Eng. A 2006, 438–440, 593.

240. G. Fan, W. Chen, S. Yang, J. Zhu, X. Ren, K. Otsuka, Acta Mater. 2004, 52, 4351.

241. V.Ya. Abramov, N.M. Aleksandrova, D.V. Borovkov, I.Yu. Khmelevskaya, A.V. Korotitskiy, S. Yu. Makushev, N.A. Polyakova, N.N. Popov, S.D. Prokoshkin, Mater. Sci. Eng. A 2006, 438-440, 553.

242. M. Peltonen, T. Lindroos, M. Kallio, J. Alloy. Compd. 2008, 460, 237.

243. K. Gall, H. Sehitoglu, Y.I Chumlyakov, I.V. Kireeva, H.J. Maier, J. Eng. Mater. Tech. 1999, 121, 20.

244. H. Rösner, P. Schloßmacher, A.V. Shelyakov, M. Glezer, Mater. Trans. 2001, 42, 1758.

245. X.L. Meng, W. Cai, Y.D. Fu, Q.F. Li, J.X. Zhang, L.C. Zhao, Intermetallics 2008, 16, 698.

246. X.D. Han, R. Wang, Z. Zhang, D.Z. Yang, Acta Mater. 1998, 46, 273.

247. X.D. Han, W.H. Zhou, R. Wang, Z. Zhang, D.Z. Yang, Acta Mater. 1996, 44, 3711.

248. G. Eggeler, J. Khalil-Allafi, S. Gollerthan, C. Somsen1, W. Schmahl, D. Sheptyakov, Smart Mater. Struct. 2005, 14, S186.

249. J. Michutta, Ch. Somsen, A. Yawny, A. Dlouhy, G. Eggeler, Acta Mater. 2006,54, 3525.

250. S. Shimizu, Y. Xu, E. Okunishi, S. Tanaka, K. Otsuka, K. Mitose, Mater. Lett. 1998, 34, 23.

251. T. Sawaguchi, M. Sato, A. Ishida, Mater. Sci. Eng. A 2002, 332, 47.

252. Q. Tian, J. Wu, Intermetallics 2002, 10, 675.

253. Z.L. Xie, J. Van Humbeeck, Y. Liu, L. Delaey, Scripta Mater. 1997, 37, 363.

254. S.H. Chang, S.K. Wu, H. Kimura, Mater. Sci. Eng. A 2008, 476, 316.

255. P. Schloßmacher, N. Bouncharat, H. Rösner, G. Wilde, A.V. Shelyakov, J. Phys. IV France 2003, 112, 731.

256. R. Santamarta, D. Schryvers, Mater. Trans. 2003, 44, 1760.

257. Y. Liu, Mater. Sci. Eng. A 2003, 354, 286.

258. G.P. Cheng, Z.L. Xie, J. Alloys. Compd. 2005, 396, 128.

259. S.H. Chang, S.K. Wu, H. Kimura, Mater. Trans. 2006, 47, 2489.

260. Y. Liu, Z.L. Xie, Y.X. Tong, C.W. Lim, J. Alloys. Compd. 2006, 416, 188.

261. S.H. Chang, S.K. Wu, H. Kimura, Intermetallics 2007, 15, 233.

262. G.P. Cheng, Z.L. Xie, Y. Liu, Mater. Sci. Eng. A 2006, 425, 268.

263. Z.L. Xie, G.P. Cheng, Y. Liu, Acta Mater. 2007, 55, 361.

264. H. Miyamoto, T. Taniwaki, T. Ohba, K. Otsuka, S. Nishigori, K. Kato, Scripta Mater. 2005, 53, 171.

265. S. Miyazaki, K. Mizukoshi, T. Ueki, T. Sakuma, Y.N. Liu, Mater. Sci. Eng. A 1999, 273–275, 658.

266. L. Yang, J.Z. Jiang, T. Liu, T.D. Hu, T. Uruga, Appl. Phys. Lett. 2005, 87, 61918.

267. D.R. Nelson, F. Spaepen, Solid State Phys. :Adv. Res. Appl. 1989, 42, 1.

268. J.P.K. Doye, D. J. Wales, Science 1986, 271, 484.

269. F. Spaepen, Nature 2000, 408, 781.

270. J.D. Bernal, Nature 1960, 185, 68.

271. P.H. Gaskell, Nature 1978, 276, 484.

272. P.H. Gaskell, J. Non-Cryst. Solids 2005, 351, 1003.

273. S.R. Elliot, Physics of Amorphous Materials 2nd ed. (Longman, London, 1990).

274. D.B. Miracle, Nature Mater. 2004, 3, 697.

275. L.Q. Xinq, T.C. Hufnagel, J. Eckert, W. Löser, L. Schultz, Appl. Phys. Lett. 2001, 79, 42.

276. K. Saksl, H. Franz, P. Jovari, K. Klementiev, E. Welter, A. Ehnes, J, Saida, A. Inoue, J. Z. Jiang, Appl. Phys. Lett. 2003, 83, 3924.

277. J. Saida, N. Matsushita, A. Inoue, Appl. Phys. Lett. 2001, 79, 412.

278. T. Takagi, T. Ohkubo, Y. Hirotsu, B.S. Murty, K. Hono, D. Shindo, Appl. Phys. Lett. 2001, 79, 485.

279. M.W. Chen, I. Dutta, T. Zhang, A. Inoue, T. Sakurai, Appl. Phys. Lett. 2001, 79, 42.

280. W.K. Luo, H.W. Sheng, F.M. Alamgir, J.M. Bai, J.H. He, E. Ma, Phys. Rev. Lett. 2004, 92, 145502.

281. J. Jonsson, H.C. Anderson, Phys. Rev. Lett. 1988, 60, 2295.

282. F. Yonezawa, Solid State Phys. 1991, 45, 179.

283. A.S. Clarke, H. Jonsson, Phys. Rev. E 1993, 47, 3975.

284. H.W. Sheng, W.K. Luo, F.M. Alamgir, J.M. Bai, E. Ma, Nature (London) 2006, 439, 419.

285. D.B. Miracle, W.S. Sanders, O.N. Senkov, Phil. Mag. A 2003, 83, 2409.

286. T. Egami, Y. Waseda, J. Non-Cryst. Solids 1984, 64, 113.

287. C. Fan, P.K. Liaw, V. Haas, J.J. Wall, H. Choo, A. Inoue, C.T. Liu, Phys. Rev. B 2006, 74, 014205.

288. X.D. Wang, S. Yin, Q.P. Cao, J.Z. Jiang, H. Franz, Z.H. Jin, Appl. Phys. Lett. 2008, 92, 011902.

289. D. Turnbull, M.H. Cohen, J. Chem. Phys. 1961, 34, 120.

290. T. Egami, S.J. Poon, Z. Zhang, V. Keppens, Phys. Rev. B 2007, 76, 024203.

291. J.W. Martin, R.D. Doherty, B. Cantor, Stability of microstructure in metallic systems (second edition), United Kingdom, Cambridge University Press, 1997.

292. X.J. Liu, G.L. Chen, X. Hui, T. Liu, Z.P. Lu, Appl. Phys. Lett. 2008, 93, 011911.

**References**